GL Noble Denton

R8928 Issue 2 *February 2010*

PROJECT #153K: THE ASSESSMENT OF CORROSION DAMAGE IN PIPELINES SUBJECTED TO CYCLIC PRESSURE LOADING

Not Restricted *Restricted to US DOT, PRCI & GL Noble Denton*

PREPARED FOR:

R Smith

US Dept of Transportation
Pipelines and Hazardous Materials Safety Administration
1200 New Jersey Avenue
SE Building, Second Floor
Washington DC 20590
USA

PREPARED BY:

T Swankie, M Robinson, J Liu, J Crossley and G Morgan

GL Industrial Services UK Ltd trading as GL Noble Denton
Ashby Road
Loughborough
Leicestershire
LE11 3GR
United Kingdom
Tel: +44 (0)1509 282057
Fax: +44 (0)1509 283119
E-mail: troy.swankie@gl-group.com
Website: www.gl-nobledenton.com

Customer Reference: DTPH56-05-T-0003 – Project 153

ISO 9001 FS 45127

This Report is protected by copyright and may not be reproduced in whole or in part by any means without the approval in writing of GL Noble Denton. No Person, other than the Customer for whom it has been prepared, may place reliance on its contents and no duty of care is assumed by GL Noble Denton toward any Person other than the Customer.
This Report must be read in its entirety and is subject to any assumptions and qualifications expressed therein. Elements of this Report contain detailed technical data which is intended for analysis only by persons possessing requisite expertise in its subject matter.

GL Noble Denton is the trading name of GL Industrial Services UK Ltd
Registered in England and Wales No. 3294136 Registered Office: Holywell Park, Ashby Road, Loughborough, Leicestershire, LE11 3GR UK.

REPORT ISSUE / AMENDMENT RECORD

Report Title:	**PROJECT #153K: The assessment of corrosion damage in pipelines subjected to cyclic pressure loading**
Report Number: R8928, Issue 2	**Project SAP Code: 1/07620**

Amendment details

Issue	Description of Amendment	Originator/Author
Draft 1.0	Draft for PRCI project team – no comments	R M Andrews, T Swankie, J Liu and J Crossley
Draft 2.0	Draft for PRCI project team	T Swankie, M Robinson, J Liu, J Crossley and G Morgan
	Comments from BP: Minor editorial comments Inclusion of additional graph to compare test results with BS 7608 S-N curve	T Swankie
Issue 1.0	Source: T Swankie (GL) Typo - Last term in Equations 3 and 4 should be $A_5(CD)^2$….instead of $A_5(CD)$….	T Swankie

Report approval

Issue	Checked by	Approved by	Date
Draft 1.0	R M Andrews and V Chauhan	P Ingham	October 2006
Draft 2.0	V Chauhan	P Ingham	November 2008
Issue 1.0	V Chauhan	P Ingham	January 2009
Issue 2.0	V Chauhan	P Ingham	February 2010

Previous issues of this document shall be destroyed or marked SUPERSEDED

Project code: 1/12434 (ex 1/10652)

Distribution

Name	Company
S Nanney R Smith A Mayberry J Merritt	US Dept of Transportation
M Piazza R Owen R Espiner D Johnson D Batte	PRCI
I Wood B Dudley	Electricore, Inc.

DISCLAIMER

This report is furnished to the U.S. Department of Transportation (DOT), Electricore, Inc. (Electricore) and Pipeline Research Council International, Inc. (PRCI) under the terms of DOT contract DTPH56-05-T-0003 between DOT and Electricore, Electricore agreement DTPH56-05-T-0003 between Electricore and Advantica, Inc. (Advantica), and PRCI contract PR-273-0323 between PRCI and Advantica. The contents of this report are published as received from Advantica. The opinions, findings and conclusions expressed in this report are those of the authors and not necessarily those of DOT, Electricore or PRCI, including PRCI's member companies or their representatives. Publication of this report by Electricore or PRCI should not be considered an endorsement by Electricore, PRCI or Advantica, or the accuracy or validity of any opinions, findings or conclusions expressed herein.

In publishing this report, Electricore, PRCI and Advantica make no warranty or representation, expressed or implied, with respect to the accuracy, completeness, usefulness, or fitness for purpose of the information contained herein, or that the use of any information, method, process, or apparatus disclosed in this report may not infringe on privately owned rights. Electricore, PRCI and Advantica assume no liability with respect to the use of, or for damages resulting from the use of, any information method, process, or apparatus described in this report. The text of this publication, or any part thereof, may not be reproduced or transmitted in any form by any means, electronic or mechanical, including photocopying, recording, storage in an information retrieval system, or otherwise, without written approval of Electricore, Advantica and PRCI.

Executive Summary

A range of methods exist for assessing the remaining strength of a corroded pipeline under static pressure loading and these have now matured to the extent that they are incorporated in regulations and standards. However, there is currently no guidance for assessing the performance of a corroded pipeline under cyclic pressure loading. This is of potential concern to operators where there are significant pressure variations, for example where there is a demand for linepack storage and in liquid pipelines. It is possible that a corrosion defect could be assessed as acceptable for the maximum operating pressure of a pipeline, but fail by fatigue due to internal pressure fluctuations.

Advantica has been contracted by PRCI and DOT to develop an assessment method for pipelines containing corrosion defects which are subject to fluctuating pressure loadings. This forms the subject of the present report.

The method involves estimating the stress raising effect of the corrosion defect to determine the enhanced cyclic stress range associated with the feature. This stress range is then used with a stress – life (S-N) curve to derive the fatigue life of the corrosion defect. This life can then be used to determine if the defect is acceptable, or the time until a repair is required.

The following main conclusions can be drawn from this work:

1. There is no available published method for assessing the life of volumetric corrosion defects in transmission pipelines under cyclic loading. An assessment method based on determining the stress raising effect of the corrosion defect combined with a *S-N* curve for parent plate material in a corrosive environment is proposed.

2. A wide range of defect geometries have been analyzed to determine elastic stress concentration factors which can be used to determine the effect of cyclic loading.

3. The assessment method derived has been validated for the following pipe and defect sizes:

Pipe diameter (D)	:	up to 1270mm (50”)
Wall thickness (t)	:	9.5mm to 19.1mm (0.37” to 0.75”)
D/t ratio	:	40 to 100
Corrosion length	:	26mm to 1000mm (1” to 40”)
Corrosion width	:	26mm to 1000mm (1” to 40”)
Corrosion depth	:	not greater than 60% of the wall thickness

4. The proposed approach has been validated by a small set of full-scale fatigue tests. The experimental results were generally consistent with the predictions, but with longer fatigue lives.

It is recommended that the work completed in this project be extended to cover the following activity to enhance the method described in this report:

1. The range of applicability of the assessment method should be investigated by considering the variation of stress concentration factor (SCF) with pipe geometry.
2. Review of the experimental data from the X100 operational trial.

Contents

1 INTRODUCTION 1
2 LITERATURE REVIEW 2
2.1 Issues Associated with Fatigue of Corrosion Defects 2
2.2 Existing Assessment Methods 3
2.3 Methods of Determining Stress Concentration Factors 3
3 FINITE ELEMENT ANALYSIS 4
3.1 Geometry and Material Properties 4
3.2 Finite Element Models 4
3.3 Loading and Boundary Conditions 5
3.4 Finite Element Results and Assessment 6
3.5 Conclusions from the FE Studies 8
3.6 Closed Form Equation to Determine SCFs 9
4 CYCLIC PRESSURE TEST 13
4.1 Material 13
4.2 Test vessel design and construction 13
4.3 Test Results 18
4.4 Metallurgical Examination 20
4.5 Experimental Stress Concentration Factors 22
5 ANALYTICAL FATIGUE LIFE ASSESSMENT 22
5.1 Fatigue Life – Based on Experimental SCFs 23
5.2 Fatigue Life – Based on Predicted SCFs 24
6 DISCUSSION 24
6.1 Closed Form Equation to Determine SCF 24
6.2 Comparison of Strain Gauge and Finite Element Results 25
6.3 General Remarks 27
7 OUTLINE OF PROPOSED ASSESSMENT METHOD 30
8 CONCLUSIONS 31
9 RECOMMENDATIONS 31
10 REFERENCES 32
APPENDIX A MATERIAL INFORMATION. 95
APPENDIX B INSPECTION CERTIFICATE (DEFECTS) 102

1 INTRODUCTION

A range of methods exist for assessing the remaining strength of a corroded pipeline under static pressure loading and these have now matured to the extent that they are incorporated in regulations and standards. However, there is currently no guidance for assessing the performance of a corroded pipeline under cyclic pressure loading. This is of potential concern to operators where there are significant pressure variations, for example where there is a demand for linepack storage and in liquid pipelines. It is possible that a corrosion defect could be assessed as acceptable for the maximum operating pressure of a pipeline, but fail by fatigue due to internal pressure fluctuations.

Advantica has been contracted by PRCI and DOT to develop an assessment method for pipelines containing corrosion defects which are subject to fluctuating pressure loadings. This forms the subject of the present report.

The method developed is based on the approach to the fatigue design of welded structures in codes such as API RP 2A [1] and BS 7608 [2] and API 579-1/ASME FFS-1 [3]. In these a set of stress – life, or S-N curves are presented in terms of the nominal stress range acting on a particular weld detail. If necessary the nominal stress range is magnified by a stress concentration factor to take account of the local structural geometry at the weld detail. The stress raising effect of the actual weld geometry is included in the S-N curve. For the present application the stress concentration is derived for the corrosion feature. This can then be used in conjunction with an appropriate S-N curve for the particular material and environment.

Section 2 of this report reviews the available literature relevant to the project. The finite element analyses carried out to derive stress concentration factors are presented in Section 3. Two fatigue tests under cyclic pressure loading have been carried out on vessels containing machined simulated corrosion defects; this also provided experimental measurements of the stress concentration factors for comparison with the numerical predictions. The details of each test are given in Section 4. Predictions of fatigue life of the defects in the full scale fatigue tests are presented in Section 5. The discussion in Section 6 considers the fitting of a closed form equation to the numerical results, comparison of the numerical predictions and experimental stress concentration factors and the results of the cyclic pressure tests. Based on the work carried out, an outline of the proposed assessment method for corrosion defects subject to cyclic pressure loading is given in Section 7. Conclusions are given in Section 8 and recommendations in Section 9.

2 LITERATURE REVIEW

2.1 Issues Associated with Fatigue of Corrosion Defects

It was not possible to locate any public domain information on the behavior of volumetric corrosion (as opposed to stress corrosion cracking) defects in pipelines. However, it is intuitively obvious that the environment giving rise to the volumetric metal loss would have an effect on the fatigue performance of the exposed pipe surface[1]. The voluminous literature on metal fatigue recognizes that a corrosive environment will reduce the fatigue life of a component below the life which would be obtained in air. There are many factors that contribute towards this reduction, and a review of these is outside the scope of the present project. However, the factors can generally be grouped into two main areas, the effects on crack initiation and effects on crack propagation.

A corrosive environment will reduce, or even eliminate entirely, the crack initiation period. It is generally accepted that the bulk of the fatigue life of smooth components at low to medium stresses is consumed by the initiation of a crack. The initiation period, and hence the fatigue life, is sensitive to factors such as surface roughness and residual stresses. In a corrosive environment pitting and other forms of surface attack provide initiation points for cracks and so the initiation period is largely removed. This gives rise to the fact that in many corrosive environments there is no fatigue limit.

Once a crack has initiated, there will be a period of crack growth until final failure occurs. During this period a corrosive environment will cause accelerated crack growth. For example, in Section 8.2.3.5 of BS 7910 [4] a freely corroding seawater environment increases the crack growth rate by a factor of 4.4 compared with an air environment when using the “screening” crack growth curves. Fatigue crack growth data for X65 linepipe exposed to sour crude oil showed similar levels of increase [5] [6] when compared to data obtained in air.

This brief analysis shows that predicting the effect of a corrosive environment on fatigue life is complex. For pipelines with significant metal loss, there is a further complication. This is that the stress raising effects of the corrosion defect would reduce life as this area is exposed to higher stresses (in addition to the environment). This stress raising effect is still present, even if the underlying corrosion problem is resolved by coating repairs or the introduction of corrosion inhibitor. Hence it is considered that an assessment method for pipeline corrosion defects should include both effects. The approach taken in this project is to separate the two. The stress raising effect of the metal loss defect is considered by an estimation based on the geometry and elastic stress analysis. This is then combined with a fatigue life estimation which includes the effect of a corrosive environment.

[1] If remedial action is taken, for example coat and re-wrap or the introduction of an effective inhibitor system, then the corrosive environment would no longer be affecting the life.

2.2 Existing Assessment Methods

A Code Case for the ASME Boiler and Pressure Vessel Code, N597-2 [7], was located. This is principally concerned with the assessment of nuclear power station piping which has suffered wall loss due to erosion or erosion – corrosion. The main loading is pressure or system loading, but there is a brief consideration of cyclic loading in paragraph –3625. If the loss in wall thickness is less than 25% of the nominal thickness and the loading is less than 150 full temperature cycles, the defect is considered acceptable. If this criterion is not met, a code pipe stress analysis is required using stress intensification[2] factors revised to take account of the geometry of the thinned areas. No guidance is given on how these revised factors should be determined. Alternatively, a set of stress range reduction factors are given which assume that the stress intensification factors increase linearly over the fatigue life by a factor of 2. This degree of stress increase at the defect may not be large enough for some cases, and it is also not clear how this should be applied to plain pipe. Furthermore, this approach does not appear to take account of aggressive environments. However, it is consistent with the general approach taken in the present project of modifying the basic fatigue performance by a factor to take account of the stress raising effect of the feature.

A search of the published literature using the "Compendex" database revealed a number of papers published in Japan concerning the assessment of thinned pipework. However, these were found to consider the behavior of power station piping under external seismic loads, with stresses exceeding yield, and were not relevant to corrosion defects in typical transmission pipelines.

One paper was located which is relevant to the present work. This study by Kim and Son [8] used three-dimensional finite element (FE) analysis to calculate stress concentration factors for ellipsoidal defects located at the bore of pipes. The loading was either internal pressure or external bending moment. The results from this work are discussed in more detail in Section 6.3.1.

2.3 Methods of Determining Stress Concentration Factors

There are published collections of stress concentration factors (SCFs) and these were reviewed to determine if there were any available solutions which could be used. None were found to be suitable, as they mainly related to two-dimensional cases such as a hole in a plate or a notch in the edge of a strip. These are not directly relevant to the three-dimensional case of a groove or pit[3] in a curved shell. Hence these could not be

[2] These are the ASME code stress intensification factors for pipework, and should not be confused with the stress intensity factor used in fracture mechanics analysis.
[3] Pits are defined as localized regions of metal loss, often referred to as circular patches. Grooves are defined as long elongated thinned areas caused by directional corrosion (or erosion). The length of the groove is much greater than the width

used for the determination of SCFs for volumetric defects. An equation derived using the finite element results was therefore considered.

3 FINITE ELEMENT ANALYSIS

SCFs have been derived using linear elastic FE analysis for a range of idealized corrosion defects. The analysis and results are presented in this section. Note that, although the analyses have been presented for specific dimensions typical of service pipelines, as the analyses are linear elastic the results can be applied to other geometrically similar cases.

3.1 Geometry and Material Properties

Three pipes were chosen with outside diameters (D) and wall thicknesses (t) of 914.4 mm (36”) x 12.7 mm (0.5”), 508 mm (20”) x 12.7 mm and 1270 mm (50”) x 12.7 mm, with D/t ratios of 72, 40 and 100, respectively. These were chosen to represent the typical range of geometries encountered in transmission pipelines. The majority of the analyses were carried out on the D/t=72 geometry, with a smaller range of cases being analyzed for D/t=40 and D/t=100 to investigate the effect of the D/t ratio on the SCF.

Both the axial corrosion length (ACL) and the circumferential corrosion length (CCL) in Figure 1 vary from 13 mm (0.5”) to 500 mm (19.7”). The corrosion depths (CD) modeled were 20%, 40%, 60% and 80% of the pipe wall thickness. These were chosen to cover a range slightly deeper than the typical manufacturing under tolerance of 10% through to a depth of 80%, where assessment codes such as ASME B31G [9] require repair. It should be noted that only one quarter of the corrosion area is shown in Figure 1, therefore ACL and CCL represent half of the total axial corrosion length and half of the total circumferential corrosion length, respectively. The corrosion defects have been idealized as having a smooth transition radius and a flat bottom.

The radius at the transition region around the corrosion edge in Figure 1 is r=t (i.e., r/t=1) for most of analyses. The effect of varying the radius r was investigated for 914.4x12.7 mm (36x0.5”) pipes by reducing the transition radius to r/t=0.5.

The assumed elastic properties were appropriate for a ferritic steel, a Young’s modulus of 210×10^3 N/mm^2 (30,460,000 psi) and a Poisson’s ratio of 0.3.

3.2 Finite Element Models

The finite element (FE) models were constructed using the PATRAN 2001 r3 [10] mesh generating software and analyzed using the general-purpose FE code ABAQUS version 6.4 [11]. Typical meshes generated for the assessment are shown in Figure 2 - Figure 6

with r/t=1, CD=0.4 and the corrosion size ACLxCCL=13x13 mm (0.5x0.5”), 13x500 mm (0.5x19.7”), 500x13 mm (19.7x0.5”) and 500x500 mm (19.7x19.7”), respectively. The models used quadratic cubic elements (20 node bricks), with the mesh design based on previous studies of the behavior of corrosion defects carried out by Advantica. Figure 2 represents a small circular pit, whilst Figure 3 is a long circumferentially oriented groove, such as might occur with preferential corrosion at a girth weld. In Figure 4 the groove orientation is axial. A square patch is shown in Figure 5; this has radiused sides and corners. Figure 6 shows the mesh for a defect with a smaller transition radius, r/t=0.5 but with the other dimensions, (CD=0.4 and ACLxCCL=13x13 mm [0.5x0.5”]) identical to those in Figure 2. The smaller transition radius has resulted in short straight sections at the edges.

A mesh sensitivity study using a finer mesh with 10 elements through the remaining ligament at the base of the corrosion defect showed only a 1% increase in the stress concentration factor, and so it was concluded that the mesh design was sufficiently refined.

3.3 Loading and Boundary Conditions

The internal pressure (*p*) was calculated to generate a hoop stress $\sigma_h = 1$ N/mm^2 (145 psi) based on the internal diameter,

$$p = \frac{\sigma_h t}{R - t} = \frac{t}{R - t} \tag{1}$$

where, R = Pipe outside radius (units: mm (“))

t = Pipe wall thickness (units: mm (“))

In order to represent the pipe sections being ‘capped off’ downstream, a distributed load (*q*) was applied to the pipe surfaces, given by:

$$q = \frac{\pi p (R - t)^2}{\pi \left[R^2 - (R - t)^2 \right]} = \frac{R - t}{2R - t} \,. \tag{2}$$

Equation (2) shows that if the internal pressure is given by equation (1), the circumferential stress in the pipe will be $\sigma_h = 1$ N/mm^2 (145 psi) and the axial stress from equation (2) will be about 0.5 N/mm^2 (72.5 psi) when R >> t. A limited number of analyses were carried out without this end load to investigate the effect of this load on the results, particularly for long circumferential grooves.

Nodal restraints were applied to the symmetry faces so that the quarter model represented a complete pipe with the defect. Additional restraints were also applied to the bottom of the pipe to prevent rigid body movement.

3.4 Finite Element Results and Assessment

3.4.1 Pipe: 914.4mm x 12.7mm

A total of 222 analyses were carried out on the 914.4x12.7 mm (36x0.5”) pipe geometry. The maximum principal stresses from these analyses are listed in Table 1 - Table 7 as functions of the ACL, CCL and CD.

Figure 7 shows that maximum principal stresses at locations away from corrosion are apparently in the range 0.54 N/mm^2 to 1.12 N/mm^2 (78.3 to 162.4 psi). This large apparent range is due to the automatic scaling of contour levels by the post-processing software. Further investigation shows that results were in the range 0.93 N/mm^2 to 1.1 N/mm^2 (134.9 to 159.5 psi). The circumferential stress of the pipe with the internal pressure given by equation (1) is equal to unity, and hence provides confidence in the FE model. The highest maximum principal stress (HMPS) (8.7 N/mm^2 (1261.8 psi) in Figure 7), which occurred in the corroded region, is defined as the stress concentration factor (SCF) for the corrosion defect. In most cases, the highest maximum principal stress occurred either around the centre of the corrosion shown in Figure 8 or around the corrosion transition region shown in Figure 9.

3.4.1.1 Effect of corrosion size (length, width and depth)

The SCFs in Table 1 to Table 4 are from FE analyses on corroded pipes with r/t=1 and with CD=0.2, 0.4, 0.6 and 0.8 wall thickness, respectively. These SCFs are also plotted in Figure 10 - Figure 13 as functions of the ACL and CCL. The figures show that, in general, the SCF increases with an increase of ACL but decreases with an increase of CCL until it reaches an approximately constant plateau value. However, for corroded pipes with a short ACL (13 mm or 20 mm, 0.5” or 0.75”), the SCF may decrease with an increase of ACL and increase with a decrease of CCL, as clearly shown in Figure 12 and Figure 13.

The SCFs are also plotted in Figure 14a – f with variation of the corrosion depth CD, showing that both the SCF and the gradient increase as corrosion depth becomes greater.

3.4.1.2 Effect of ‘Capped End Force’

For corroded pipes with a short ACL but long CCL (i.e. circumferential grooves), the distributed load defined by equation (2) due to the ‘capped end force’, may play a major role on SCFs. Local axial, hoop and radial component stresses have been extracted from the results at the location of the highest maximum principal stress. Table 8 lists these stresses for pipes with CD=0.8. It shows that

- For ACL larger than or equal to 50 mm (2”), the maximum principal stress is approximately equal to the local circumferential stress.

- When ACL equals 13 mm and 20 mm (0.5” and 0.75”), the axis of maximum principal stress changes from the circumferential direction to the pipe axial direction with an increase of CCL, i.e., for CCL less than about 50 mm (2”), the maximum principal stress is approximately equal to the local circumferential stress. However, for CCL larger than or equal to 50 mm (2”), the maximum principal stress is approximately equal to the local axial stress.

Local axial, circumferential and radial stresses for pipes with short ACL (13 mm and 20 mm, 0.5” and 0.75”) and with CD=0.2 and 0.4 are also given in Table 9 and Table 10 respectively. These tables show that

- For CD=0.2 with both ACL=13 mm (0.5”) and ACL=20 mm (0.75”), the maximum principal stress in Table 9 is approximately equal to the local circumferential stress, hence the axis of maximum principal stress remains the circumferential direction with the increase of CCL.

- For CD=0.4 with ACL=20 mm (0.75”), the maximum principal stress in Table 10 is approximately equal to the local circumferential stress. However, for ACL=13 mm (0.5”), the maximum principal stress is approximately equal to the local circumferential stress only when the CCL is less than 50 mm, and for CCL greater than 100 mm (4”), the maximum principal stress is approximately equal to the local axial stress.

SCFs from FE analyses with CD=0.8 and without the ‘capped end force’ acting on the end of pipes are given in Table 5 and plotted in Figure 15. It shows that the SCF increases with an increase of ACL and decreases with an increase of CCL even for short lengths of ACL=13 mm and 20 mm (0.5” and 0.75”).

3.4.1.3 Effect of radius at the transition region

SCFs with transition radius r=0.5t are given in Table 6 and Table 7 for CD=0.2 and CD=0.4, respectively. Comparing these values with the data for r/t=1 in Table 1 and Table 2 shows that the SCF is higher for the smaller transition radius, r. The increased percentage of SCF, when the transition radius r/t=1 decreases to a more acute transition radius r/t=0.5, is listed in Table 11. It shows that the maximum percentage increase is less than 10%.

SCFs are also plotted in Figure 16 and Figure 17 for CD=0.2 and CD=0.4 respectively. The trend of the graph is similar to that in Figure 10 and Figure 11, except for the case with ACL=13 mm (0.5”) and CD=0.4 which shows that the ‘capped end force’ influence on the SCF is less when r=0.5t.

3.4.1.4 Effect of a variation in wall thickness

The SCFs in Table 12 are from additional FE analyses on the 914.4mm (36”) diameter pipe, which were undertaken to confirm whether pipe wall thickness had an underlying

effect on the calculated SCF. To complement the analyses on 12.7mm (0.5”) thick pipe, three additional wall thicknesses were considered, 9.5mm (0.37”), 15.9mm (0.63”) and 19.1mm (0.75”), but the ratio of defect depth to wall thickness was consistent for the analyses. The results are presented in Table 12, which shows that any trends appear dependent more on the defect geometry with some defects showing an increase in SCF with an increase in wall thickness and others a decrease. All of the SCFs are within 10% of the 12.7mm (0.5”) results.

3.4.2 Pipe: 508mm x 12.7mm (20” x 0.5”)

A total of 73 finite element (FE) analyses have been carried out on 508x12.7 mm (20x0.5”) pipes. The maximum principal stresses from these FE analyses are listed in Table 13 with the variation of ACL, CCL and CD. Table 13 shows that, in general, the SCF increases with an increase of ACL and decreases with an increase of CCL until it reaches an approximately constant value.

3.4.3 Pipe: 1270mm x 12.7mm (50” x 0.5”)

There are a total of 48 finite element (FE) analyses carried out on 1270x12.7 mm (50x0.5”) pipes. The maximum principal stresses from these FE analyses are listed in Table 14 with the variation of ACL, CCL and CD. Table 14 shows that SCF increases with an increase of ACL.

3.4.4 Effect of pipe size

SCFs from the three pipes (508x12.7mm (20x0.5”), 914.4x12.7 mm (36x0.5”) and 1270x12.7 mm (50x0.5”)) with CCL=13 mm (0.5”) and 20 mm (0.75”) are plotted in Figure 18 to Figure 21 for CD=0.2 to 0.8 respectively. Table 15 and Table 16 show the increment/decrement percentage in the SCF for 508 mm (20”) pipe and for 1270 mm (50”) as compared with 914.4 mm (36”) pipe, respectively. It should be noted that some care is required in comparing the results for defects in different diameter pipes, as the fixed width defects will subtend different angles in pipes of different diameter and so would be expected to have different SCFs.

3.5 Conclusions from the FE Studies

The following conclusions can be drawn directly from the finite element analysis phase of the project:

- In general, the SCF increases as the axial corrosion length increases, but decreases as the circumferential corrosion length increases until it reaches a constant value.
- For corroded pipes with a short axial corrosion length the axis of the maximum principal stress may change, due to the ‘capped end force’ effect, from the

circumferential direction to the axial direction as the circumferential length rises. Where this condition occurs, the SCF will increase with increasing circumferential corrosion length.

- The SCF increases with increasing corrosion depth.
- The effect of reducing the transition radius was small, producing typically less than 10% change in the SCF.
- Varying the wall thickness for a specific diameter has no consistent effect on the SCF. For the wall thicknesses analyzed, 9.5mm (0.37”), 15.9mm (0.63”) and 19.1mm (0.75”), all of the SCFs were within 10% of the values for a wall thickness of 12.7mm (0.5”).
- There was no consistent trend in the SCF with varying pipe diameter, but the effects were generally less than 10% when compared with the base case of D/t=72.

3.6 Closed Form Equation to Determine SCFs

The finite element analysis has generated “point” values of the SCF associated with corrosion defects for the specific dimensions modeled. For practical applications a method of obtaining SCFs for intermediate dimensions is needed. It was noted in Section 3.5 above that the effects of the transition radius and pipe D/t ratio were small. Therefore attempts to fit an equation to the SCFs were concentrated on the main set of results for *D/t*=72 (pipe diameter and wall thickness of 914.4mm (36”) and 12.7mm (0.5”)) and *r/t*=1, as presented in Table 1 to Table 4.

To simplify the equation fitting procedure the SCFs results were split into two categories; those dominated by a hoop stress component and those dominated by an axial stress component. The changing relationship between the SCFs and defect geometry for the two categories is simpler to describe using two separate equations for each component. From the finite element results it can be seen that when the CCL≥50mm (2”) and the ACL≤20mm (0.75”) the SCF can be either hoop or axial driven, but outside of this region the SCF has been found to be dominated by the hoop stress. For an area of corrosion that has dimensions, ACL and CCL in the hoop/axial boundary region the highest SCF value returned from the two equations will provide the best estimate to its “actual” value.

The basic form of each equation was determined by examining the graphical relationships between ACL, CCL and CD. Several equations were developed, each capable of predicting an SCF for the range of defects (ACL, CCL, CD) and pipe sizes (D, t and D/t) considered in the FE studies. The equations which provided the highest levels of accuracy are shown below:

The hoop SCFs are calculated using the following equations:

$$SCF_{HOOP} = A_6\left(A_1 + \left[A_2(CD)^2\left(\frac{Ln(ACL)}{Ln(CCL)}\right)^2\right] + \left[A_3\frac{CD^2}{\left(\frac{CCL}{\sqrt{Dt}}\right)}\right] + \left[A_4\frac{(CD)^2 ACL}{CCL}\right] + \left[A_5(CD)^2 Ln\left(\frac{CCL}{ACL(CD)}\right)\right]\right) \quad (3)$$

for CCL≤100mm (4”) and CD≤0.6

$$SCF_{HOOP} = A_6\left(A_1 + \left[A_2(CD)^2\left(\frac{Ln(ACL)}{Ln(100)}\right)^2\right] + \left[A_3\frac{(CD)^2}{\left(\frac{100}{\sqrt{Dt}}\right)}\right] + \left[A_4\frac{(CD)^2 ACL}{100}\right] + \left[A_5(CD)^2 Ln\left(\frac{100}{ACL(CD)}\right)\right]\right) \quad (4)$$

for CCL>100mm (4”) and CD≤0.6

where,

D	=	Pipe outside diameter (units: mm)
t	=	Pipe wall thickness (units: mm)
ACL	=	Half axial corrosion length (units: mm)
CCL	=	Half circumferential corrosion length (units: mm)
CD	=	Ratio of corrosion depth to pipe wall thickness
A_1 to A_6	=	Constants (calibrated to SI units, note units above)

The constants A_1 to A_6 are, A_1=1.40, A_2=7.40,A_3=-0.54, A_4=-0.37, A_5=0.28 and A_6=1.18.

A standard least squares approximation technique was employed to determine the equation constants A_1 to A_5, which provide a mean fit to the SCFs. Constant A_6 is included in the equation to ensure that the calculated SCF is not under predicted.

From the FE data it was noticed that beyond CCL of 100mm (4”) any further increase in SCF was negligible. To model this trend, two equations have been developed, one for CCL≤100mm (4”) and one for CCL>100mm (4”).

The axial SCFs are calculated using the following equation:

$$SCF_{AXIAL} = B_5\left(B_1 + \left(B_2 CD\left(Ln\left(\frac{CCL}{ACL}\right)\right)\right) + \left(B_3 CD\left(Ln\left(\frac{ACL}{\sqrt{Dt}}\right)\right)\right) + B_4 (CD)^2\right) \quad (5)$$

for CD≤0.6

where, B_1 to B_5 = Constants (calibrated to SI units)

The remaining terms in Equation (5) are defined above for Equations (3) and (4). The constants B_1 to B_5 are: B_1=-0.64, B_2=0.58, B_3=-2.29, B_4=1.31 and B_5=1.10. As noted above, the constants are calibrated to the parameters being input in SI units.

The constants B_1 to B_4 provide a mean fit to the SCFs. Constant B_5 is included in the equation to ensure that the calculated SCF is not under predicted.

Equations (3) and (4) which described the hoop SCF trend have a maximum error of 36% (over-prediction) and Equation (5) which describes the axial stress SCF has an error of 24% (over-prediction). Note, these errors relate to a pipe size (Dxt) of 914.4x12.7mm (36x0.5”), and a maximum corrosion depth not greater than CD=0.6. As described above, the equations ensure that the SCF is not under predicted. The mean error for the SCF_{HOOP} calculations is 14% with a standard deviation of 8.4%. This indicates that the error bounds are stretched by a small number of high inaccuracy points. Analyzing the data reveals that the upper bound errors are predominantly caused by an over estimation of defects that generate a relatively low SCF for deep defects, CD=0.6.

The equations exhibit a strong correlation between corrosion depth and accuracy, with accuracy decreasing as the corrosion depth increases. The maximum errors for CD=0.2, 0.4 and 0.6 are 25%, 31% and 36% respectively. If a higher level of accuracy is to be achieved this could be done by categorizing the corrosion defect by depth in terms of shallow, medium and deep, and developing separate equations for each category.

3.6.1 Equation Limitations

Equations (3), (4) and (5) are valid for corrosion defects of depth not greater than CD=0.6. Finite element results have been generated for CD=0.8. However, inclusion of this data in the above equations resulted in a significantly higher level of error. Although the corrosion assessment methods for static internal pressure loading extend to defects of depth, CD=0.8, for a pipeline that is pressure cycled it was considered prudent to limit the allowable depth to CD=0.6. If corrosion damage deeper than this is identified consideration should be given to either undertaking a repair or performing a case specific assessment. An insight into the reason why the fitting is so difficult for deep defects can be obtained from Figure 14. These graphs show that for certain defect sizes there are significant changes in the relationship between depth and SCF beyond CD=0.6. Separate equations, potentially of a different form to those presented above,

would be required to enable the assessment of defects ranging in depth from 0.6<CD≤0.8. Eliminating the data for defects greater than 60% in depth from the fitting procedure reduces the number of points available to perform a least squares solution. The intrinsic accuracy of a least squares solution is driven by the number and spread of data points available for the fitting process. This is not a concern for the hoop equation where 98 data points were available for CD≤0.6. However, there were only ten points available to fit the axial equation to the data. The minimum required for a least squares solution is 1+n, where n is the number of constants in the equation. Although the axial equation has more than the minimum number of points the data is still over a small range and will not have the inherent robustness of the hoop equation. Unfortunately the axial equation is only applicable over a small range of defect sizes so it is impossible to address this concern without further in depth FE analysis concentrating on that region.

3.6.2 Effect of Pipe Diameter on Accuracy

The SCF equations have been calibrated using data for a 914.4mm (36”) diameter pipe. As previously mentioned there is also a limited number of SCF data for a 508mm (20”) and 1270mm (50”) diameter pipe. All of the defects modeled for the 508mm (20”) and 1270mm (50”) diameter pipe produced hoop dominant SCFs, which restricted a sensitivity study to investigate the effect of diameter on the hoop equation. If these extra data points are added to the existing 914.4mm (36”) data set the maximum percentage error in the hoop equation is increased to 43% (an increase in error of 7%). It was not possible to incorporate a term in the equations to account for the effect of diameter on SCF using a correction factor. Further FE analyses are recommended for smaller pipe diameters, less than 508mm (20”) to extend the SCF data base as the SCFs generated in this work from 3 different pipe diameters suggests a potentially complex relationship between defect geometry and pipe diameter.

3.6.3 Effect of Wall Thickness on Accuracy

All the data points used to derive the SCF equations had a constant wall thickness of 12.7mm (0.5”). Additional FE data was generated for several defect sizes in a 914.4mm (36”) diameter pipe with a wall thickness of 9.5mm (0.37”), 15.9mm (0.63”) and 19.1mm (0.75”). The corresponding SCFs are presented in Table 12. Wall thickness has a similar inconsistent effect on SCF as diameter with some defects showing a proportional trend between wall thickness and SCF and others behaving inversely proportional. The equations proposed above only contain the wall thickness in one term and increasing the wall thickness will result in the calculated SCF being lower. This could cause a potential “stretching” of the error bounds in the SCF calculations for those defects which have an increasing trend between SCF and wall thickness. The SCF equations should be limited to pipe wall thicknesses from 9.5mm (0.37”) to 19.1mm (0.75”), until further FE studies are undertaken to extend these bounds.

4 CYCLIC PRESSURE TEST

A limited test program was undertaken to provide validation of the FE analyses described in Section 3. This used two vessels, each containing four machined metal loss defects. Both vessels were then subjected to pressure cycling. Strain measurements were made at each defect and used to determine SCFs for comparison with the finite element results. In each of the vessels tests, three of the four defects failed and the fourth defect survived beyond the predicted life. This section describes the test program and the results obtained.

4.1 Material

Two pipes were selected for testing. Both pipes were 12m (39.4 ft) in length with an outside diameter of 323.9mm (12" nominal diameter). Details of each test pipe are given below:

- Pipe 1: Constructed from Seamless line pipe of grade X52 material to API 5L [12], which has a specified minimum yield strength (SMYS) of 359 N/mm^2 (52,000 psi) and a specified minimum tensile strength (SMTS) of 455 N/mm^2 (66,000 psi). The pipe nominal wall thickness was 8.4 mm (0.33"), giving a pipe diameter to wall thickness (*D/t*) ratio of 38.5. This is marginally below the lowest *D/t* ratio analyzed in the FEA. The pipe manufacturer was Dalmine.
- Pipe 2: Constructed from HFI (High Frequency Induction welded) line pipe of grade X60 material to API 5L, which has an SMYS of 414 N/mm² (60,000 psi) and an SMTS of 517 N/mm² (75,000 psi). The pipe nominal wall thickness was 15.9 mm (0.63"), giving a *D/t* ratio of 20.4. The pipe manufacturer was Corus. Compared with pipe 1, pipe 2 was chosen for the following reasons:
    - The *D/t* ratio was approximately half that of pipe 1.
    - Pipe 2 had greater strength than pipe 1.
    - Pipe 2 was manufactured using the HFI process, unlike pipe 1 which was seamless.

The mill certificate for each pipe is provided in APPENDIX A.

4.2 Test vessel design and construction

4.2.1 Introduction of defects

Each pipe had 4 defects machined along its length. The defects machined in pipe 1 were identical in length and depth (i.e., proportion of the pipe wall thickness) to those in pipe 2. For ease of handling and machining purposes each pipe was cut in half (approximately 6m (19.7 ft) lengths). Each half contained 2 machined defects, spaced

such that when the two halves were rejoined, the defects were equally spaced along the length of the pipe, and offset to one another around the pipe circumference by approximately ¼ of the pipe circumference (note, the defects in pipe 2 were positioned approximately 120° either side of the HFI weld). The purpose of this offset was to mitigate against the possibility of a rupture from a failed defect propagating into an adjacent defect.

The defect types and target dimensions are summarized below:

Defect	Type	*CD*	*L* mm (“)	Pipe 1		Pipe 2	
				R mm (“)	*W* mm (“)	*r* mm (“)	*W* mm (“)
1	Axial groove	0.2	400 (15.75)	8.5 (0.335)	10.1 (0.398)	16.0 (0.630)	19.1 (0.750)
2	Axial groove	0.4	400 (15.75)	8.5 (0.335)	13.5 (0.531)	16.0 (0.630)	25.5 (1.004)
3	Axial groove	0.6	400 (15.75)	8.5 (0.335)	15.5 (0.610)	16.0 (0.630)	29.3 (1.154)
4	Patch	0.6	400 (15.75)	8.5 (0.335)	140 (5.512)	16.0 (0.630)	140 (5.512)

Where *t* is the pipe wall thickness, CD is the ratio of defect depth (from the outer pipe surface) to pipe wall thickness, *L* and *W* are the defect length and width in the pipe axial and circumferential directions measured along the outer surface of the pipe, and *r* is the blend radius (which is approximately equal to the pipe wall thickness).

The actual dimensions of the machined defects are compared with the target dimensions in Table 17 (see also APPENDIX B for the defect inspection certificate). A 50x50 mm (2x2”) grid was marked onto the surface of the machined-out patch defect in both pipes. At each grid intersection, ultrasonic wall thickness measurements were undertaken to determine the variation in remaining ligament thickness. The remaining ligament thickness for each groove defect was determined by subtracting the actual depth of the defect (as measured using a depth micrometer) from the local wall thickness of the pipe which was measured using an ultrasonic thickness meter.

After the defects had been machined, the surface of each defect was shot blasted. The pipe was then left outside for a period to permit the surface of the defects to corrode (this was to ensure that the number of fatigue cycles to crack initiation was truly representative of a corrosion defect and not unduly influenced by surface profile). The purpose of grit blasting the machined defects was to create a ‘highly active’ surface to promote accelerated corrosion.

4.2.2 Vessel fabrication

The two halves of pipe 1 and pipe 2 were first butt welded back together. To enable a full-scale fatigue test to be undertaken, two dome-ended pup pieces were constructed, which were welded to either end of the test pipe to form a pressure vessel. The same set of test ends were used to test both pipes.

The material used to construct the pup piece test ends was API 5L grade X52. The pup wall thickness measured 12.7 mm (0.5”). The domed ends were forged from P460 NL1 plate [13] with the same wall thickness as the test end pipe pup material. Each test end had a 1” BSPT 6,000 psi rated thread-o-let welded to the outside diameter to allow for filling (and discharging) and venting of the completed vessel.

The vessel was constructed from two test ends circumferentially welded to the test section, with the thread-o-lets positioned diametrically opposite to ensure removal of air during filling and venting of the vessel.

An illustration of the test vessel is shown in Figure 22.

4.2.3 Defect instrumentation

Each defect was strain gauged prior to testing. The groove defects each had 3 strain gauges; one located central to the length/width of the groove, and one at either end approximately 2-3 mm (0.08-0.12”) from the blend radius. The patch defect had 4 strain gauges; one located central to the length/width of the patch, one located around the patch circumference approximately 2-3 mm (0.08-0.12”) from the blend radius (central to the patch length), one located along the pipe length approximately 2-3 mm (0.08-0.12”) from the blend radius (central to the patch width), and the final gauge was located at a corner of the patch approximately 2-3 mm (0.08-0.12”) from the blend radius. The four strain gauges in the patch defect enveloped a quadrant of the patch, in the region where the thinnest remaining ligament was measured.

At the location where each strain gauge was positioned, the surface rust was locally removed to reveal bright metal to aid adhesion of the strain gauge.

Strain gauge rosettes were used at each location. Two types were used,

Type 1. CEA-06-062WT-350: two elements 90° to each other, one stacked on top of the other (see Figure 23).

Type 2. CEA-06-062UT-350: two elements 90° to each other, located side by side (see Figure 23).

Strain gauge type (1) was used where space was limited, at the blend radii. Type (2) was used at the centre (length/width) of the groove and patch defects. The locations of the strain gauges are shown in Figure 24.

4.2.4 Test facility

The test was carried out with the test vessel mounted on freestanding vee support frames with the thread-o-lets positioned at 12 and 6 o'clock around the pipe circumference. The vessel was connected to the hydraulic system and filled with water. Once the vessel was full and all air had been removed, a 160 Barg (2,320 psig) pressure transducer was connected to the upper thread-o-let of the vessel.

The test was undertaken according to a generic burst test risk assessment, which included the use of an exclusion zone and of the placement of 1 ton sand bags at either end of the vessel to help contain debris should catastrophic failure occur.

A data logger was used to log the output from the pressure transducer, and a 'K' type stainless steel sheathed thermocouple was used to measure ambient air temperature. The data was logged periodically at high frequency for a short time interval in an attempt to capture the minimum and maximum pressures associated with each pressure cycle. In addition, a strip chart recorder was used to continually monitor the pressure history during the test. The hydraulic power pack enabled a cyclic pressure rate of 5 to 6 cycles per minute.

4.2.5 Test method

Vessel 1 (pipe 1) was the first vessel to be tested. The vessel was initially pressurized to 16 Barg (232 psig), after an initial shakedown (i.e., 3 pressure cycles from 0–16–0 Barg (0-232-0 psig)) to ensure that the strain gauges were working correctly and to enable calculation of the maximum permissible pressure that each defect could sustain without yielding the remaining ligament ahead of the defect. The strain gauge data were analyzed to determine the magnitude of hoop stress σ_h in the reduced ligament of each defect, using the following equation:

$$\sigma_h = \frac{E}{1-\nu^2}\left(\varepsilon_h + \nu\varepsilon_a\right) \qquad (6)$$

where, E = Elastic modulus (210×10^3 N/mm² (30,460 kips))

ν = Poisson's ratio (assumed 0.3)

ε_h = hoop strain

ε_a = axial strain

The maximum measured hoop stress from each defect was then compared with the material's specified minimum yield strength (SMYS) of 359 N/mm² (52,000 psi) for vessel 1 (grade X52 material). For each defect the maximum pressure to give a hoop stress in the remaining ligament equal to SMYS was predicted by multiplying the initial 'calibration' pressure (16 Barg (232 psig)) by the ratio SMYS/σ_h. These maximum

pressures corresponded to the planned maximum pressure in the pressure cycle for each defect. The intention was to cycle the vessel using the lowest of these maxima, so that the other defects would not be overstressed. After failure of the first defect, the maximum pressure could be increased if necessary to that calculated for the next lowest defect.

Based on the progress and results from the test on vessel 1, the initial pressurization of vessel 2 (pipe 2), was 60 Barg (870 psig). This gave a maximum measured hoop stress in the most onerous defect (defect D3) equal to the materials measured yield strength (504 N/mm² (73,100 psi), see APPENDIX A)

The characteristics of each test are described below:

Vessel 1 (pipe 1)

The minimum pressure in the pressure cycle was initially set at 10 Barg (145 psig), and the test started. The maximum pressure was set at 33.3 Barg (479 psig), based on the strain gauge readings for the most onerous defect, D3. The strain gauge readings from the first full pressure cycle were re-analyzed to confirm elastic behavior in the remaining ligament of defect D3 (i.e., linear pressure v strain load and unload history) and to confirm earlier calculations of maximum pressure for the other defects.

After 98,951 pressure cycles of 23.3 Bar (334psi) range, the minimum pressure was decreased to 8.5 Barg (123 psig), the lowest achievable pressure whilst avoiding un-necessary lag in the pressure reversal and ensuring optimum cyclic test frequency. This increased the pressure range. In addition, the maximum pressure for each defect was increased; the maximum pressure being of sufficient magnitude to give a hoop stress equal to the material's measured yield strength of 390 N/mm^2 (56,560 psi) (see APPENDIX A, Figure A1, Test N.R7133 Heat N.990178, transverse oriented tensile test). Testing resumed based on the updated minimum and maximum pressures.

The minimum and maximum pressures in the pressure cycle for each defect are given in Table 18.

Vessel 2 (pipe 2)

The minimum pressure in the pressure cycle was set at 8 Barg (116 psig), and the test started. The maximum pressure was set at 60 Barg (870 psig), based on the strain gauge readings for the most onerous defect, D3 where the hoop stress in the remaining ligament was approximately equal to the materials measured yield strength of 504 N/mm² (73,100 psi) (see APPENDIX A, Figure A3). After 358,614 pressure cycles the test was stopped, a single pressure cycle of 0-60-0 Barg (0-870-0 psig) was applied and the strain gauge data recorded. The strain gauge data was re-analyzed and it was found that the peak pressure could be increased slightly to 66 Barg (957 psig). Testing resumed based on the updated maximum pressure.

The corresponding calculated peak pressures for the other defects were also found to increase slightly. The difference between the latter and former calculations of peak pressure is likely to be due to the system not having shaken down to an elastic response before the application of the first pressure cycle. The results from this latter analysis were used to define the peak pressures for the other defects.

The minimum and maximum pressures in the pressure cycle for each defect are given in Table 19.

4.3 Test Results

When a fatigue crack had grown through the pipe wall due to pressure cycling, the test was temporarily stopped, the vessel drained, and the defect area repaired. The fatigue life associated with that defect was then logged and testing was resumed once the vessel was re-filled. To enable the fatigue life of each defect to be determined, repairs were undertaken on each occurrence of a crack growing through the pipe wall.

The repair method used was to flame cut out a pup piece containing the defect, of length just greater than the defect length and butt weld the two remaining pipe sections together. The procedure is shown schematically in Figure 25.

The results of the two vessel tests are presented below.

4.3.1 Vessel 1 (pipe 1)

The test started with minimum and maximum pressures of 10.0 Barg (145 psig) and 33.3 Barg (483 psig) (pressure range of 23.3 bar (338 psi)), where 33.3 Barg (483 psig) was predicted to give a hoop stress in defect D3 equal to the material's specified minimum yield strength. After 98,951 cycles, the minimum pressure was decreased to 8.5 Barg (123 psig) and the maximum pressure was increased to 39.9 Barg (579 psig) (pressure range of 31.4 Bar (455 psi). The increase in maximum pressure increased the hoop stress in defect D3 to equal the material's measured yield strength. Defect D3 endured a further 229,071 cycles before failure occurred.

Defect D2 was predicted to fail next. The minimum pressure remained at 8.5 Barg (123 psig), but the maximum pressure was increased to 52.2 Barg (757 psig), giving a pressure range of 43.7 Bar (634 psi). The maximum pressure corresponded to a hoop stress in defect D2 equal to the material's measured yield strength. In addition to the previous pressure regimes and corresponding number of cycles, defect D2 endured a further 447,344 cycles of 43.7 Bar (634 psi) pressure range before failure occurred.

Defect D4 was predicted to fail next. The minimum pressure remained at 8.5 Barg (123 psig), but the maximum pressure in the cycle was increased to 62.9 Barg (912 psig), giving a pressure range of 54.4 Bar (789 psi). The maximum pressure corresponded to a hoop stress in defect D4 equal to the material's measured yield strength. In addition to the previous pressure regimes and corresponding number of cycles, defect D4 endured a further 100,575 cycles of 54.4 Bar (789 psi) pressure range before failure occurred.

With only defect D1 remaining, the maximum pressure in the pressure cycle was increased to 94.3 Barg (1,368 psig), giving a pressure range of 85.8 Bar (1,244 psi) with the minimum pressure remaining at 8.5 Barg (123 psig). Again, the maximum pressure corresponded to a hoop stress in defect 1 equal to the material's measured yield strength. In addition to the previous pressure regimes and corresponding number of cycles, defect 1 endured a further 370,419 cycles of 85.8 Bar (1,244 psi) pressure range before the test was terminated due to a failure in the pipework of the pressurization system.

The test results are summarized in Table 20.

4.3.2 Vessel 2 (pipe 2)

The test started with minimum and maximum pressures of 8 Barg (116 psig) and 60 Barg (870 psig) (pressure range of 52 Bar (754 psi)), where the peak pressure was predicted to give a hoop stress in the remaining ligament of defect D3 equal to the materials measured yield strength (504N/mm² (73,100 psi), see APPENDIX A, Figure A3).

After 358,614 pressure cycles, the test was stopped, a single pressure cycle of 0-60-0 Barg (0-870-0 psig) was applied and the strain gauge data recorded and reanalyzed. Based on the results of this latter pressure cycle, the peak pressure was increased to 66 Barg (957 psig) (58 Bar (841 psi) pressure range). After a further 98,992 pressure cycles of 58 Bar (841 psi) pressure range the test was stopped. Although defect D3 had not failed, due to the number of pressure cycles already accumulated, the peak pressure was increased to 136 Barg (1,973 psig) (128 Bar (1,856 psi) pressure range), which gave a hoop stress in the ligament of defect D2 equal to the materials measured yield strength. At this pressure the hoop stress in the remaining ligament of defect D3 was approximately 1.93 times the material measured yield strength. Despite exceeding the yield strength of the material, plasticity effects do not need to be considered in the analysis unless the stress range exceeds twice the

materials measured yield strength [14]. Defect D3 failed after 5,231 pressure cycles, in addition to the previous pressure regimes and corresponding number of cycles. Defect D4 then failed after a further 230,819 cycles. This was unexpected since analysis of the strain gauge data suggested that defect D2 would fail first.

The peak pressure was increased to 200 Barg (2,900 psig) (192 Bar (2,784 psi) pressure range), which increased the hoop stress in the remaining ligament of defect D2 to approximately 1.40 times the materials measured yield strength. Defect D2 endured a further 18,606 cycles in addition to the previous pressure regimes and corresponding number of cycles before failure occurred.

The peak pressure was increased to the system limit of 250 Barg (3,626 psig), which was just short of the pressure required to give a hoop stress in the remaining ligament of defect D1 equal to the materials measured yield strength. After 9,019 pressure cycles of 242 Bar (3,510 psi) pressure range the test was terminated without failure of the defect.

The test results are summarized in Table 21.

4.4 Metallurgical Examination

The pipe samples were examined visually using a stereo optical microscope to determine the location and size of through wall cracks present within the simulated defects. The samples were sectioned to remove the cracks found; the cracks were then opened by cooling in liquid nitrogen and fracturing the remaining ligaments at the ends. After sectioning the cracks were examined by eye and using a stereo optical microscope. The crack faces were examined as-opened and after cleaning of deposits using Clarke's solution (inhibited acid).

The features from each vessel test are described below.

4.4.1 Vessel 1 (pipe 1)

The crack faces as opened and after removal of surface deposits are shown in Figure 26 for defect D3, Figure 27 for D2 and Figure 28 for D4. The crack surfaces were characteristic of low stress, high cycle fatigue crack propagation. Step markings on D3 (Figure 26) along the outer surface suggested multiple crack initiation. Beach markings on cracks D2 and D3 were consistent with crack initiation at the outer surface and crack propagation across the remaining pipe wall ligament at the defect. In contrast, for defect D4 multiple crack initiation sites were observed on the inner pipe surface and the crack propagated across the remaining pipe wall ligament to the outer pipe surface. This is likely to be due to the increased surface roughness on the inner surface of the pipe compared with the smooth machined finish of the patch on the outer pipe surface.

The cleaned crack surfaces were examined using a CAMSCAN S4 scanning electron microscope to confirm the mode of failure. The appearance of the crack faces towards

the outer and inner surfaces is shown in Figure 29 for defect D3, Figure 30 for D2 and Figure 31 for D4. The appearance of all crack faces was very similar, consistent with transgranular separation with crack propagation on multiple fine scale paths. Fine striations were also visible at high magnification. These observations are characteristic of low stress, high cycle fatigue crack propagation. On cracks D2 and D3, numerous secondary cracks were also visible towards the inner surface, orientated perpendicular to the direction of crack propagation. These secondary cracks are also characteristic of low stress, high cycle fatigue crack propagation, and are generally more apparent when crack propagation velocity is high.

4.4.2 Vessel 2 (pipe 2)

The crack faces as opened and after removal of surface deposits are shown in Figure 32 for defect D2, Figure 33 for defect D3 and Figure 34 for defect D4. The crack surfaces were characteristic of low stress, high cycle fatigue crack propagation. The crack faces were mostly flat and appeared to have formed with little evident bulk plastic deformation in adjacent material. The cracks extended further along one surface than the other, with clearly defined curved boundaries within the wall thickness and faint concentric 'beach' markings present on the crack faces. The shape of the crack faces and pattern of beach markings on the D2 and D3 defects indicated crack initiation within the outer surface at the defect and crack propagation approximately directly across the wall thickness to emerge at the inner surface. For defect D4 the appearance of the crack faces and beach markings indicated initiation within the inner surface under the defect; the crack had initiated under one side of the patch defect and had propagated through the wall thickness to emerge at the outer surface within and at the top of the machined radius. Step markings present on all crack faces along the initiating surface, particularly apparent on the defect D2 crack face, are consistent with multiple crack initiation.

The cleaned crack faces were examined using a CAMSCAN S4 scanning electron microscope to confirm mode of failure. The appearance of the crack faces towards the outer and inner surfaces is shown in Figure 35 for defect D2, Figure 36 for defect D3 and Figure 37 for defect D4. The detail on the surface of the D4 defect crack face at the inner surface close to the initiation area was not clear due to deposits and mechanical degradation, and the images included in the Figure show an adjacent area where the crack was propagating in a direction approximately parallel to the surface. The appearance of all crack faces was essentially similar, and consistent with transgranular separation and crack propagation on multiple fine scale paths. Fine striations were evident in places at higher magnification, aligned perpendicular to the direction of crack growth. Towards the inner surface, i.e. approaching perforation, concentric markings were present on the defect D2 (in particular) and D3 crack faces; these appeared to be consistent with narrow bands of tearing, possibly due to increasing stress intensity associated with the growing crack and lack of restraint as the remaining ligament reduced.

4.5 Experimental Stress Concentration Factors

Experimental stress concentration factors have been obtained from the strain gauge readings for comparison with the finite element predictions. Equation (6) was used to obtain the hoop stress range corresponding to the strain change during a pressure cycle. This stress range was then normalized by the corresponding nominal stress range due to the pressure swing calculated using the external diameter and the *nominal* wall thickness of the pipe (8.4 mm (0.33”) for vessel 1, 15.9 mm (0.63”) for vessel 2). The experimental SCFs are given in Table 22. This table also shows the actual measured wall thicknesses local to the defect. A comparison of the measured SCFs and the finite element predictions is given in Section 6.2, which also considers the significance of variations in wall thickness from the nominal when evaluating the SCFs.

5 ANALYTICAL FATIGUE LIFE ASSESSMENT

The procedures described in BS 7608 [2] have been used to calculate the fatigue life of the defects. The procedures are based on the quantitative relationship between fatigue strength (*S*) and the number of cycles (*N*) corresponding to a specific probability of failure.

The analysis is based on the maximum local hoop stress range in the defect, which for these tests was determined from strain gauges located in the defect area. The fatigue life using this approach is given by,

$$LogN = LogC_o - d\sigma - mLogS_r \qquad (7)^4$$

where, N = Number of cycles to failure

C_o = A constant relating to the mean S_r-N curve

d = Number of standard deviations below the mean

σ = Standard deviation of *Log N* about the mean line

S_r = Maximum local hoop stress range (units: N/mm^2)

m = The inverse slope of the *Log* S_r versus *Log N* curve

Despite the mild corrosion on the surface of the defects, for these assessments the Class B fatigue design curve was considered appropriate as it is considered representative of a plate with mill scale or an equivalent rough surface finish. The

[4] The equation taken from BS 7608:1993 contains a typographical error in the British Standard document. The original equation, expressed as $log(N) = log(C_o)-(d/\sigma)-m\ log(S_r)$ is shown in its corrected form above.

constants C_o, σ and m are 15.3697, 0.1821 and 4.0 respectively. Logarithms are to base 10.

For each defect, fatigue life has been calculated based on the mean *S-N* curve (representative of a 50% probability of survival), 1 standard deviation below the mean (representative of an 84% probability of survival) and 1 standard deviation above the mean (representative of a 16% probability of survival).

As discussed in Section 4.3, each defect was subjected to two or more pressure ranges during the fatigue test. To enable a direct comparison with the predicted fatigue lives the equivalent number of pressure cycles (N_{eq}) corresponding to the final test pressure range (ΔP) for each defect is determined from,

$$N_{eq} = N_1\left(\frac{\Delta P_1}{\Delta P}\right)^m + N_2\left(\frac{\Delta P_2}{\Delta P}\right)^m + N_3\left(\frac{\Delta P_3}{\Delta P}\right)^m + ...N_n\left(\frac{\Delta P_n}{\Delta P}\right)^m \qquad (8)$$

where, N_{eq} = Number of cycles to failure of ΔP

ΔP = Pressure range for which *N* is to be calculated

$\Delta P_{1,2,3....n}$ = Pressure range for stage 1, 2, 3…….n

$N_{1,2,3....n}$ = Number of cycles for stages 1, 2, 3…….n

m = The inverse slope of the *Log* S_r versus *Log N* curve (see [2])

The equivalent numbers of pressure cycles are presented in Table 23.

5.1 Fatigue Life – Based on Experimental SCFs

The predicted fatigue life of each defect, based on an SCF determined from the corresponding strain gauge data is given in Table 24 for Vessel 1 (Pipe 1) and Table 25 for Vessel 2 (Pipe 2). The predictions are also compared with the equivalent number of pressure cycles for the corresponding defect.

The results are also presented in Figure 41, compared with the mean and mean -1 standard deviation Class B fatigue design curves.

As can be seen for Vessel 1 with the exception of defect D3 (groove, CD_{max}=0.57), the actual fatigue life of each defect is equivalent to, or greater than the predicted fatigue life based on the mean +1 standard deviation Class B *S-N* curve (note, defect D1 did not fail). The actual fatigue life of defect D3 was equivalent to the predicted fatigue life based on the mean Class B *S-N* curve.

As can be seen for Vessel 2, the actual fatigue life of defects D2, D3 and D4 is greater than the predicted fatigue life based on the mean +1 standard deviation Class B *S-N* curve. The test was terminated without failure of Defect D1.

5.2 Fatigue Life – Based on Predicted SCFs

The predicted fatigue life of each defect, based on an SCF determined using the SCF prediction method (Section 3.6) the corresponding strain gauge data is given in Table 26 for Vessel 1 (Pipe 1) and Table 27 for Vessel 2 (Pipe 2). The predictions are also compared with the equivalent number of pressure cycles for the corresponding defect.

The results are also presented in Figure 42, compared with the mean and mean -1 standard deviation Class B fatigue design curves.

As can be seen for Vessel 1 and Vessel 2, the actual fatigue life of each defect is much greater than the predicted fatigue life based on the mean +1 standard deviation Class B *S-N* curve (note, defects D1 in vessel 1 and D1 in vessel 2 did not fail).

The significant difference between actual and predicted fatigue life is due to the error associated with the method for predicting an SCF. As discussed in Section 3.6 the mean SCF curves are increased by constant A_6 for the hoop SCFs and B_5 for the axial SCFs. This is to ensure that the SCF is not under predicted (i.e., the error is always 'positive', ranging from 0% up to 36%, the mean error being 14% with a standard deviation of 8.4%). Given that fatigue life is inversely proportional to the 'm' power of the stress range, Equation (7), a small error for SCF can have a significant effect on the calculated fatigue life. For example:

- an error of +5% on SCF will reduce the predicted fatigue life by 18%
- an error of +10% on SCF will reduce the predicted fatigue life by 32%
- an error of +15% on SCF will reduce the predicted fatigue life by 43%, and
- an error of +20% on SCF will reduce the predicted fatigue life by 52%.

6 DISCUSSION

6.1 Closed Form Equation to Determine SCF

The Hoop and Axial SCF equations presented in section 3.6 are for defects of depth, CD≤0.6. Inclusion of the FE data for CD=0.8 significantly increases the 'error' bound of the SCF prediction method. Although the corrosion assessment methods for static internal pressure loading extend to defects of depth, CD=0.8, for a pipeline that is pressure cycled it was considered prudent to limit the allowable depth to CD=0.6. If corrosion damage deeper than this is identified in a pipeline subjected to pressure cycling consideration should be given to either undertaking a repair or performing a case specific assessment whereby the actual pipe geometry and metal loss dimensions are modeled using FE to obtain more accurate SCFs.

The two equations were primarily calibrated using FE data obtained using a 914.4mm (36”) diameter pipe. A limited data set was available for pipe diameters 508mm (20”) and 1270mm (50”). Selected defects were re-analyzed for the 914.4mm (36”) diameter pipe with a range of wall thicknesses, 9.5mm (0.37”), 15.9mm (0.63”) and 19.1mm (0.75”). All of the additional defects produced hoop dominant SCFs restricting a sensitivity investigation to the hoop equation. The diameter change resulted in a 7% increase in percentage error and the effect of the wall thickness variation is shown in Table 28.

The diameter and wall thicknesses used cover a wide range of D/t values over which the equations have been found to be applicable. Although the equations have been shown to be acceptable for different diameters and wall thicknesses a method of quantifying their effects within the equations would be preferable. However, that would require significantly more FE data points than was available for this study. From the analyses undertaken, the equations are limited to the following:

Pipe diameter	:	up to 1270mm (50”)
Wall thickness	:	9.5mm to 19.1mm (0.37” to 0.75”)
D/t ratio	:	40 to 100
Corrosion length	:	26mm (1”) up to 1000mm (40”) (13<ACL≤500mm, 0.5<ACL≤20”)
Corrosion width	:	26mm (1”) up to 1000mm (40”) (13<CCL≤500mm, 0.5<CCL≤20”)
Corrosion depth	:	not greater than 60% of the wall thickness (CD≤0.6)

6.2 Comparison of Strain Gauge and Finite Element Results

This section presents a comparison of the experimental and numerical SCFs and also presents the results of limited further work carried out to investigate the effects of wall thickness tolerances in seamless pipe.

6.2.1 Comparisons

The experimentally determined SCFs have been compared against the proposed equation described in Section 3.6. The experiments described in Section 4 used a radius equal to the nominal wall thickness, i.e. r/t=1, and so this is an appropriate comparison.

The calculated and experimental SCFs are shown in Table 29. It is apparent that the experimental values are consistently below the numerical predictions when the nominal wall thickness is used, with the discrepancy increasing as the defect becomes deeper. When the actual wall thickness local to the defect is used, the SCF varies slightly due to

the differences in CD. Although the equation provided consistently higher SCF results the values follow a similar trend to the experimentally derived SCFs.

The pipe used to obtain the experimental SCFs had a diameter, 323.9mm (12.75”), significantly removed from those used in the FE analyses. The discrepancies highlight the difficulties encountered in maintaining high levels of accuracy for different diameters and wall thicknesses. Extensive FE analyses over a wide range of diameters would be required to ascertain if it is possible to derive a general equation for all pipe sizes without introducing unwanted complexity.

It was speculated that one cause of the discrepancies between the experimental and numerical results was errors in the positioning of the gauge. The effects of averaging the strain over the active area of a strain gauge rather than taking point values were considered, as the grooves in the test vessel were relatively small. This study also considered the effect of the gauge being slightly offset circumferentially. The maximum difference, from the value at the centre point, was about 5.2% decrease in SCF and 6.6% decrease in strain, when averaged over the area of the strain gauge and offset by 1mm. Thus it was concluded that these errors are unlikely to account for all of the discrepancies.

6.2.2 Effects of pipe dimensional tolerances

Two-dimensional plane strain models were developed to investigate the effect of tolerances on wall thickness on the predicted SCFs. The models were based on Defect 3 of the test vessel, with a groove 5.2 mm (0.205”) deep and a groove radius of 8.5 mm (0.335”). The pipe outside diameter was fixed at 323.9 mm (12.75”).

Figure 38 shows stress contours from models of an offset bore. The bore diameter is 305.7 mm (12.03”), giving a basic wall thickness of 9.1 mm (0.36”). The pressure is calculated to give a hoop stress of 1.0 N/mm^2 (145 psi) based on these dimensions, and is the same in all three cases. In the top part of the figure, the bore is centrally located and the peak stress (equivalent to the SCF as the hoop stress is unity) at the bottom of the groove is 9.83 N/mm^2 (1,425 psi). When the bore is located eccentrically giving the maximum thickness at the groove position, the SCF falls to 7.80. Note that the change in wall thickness is only about 8%, but the SCF has reduced by 21%. In the bottom part of Figure 38 the bore is offset in the opposite direction, so that the corrosion groove is now located at the minimum thickness. The SCF now increases to 12.8, an increase of 31% compared with the value for a concentric bore.

This analysis shows that eccentricity of the bore may have a significant effect on the stresses at the corrosion feature, beyond that due solely to changes in the wall thickness or the remaining ligament under the defect. In the case analyzed above the basic wall thickness changed by about 8% and the ligament under the defect by 18%, but the SCF increased by 30%. To investigate this effect further, this pipe geometry was analyzed without the corrosion groove, simulating a plain pipe with an eccentric bore.

The results are shown in Figure 39. It is apparent that, even in the absence of a corrosion defect, it would be possible to obtain large local increases in stress if the pipe bore is offset by amounts allowable for seamless pipe in the basic API 5L specification [12].

The effect of varying the wall thickness of the pipe is investigated further in the results shown in Figure 40. In this case the bore is concentric with the outer diameter, but is varied to modify the wall thickness. The internal pressure loading was adjusted to maintain the nominal hoop stress at 1 N/mm^2 (145 psi) based on the outside diameter. The SCFs are shown in the figure. In this case the relative changes in the SCF are approximately the same as the changes in the remaining ligament under the groove, provided the analysis is based on the actual pipe wall thickness rather than a nominal value.

Overall, it is considered that the analyses in this section have shown that typical manufacturing tolerances on wall thickness can have a significant effect on the estimated SCF, and hence on any calculated fatigue life. This effect is likely to be greatest for seamless pipe, where the bore may be eccentric relative to the outside diameter producing a varying wall thickness. Where the pipe is formed from rolled plate or strip there is likely to be less variation in wall thickness.

It is recommended that the application of the method proposed in this report should be based on the actual wall thickness of the pipe joint in which the corrosion defect is located. If this is not possible, the minimum wall thickness should be used.

6.3 General Remarks

6.3.1 Validity of results

The SCF equations, calibrated using the FE data, have been compared with the similar predictions by Kim and Son [8]. The Advantica results were calculated as described in Section 3.6 for comparison with the tabulated values in [8]. The Advantica results varied from those in [8]. There did not appear to be a consistent trend to the differences. However, there are differences in the geometries analyzed, as the present work has considered essentially rectangular defects with radiused corners and a constant reduced ligament over the main area of the defect. In contrast, the defects modeled in [8] were essentially ellipsoidal defects, so that the ligament was continuously varying. The work in [7] also did not include information regarding the pipe size used in the FE analysis, only giving the normalized defect sizes. As has been mentioned above, accuracy of SCF prediction could be reduced for pipes with geometry sufficiently removed from that used for this work, 914.4x12.7mm (36x0.5”). Thus, it is considered that the results in [8] are not at variance with those generated in the current work.

6.3.2 Effects of high SCFs

A concern is that when the elastic SCF is applied to a large hoop stress range, or the elastic SCF is itself large, the resultant local stress range may exceed SMYS. As the high stress area is contained, rather than the plasticity extending through the cross section, shakedown to elastic cycling should occur as long as the stress range does not exceed twice SMYS. If the stress range does exceed twice SMYS, cyclic plasticity will occur which may lead to a low cycle fatigue failure.

This effect is considered in Annex C of PD 5500 [14], where a plasticity correction factor is applied to stress ranges which exceed twice SMYS. The factor depends on the tensile and yield strengths of the material in addition to the stress range. As this correction is relatively complex, it is recommended that it is not used, and a simple criterion is adopted such that the local stress range in the corrosion defect calculated using the elastic SCF is limited to twice SMYS.

6.3.3 Effect of corrosion length in the pipe circumferential direction

The acceptance methods for static strength of corrosion defects such as RSTRENG [15][16] and the LPC-1 method [17] do not take account of the circumferential extent of the defect, as they require only the axial length and the defect depth. This work has shown that under cyclic loading the circumferential extent of the defect should be considered. The stress raising effect appears to be more onerous for deep, narrow axial defects, where there is effectively a long notch. As the circumferential size increases, the SCF drops to a plateau level.

Thus, if there is linepacking the restrictions on circumferential size may be more onerous than if the pipeline is only subject to static pressure loading. It is recommended that the results obtained in this work be further analyzed to determine screening criteria to highlight the areas where acceptable defect sizes are obtained.

6.3.4 Recommended Fatigue Assessment Code

The approach developed in this project is to combine the stress raising effect of the corrosion defect with a *S*–*N* curve for the material and the environment. As discussed in Section 2.1, the determination of fatigue lives in corrosive conditions is complex. If an appropriate *S*–*N* curve is available for the material and the environment, this should be used.

In most cases, it is unlikely that detailed guidance will be available. For ferritic steels, general guidance is available in BS 7608. This places different welded details into one of a set of *S*-*N* curves. These are presented in terms of the nominal stress range acting on a feature. For parent plate, the most appropriate class is B, described as “as rolled” plate or sections. This implies some surface roughness, which would be appropriate for

a corroded surface. The mean minus two standard deviations (i.e. approximately 1 in 40 failure probability) *S–N* relationship for Class B is:

$$S^4 N = 1.01 * 10^{15} \quad (8)$$

where, S = stress range (N/mm^2)

N = number of cycles to failure under constant amplitude cycling at stress range S

Equation (8) applies to a non-corrosive environment. In freely corroding seawater, Section 4.3.3 of BS 7608 recommends that the calculated life is reduced by a factor of 2 and there is no fatigue limit, so that all stress cycles are assumed to contribute to failure. The standard cautions that this correction may not apply to high strength materials with a yield strength above 400 N/mm^2 (58,000 psi), this would affect pipeline steels of Grade X65 or above. However, the *S-N* curve approach of BS 7608 has been used for quenched and tempered materials up to 700 N/mm^2 (101,500 psi) yield (e.g. RQT 701), and Section 1.1 of the standard states that the scope includes steels with a specified minimum yield strength up to this level. A review carried out for the UK Health and Safety Executive [18] suggests there is no significant difference in the corrosion fatigue behavior of steel structures and weldments up to 900 N/mm^2 (130,500 psi) yield strength when compared with that of lower strength structural steels. Thus it is considered that the BS 7608 approach and *S-N* curves are currently the best available for assessing the base fatigue life.

Further validation of the assessment method for high strength steel pipelines will be possible following completion of a full-scale operational trial of a 1220mm (48”) diameter, grade X100 pipeline section, which Advantica is undertaking on behalf of BP Exploration [19]. The test section comprises a number of simulated groove and patch metal loss defects, and is being subjected to pressure cycling over a two year period which will be equivalent to 40 years operation. The testing is due to be completed mid 2009.

BS 7608 also includes a “thickness correction”. This accounts for the fact that it has been shown by experiment and by theoretical fracture mechanics analyses that the fatigue life of a *welded* joint falls as the thickness increases. Hence a penalty is applied to the predicted life where the material thickness is greater than a reference thickness. For BS 7608 the reference thickness is 16 mm (0.63”), so that the thickness correction would be required for some heavier walled pipelines. A similar thickness correction is included in Annex C of the UK pressure vessel curve PD 5500 [14] but with a higher reference thickness of 22 mm (0.866”). Advantica’s opinion is that the correction is over-conservative for volumetric corrosion defects, which are relatively smooth compared with the sharp notch at the toe of a fusion weld. Hence the use of this correction is not recommended.

This approach to setting the fatigue life could be considered conservative compared with the situation in a real pipeline, as the defect is introduced at full depth, with the highest SCF, at the start of life and the pressure cycling is applied to this full size. In a real pipeline the corrosion defects would be small during the earlier parts of the lifetime, and so the SCF and the resulting fatigue damage would be less during the earlier part of the life. However, the approach is appropriate for the situation where a defect is discovered by inspection and is being assessed at its current size for future operation.

7 OUTLINE OF PROPOSED ASSESSMENT METHOD

The proposed assessment method for volumetric corrosion defects subject to cyclic pressure loading is as follows. (It is assumed that a pressure-loading spectrum of pressure ranges and the number of occurrences of each range is available either from historical SCADA data or from predictions of the future operational regime of the pipeline.)

1. Determine the diameter, actual wall thickness and grade of the joint containing the defect.
2. Determine the maximum depth, the axial length and the circumferential extent of the defect.
3. Using the SCF equations presented in Section 3.6 of this report, determine the elastic stress concentration factor. Care should be taken if the pipe dimensions deviate from those covered in this report.
4. Calculate the hoop stress range for the largest pressure range in the loading spectrum. Multiply this range by the SCF determined in step (3) to determine the maximum elastic stress range for the defect.
5. If the maximum elastic stress range for the defect calculated for step (4) exceeds twice the specification minimum yield strength for the pipe, shakedown to elastic cycling cannot be guaranteed and the defect is not acceptable. Remedial action is required, or the cyclic loading must be reduced by changing the operational parameters of the pipeline.
6. Carry out a conventional fatigue analysis using the hoop stress ranges calculated from the pressure spectrum multiplied by the elastic SCF from step (3). The recommended method is that given in BS 7608, using the Class B fatigue design curve corrected for a freely corroding environment, if appropriate.
7. Compare the calculated fatigue life with the required life of the pipeline to determine when repair is required.

8 CONCLUSIONS

The following main conclusions can be drawn from this work:

1. There is no available published method for assessing the life of volumetric corrosion defects in transmission pipelines under cyclic loading. An assessment method based on determining the stress raising effect of the corrosion defect combined with an *S-N* curve for parent plate material in a corrosive environment is proposed.
2. A wide range of defect geometries have been analyzed to determine elastic stress concentration factors which can be used to determine the effect of cyclic loading.
3. The assessment method derived has been validated for the following pipe and defect sizes:

Pipe diameter	:	up to 1270mm (50”)
Wall thickness	:	9.5mm to 19.1mm (0.37” to 0.75”)
D/t ratio	:	40 to 100
Corrosion length	:	from 26mm (1”) to 1000mm (40”) (13<ACL≤500mm, 0.5<ACL≤20”)
Corrosion width	:	from 26mm (1”) to 1000mm (40”) (13<CCL≤500mm, 0.5<CCL≤20”)
Corrosion depth	:	not greater than 60% of the wall thickness (CD≤0.6)

4. The proposed approach has been validated by a small set of full-scale fatigue tests. The experimental results were generally consistent with the predictions, but with longer fatigue lives.

9 RECOMMENDATIONS

1. The range of applicability of the assessment method should be investigated by considering the variation of SCF with pipe geometry.
2. Review of the experimental data from the X100 operational trial.

10 REFERENCES

[1] API. Recommended practice for planning, designing and constructing fixed offshore platforms - working stress design API RP 2A-WSD 21st Edition. Washington: American Petroleum Institute; 2000.

[2] BSI. Code of practice for fatigue design and assessment of steel structures BS 7608 Incorporating amendment No.1. London: British Standards Institution; 1993.

[3] API/ASME. Fitness for Service API 579-1/ASME FFS-1 (API 579 Second Edition). Washington: American Petroleum Institute and New York: American Society of Mechanical Engineers; June 5, 2007

[4] BSI. Guide to methods for assessing the acceptability of flaws in metallic structures BS 7910:2005 Incorporating amendment No.1, London: British Standards Institution; 2007.

[5] Vosikovsky O. Fatigue crack growth in an X65 line-pipe steel in sour crude oil. Corrosion NACE 1976;32:472-5.

[6] Vosikovsky O, Rivard A. Effect of hydrogen sulfide in crude oil on fatigue crack growth in a pipe line steel. Corrosion NACE 1982;38(1):19-22.

[7] ASME. Case N-597-2 Requirements for analytical evaluation of pipe wall thinning, Section XI, Division 1. New York: American Society of Mechanical Engineers; 2003.

[8] Kim Y-J, Son B-G. Finite element based stress concentration factors for pipes with local wall thinning. International Journal of Pressure Vessels and Piping 2004;81:897-906.

[9] ASME B31G. Manual for Determining the Remaining Strength of Corroded Pipelines A Supplement to ASME B31 Code for Pressure Piping, American Society of Mechanical Engineers, 1991.

[10] MSC/PATRAN 2001 r3, MacNeal-Schwendler Corporation.

[11] ABAQUS/Standard Version 6.4, Hibbitt, Karlsson & Sorensen Inc., 2003.

[12] ANSI/API Specification 5L, 'Specification for line pipe', 44th Edition, October 2007, Approved American National Standard/American Petroleum Institute, USA.

[13] BSI: Specification for flat products made of steels for pressure purposes. Part 3: Weldable fine grain steels, normalized. London: British Standards Institution, BS EN 10028-3, 2003.

[14] BSI: Unfired fusion welded pressure vessels. London: British Standards Institution; PD 5500, 2006.

[15] Kiefner JF and Veith PH: A Modified Criterion for Evaluating the Remaining Strength of Corroded Pipe, Final Report on PR-3-805 to the Pipeline Research Committee of the American Gas Association, Battelle, Ohio, 1989

[16] Vieth PH and Kiefner JF: RSTRENG2 User's Manual, Final report on PR-218-9205 to Corrosion Supervisory Committee, Pipeline Research Committee, American Gas Association, Kiefner & Associates, Inc., Ohio, 1993

[17] Fu B. and Batte AD: Advanced Methods for the Assessment of Corrosion in Linepipe. Summary Report OTO 97065, UK Health and Safety Executive.

[18] Healy J and Billingham J: A review of the corrosion fatigue behaviour of structural steels in the strength range 350-900 MPa and associated high strength weldments. HSE Offshore Technology Report OTH 97 532. London: HSE Books; 1997.

[19] Andrews RM: Operational Trial for X100 Pipelines – Technical Description for DoT OPS. Advantica, 6 February 2006.

CCL (mm)	ACL (mm)					
	13	**20**	**50**	**100**	**200**	**500**
13	1.77	1.89	2.19	2.32	2.35	2.37
20	1.66	1.76	2.03	2.19	2.25	2.30
50	1.63	1.70	1.86	1.97	2.02	2.11
100	1.60	1.67	1.79	1.84	1.85	1.90
200	1.60	1.66	1.77	1.81	1.79	1.80
500	1.66	1.70	1.82	1.86	1.82	1.80

Table 1. SCF for 914.4x12.7mm (36x0.5”) pipe with CD=0.2 (r/t=1).

CCL (mm)	ACL (mm)					
	13	**20**	**50**	**100**	**200**	**500**
13	2.16	2.59	3.68	4.39	4.70	4.90
20	2.04	2.32	3.22	3.95	4.32	4.58
50	2.04	2.22	2.69	3.13	3.35	3.64
100	2.17	2.24	2.59	2.85	2.86	2.99
200	2.21	2.21	2.58	2.84	2.83	2.80
500	2.11	2.21	2.57	2.83	2.84	2.83

Table 2. SCF for 914.4x12.7 mm (36x0.5”) pipe with CD=0.4 (r/t=1).

CCL (mm)	ACL (mm)					
	13	**20**	**50**	**100**	**200**	**500**
13	2.44	3.26	5.66	8.14	9.74	10.70
20	2.18	2.58	4.22	6.24	7.67	8.70
50	2.68	2.59	3.39	4.41	5.09	5.52
100	3.64	2.78	3.39	4.29	4.59	4.61
200	4.05	3.16	3.37	4.34	4.64	4.62
500	3.95	2.99	3.33	4.30	4.62	4.59

Table 3. SCF for 914.4x12.7 mm (36x0.5”) pipe with CD=0.6 (r/t=1).

CCL (mm)	ACL (mm)							
	13	**20**	**50**	**100**	**200**	**350**	**500**	**800**
13	2.74	4.08	7.94	13.90	19.80	21.90	23.30	25.4
20	2.31	2.79	5.11	8.87	12.70	13.70	14.60	
50	3.40	3.00	5.40	6.84	8.95	8.71	8.94	
100	5.43	3.62	5.34	6.34	8.69	9.10	8.77	
200	7.35	4.91	5.46	6.50	8.35	8.70	8.98	
500	8.43	5.13	5.42	6.69	8.55	8.77	8.70	

Table 4. SCF for 914.4x12.7 mm (36x0.5”) pipe with CD=0.8 (r/t=1).

CCL (mm)	ACL (mm)					
	13	**20**	**50**	**100**	**200**	**500**
13	2.70	4.17	7.98	13.90	19.80	23.30
20	2.23	2.94	5.15	8.90	12.70	14.60
50	2.13	2.68	5.40	6.76	9.10	8.98
100	2.17	2.72	4.96	6.51	9.23	9.12
200	2.22	2.80	4.95	6.56	8.97	9.75
500	2.29	2.87	4.95	6.66	9.01	8.96

Table 5. SCF for 914.4x12.7 mm (36x0.5”) pipe with CD=0.8 (r/t=1) and without ‘capped end force’.

CCL (mm)	ACL (mm)					
	13	**20**	**50**	**100**	**200**	**500**
13	1.83	1.96	2.25	2.39	2.44	2.49
20	1.82	1.91	2.18	2.34	2.40	2.45
50	1.78	1.84	2.00	2.11	2.16	2.25
100	1.74	1.80	1.91	1.95	1.96	2.02
200	1.73	1.79	1.90	1.93	1.91	1.91
500	1.73	1.79	1.90	1.93	1.91	1.91

Table 6. SCF for 914.4x12.7 mm (36x0.5”) pipe with CD=0.2 (r/t=0.5).

CCL (mm)	ACL (mm)					
	13	**20**	**50**	**100**	**200**	**500**
13	2.34	2.69	3.72	4.50	4.86	5.11
20	2.22	2.47	3.30	4.04	4.43	4.75
50	2.24	2.43	2.84	3.28	3.48	3.81
100	2.27	2.45	2.81	3.09	3.08	3.20
200	2.24	2.41	2.75	3.02	3.02	2.99
500	2.24	2.40	2.76	3.04	3.04	3.02

Table 7. SCF for 914.4x12.7 mm (36x0.5”) pipe with CD=0.4 (r/t=0.5).

Corrosion Defect Size ACL x CCL (mm)	Max. Principal Stress (N/mm^2)	Stresses (N/mm^2)		
		Axial	Circumferential	Radial
13x13	2.74	1.33	2.71	0.03
13x20	2.31	1.56	2.29	0.01
13x50	3.4	3.39	2.00	0.01
13x100	5.43	5.43	2.86	0.02
13x200	7.35	7.34	3.91	0.02
13x500	8.43	8.43	4.37	0.10
20x13	4.08	1.26	4.08	0.00
20x20	2.79	1.21	2.79	0.02
20x50	3	HMPS occurs at the middle of corrosion corner		
20x100	3.62	3.62	2.58	0.00
20x200	4.91	4.91	3.50	0.00
20x500	5.13	5.13	3.75	0.00
50x13	7.94	1.87	7.94	0.00
50x20	5.11	1.16	5.11	0.00
50x50	5.4	3.36	5.40	0.00
50x100	5.34	0.93	5.34	-0.02
50x200	5.46	1.18	5.46	-0.02
50x500	5.42	1.13	5.42	-0.02
100x13	13.9	3.53	13.87	0.00
100x20	8.87	2.07	8.86	0.08
100x50	6.84	1.95	6.84	0.00
100x100	6.34	1.85	6.34	0.03
100x200	6.5	2.06	6.49	0.06
100x500	6.69	1.95	6.68	0.09
200x13	19.8	5.88	19.82	-0.01
200x20	12.7	3.78	12.69	0.11
200x50	8.95	2.85	8.94	0.07
200x100	8.69	2.96	8.67	0.07
200x200	8.35	2.94	8.34	0.08
200x500	8.55	2.81	8.54	0.11
500x13	23.3	7.42	23.34	-0.01
500x20	14.6	4.89	14.63	0.12
500x50	8.94	3.08	8.92	0.07
500x100	8.77	3.21	8.76	0.08
500x200	8.98	3.30	8.97	0.09
500x500	8.7	2.92	8.68	0.10

Table 8. Axial, circumferential and radial stress at locations of HMPS for 914.4x12.7 mm (36x0.5”) pipe with CD=0.8 (r/t=1).

Corrosion Defect Size ACL x CCL (mm)	Max. Principal Stress (N/mm^2)	Stresses (N/mm^2)		
		Axial	Circumferential	Radial
13x13	1.77	0.87	1.76	0.04
13x20	1.66	0.89	1.65	0.04
13x50	1.63	0.93	1.62	0.04
13x100	1.60	1.01	1.58	0.05
13x200	1.60	1.01	1.57	0.06
13x500	1.66	0.92	1.65	0.03
20x13	1.89	0.88	1.88	0.04
20x20	1.76	0.89	1.75	0.04
20x50	1.70	0.92	1.69	0.04
20x100	1.67	0.92	1.66	0.04
20x200	1.66	0.91	1.65	0.03
20x500	1.70	0.91	1.69	0.03

Table 9. Axial, circumferential and radial stress at locations of HMPS for 914.4x12.7 mm (36x0.5”) pipe with CD=0.2 (r/t=1).

Corrosion Defect Size ACL x CCL (mm)	Max. Principal Stress (N/mm^2)	Stresses (N/mm^2)		
		Axial	Circumferential	Radial
13x13	2.16	1.14	2.15	0.04
13x20	2.04	1.22	2.02	0.05
13x50	2.04	1.51	1.98	0.04
13x100	2.17	2.16	1.70	0.01
13x200	2.21	2.20	1.73	0.01
13x500	2.11	2.10	1.70	0.01
20x13	2.59	1.17	2.58	0.03
20x20	2.32	1.19	2.30	0.04
20x50	2.22	1.40	2.10	0.07
20x100	2.24	1.43	2.11	0.07
20x200	2.21	1.39	2.09	0.07
20x500	2.21	1.38	2.09	0.07

Table 10. Axial, circumferential and radial stress at locations of HMPS for 914.4x12.7 mm (36x0.5”) pipe with CD=0.4 (r/t=1).

CD	CCL (mm)	ACL (mm)					
		13	**20**	**50**	**100**	**200**	**500**
0.2	**13**	3.39	3.70	2.74	3.02	3.83	5.06
	20	9.64	8.52	7.39	6.85	6.67	6.52
	50	9.20	8.24	7.53	7.11	6.93	6.64
	100	8.75	7.78	6.70	5.98	5.95	6.32
	200	8.12	7.83	7.34	6.63	6.70	6.11
	500	4.22	5.29	4.40	3.76	4.95	6.11
0.4	**13**	8.33	3.86	1.09	2.51	3.40	4.29
	20	8.82	6.47	2.48	2.28	2.55	3.71
	50	9.80	9.46	5.58	4.79	3.88	4.67
	100	4.61	9.38	8.49	8.42	7.69	7.02
	200	1.36	9.05	6.59	6.34	6.71	6.79
	500	6.16	8.60	7.39	7.42	7.04	6.71

Table 11. Percentage increase in SCF as transition radius decreases from r/t=1.0 to r/t=0.5.

Diameter (mm)	CCL (mm)	ACL (mm)	CD	SCF t=9.5mm	SCF t=12.7mm	SCF t=15.9mm	SCF t=19.1mm
914.4	50	100	0.4	3.08	3.13	3.10	3.13
914.4	200	100	0.4	2.87	2.84	2.78	2.77
914.4	20	50	0.6	4.18	4.22	4.34	4.50
914.4	20	100	0.6	6.05	6.24	6.49	6.73
914.4	50	100	0.6	4.54	4.41	4.36	4.28
914.4	200	100	0.6	4.48	4.34	4.15	4.02

Table 12 SCFs for differing wall thicknesses (t) for 914.4mm (36”) diameter pipe

CD	CCL (mm)	ACL (mm)					
		13	**20**	**50**	**100**	**200**	**500**
0.2	**13**	1.70	1.84	2.12	2.22	2.26	2.30
	20	1.65	1.76	2.01	2.13	2.18	2.24
	50	1.64	1.71	1.85	1.90	1.94	2.02
	100	1.62	1.69	1.79	1.79	1.79	1.82
	200	1.60	1.67	1.78	1.78	1.78	1.77
	500	1.63	1.69	1.81	1.82	1.81	1.84
0.4	**13**	2.2	2.66	3.76	4.33	4.55	4.74
	20	2.07	2.38	3.27	3.83	4.07	4.34
0.6	**13**	2.52	3.4	6.01	8.16	9.1	9.97
	20	2.27	2.74	4.59	6.3	7.06	7.9
0.8	**13**	2.93	4.37	8.91	14.9	18.2	20.5
	20	2.75	3.03	6.12	9.88	11.7	12.8

Table 13. SCFs for 508x12.7 mm (20x0.5”) pipe with r/t=1.

CD	CCL (mm)	ACL (mm)					
		13	20	50	100	200	500
0.2	13	1.71	1.85	2.14	2.29	2.33	2.36
	20	1.68	1.78	2.05	2.23	2.29	2.33
0.4	13	2.16	2.58	3.67	4.42	4.80	4.99
	20	2.03	2.30	3.18	3.97	4.43	4.68
0.6	13	2.41	3.20	5.50	8.02	9.99	11.00
	20	2.15	2.52	4.05	6.11	7.92	9.07
0.8	13	2.76	3.98	7.51	13.10	20.20	24.70
	20	2.59	2.79	4.70	8.35	12.90	15.40

Table 14. SCFs for 1270x12.7 mm (50x0.5”) pipe with r/t=1.

CD	CCL (mm)	ACL (mm)					
		13	20	50	100	200	500
0.2	13	-3.95	-2.65	-3.20	-4.31	-3.83	-2.95
	20	-0.60	0.00	-0.99	-2.74	-3.11	-2.61
0.4	13	1.85	2.70	2.17	-1.37	-3.19	-3.27
	20	1.47	2.59	1.55	-3.04	-5.79	-5.24
0.6	13	3.28	4.29	6.18	0.25	-6.57	-6.82
	20	4.13	6.20	8.77	0.96	-7.95	-9.20
0.8	13	6.93	7.11	12.22	7.19	-8.08	-12.02
	20	19.05	8.60	19.77	11.39	-7.87	-12.33

Table 15. SCF percentage increase for 508x12.7 mm (20x0.5”) pipe over 914.4x12.7 mm (36x0.5”) pipe for the same corrosion defect.

CD (%)	CCL (mm)	ACL (mm)					
		13	**20**	**50**	**100**	**200**	**500**
20	**13**	-3.39	-2.12	-2.28	-1.29	-0.85	-0.42
	20	1.20	1.14	0.99	1.83	1.78	1.30
40	**13**	0.00	-0.39	-0.27	0.68	2.13	1.84
	20	-0.49	-0.86	-1.24	0.51	2.55	2.18
60	**13**	-1.23	-1.84	-2.83	-1.47	2.57	2.80
	20	-1.38	-2.33	-4.03	-2.08	3.26	4.25
80	**13**	0.73	-2.45	-5.42	-5.76	2.02	6.01
	20	12.12	0.00	-8.02	-5.86	1.57	5.48

Table 16. SCF percentage increase for 1270x12.7 mm (50x0.5”) pipe over 914.4x12.7 mm (36x0.5”) pipe for the same corrosion defect.

Defect	Type	Defect dimensions			
		CD*	***L*** **(mm)**	***r*** **(mm)**	***W*** **(mm)**
Pipe 1: 323.9mm x 8.4mm, seamless pipe, grade X52.					
D1	Groove	0.22 (0.2)	399.0 (400)	8.5 (8.5)	11.2 (10.1)
D2	Groove	0.40 (0.4)	404.5 (400)	8.5 (8.5)	13.9 (13.5)
D3	Groove	0.57 (0.6)	405.8 (400)	8.5 (8.5)	16.2 (15.5)
D4	Patch	0.68 (0.6)	398.5 (400)	8.5 (8.5)	137.8 (140)
Pipe 2: 323.9mm x 15.9mm, HFI pipe, grade X60.					
D1	Groove	0.19 (0.2)	399.0 (400)	12.7 (16.0)	16.7 (19.1)
D2	Groove	0.39 (0.4)	399.0 (400)	12.7 (16.0)	21.8 (25.5)
D3	Groove	0.59 (0.6)	400.0 (400)	12.7 (16.0)	24.0 (29.3)
D4	Patch	0.59 (0.6)	399.0 (400)	12.7 (16.0)	136.0 (140)

Notes: ***CD**** is the ratio of maximum measured defect depth measured (see Appendix B) to pipe wall thickness, ***d*** is defect depth, ***L*** and ***W*** are defect length and width in the pipe axial and circumferential directions respectively (measured along the outer surface of the pipe) and ***r*** is the blend radius.

Table 17. Comparison of target and actual defect dimensions.

Defect	Pressure limits		Pressure range	Stress range
	P_{min} bar	**P_{max} bar**	**ΔP bar**	**$\Delta\sigma$ N/mm²**
D1 – Groove (CD_{max}=0.22)	8.5	94.3	85.8	336
D2 – Groove (CD_{max}=0.40)	8.5	52.2	43.7	318
D3 – Groove (CD_{max}=0.57)	8.5	39.9	31.4	283
D4 – Patch (CD_{max}=0.68)	8.5	62.9	54.4	319

Note: The vessel was initially pressure cycled between P_{min} and P_{max} limits of 10.0 and 33.3 Barg for 98,951 cycles before the limits were adjusted to those shown above. The stress range is calculated from the strain gauge data.

Table 18. Vessel 1 (pipe 1): Minimum and maximum pressures in the pressure cycle for each defect.

Defect	Pressure limits		Pressure range	Stress range
	P_{min} bar	P_{max} bar	ΔP bar	$\Delta\sigma$ N/mm²
D1 – Groove (CD_{max}=0.19)	8.0	250.0	242.0	482
D2 – Groove (CD_{max}=0.39)	8.0	200.0	192.0	709
D3 – Groove (CD_{max}=0.59)	8.0	136.0	128.0	981
D4 – Patch (CD_{max}=0.59)	8.0	136.0	128.0	388

Note: The vessel was initially pressure cycled between P_{min} and P_{max} limits of 8.0 and 60.0 Barg for 358,614 cycles before the limits were adjusted to those shown above. The stress range is calculated from the strain gauge data.

Table 19. Vessel 2 (pipe 2): Minimum and maximum pressures in the pressure cycle for each defect.

Defect	Number of cycles for a given pressure range (ΔP)				
	23.3bar	31.4bar	43.7bar	54.4bar	85.8bar
D1 – Groove (CD_{max}=0.22)	98,951	229,071	447,344	100,575	370,419
D2 – Groove (CD_{max}=0.40)	98,951	229,071	447,344		
D3 – Groove (CD_{max}=0.57)	98,951	229,071			
D4 – Patch (CD_{max}=0.68)	98,951	229,071	447,344	100,575	

Table 20. Vessel 1 (pipe 1) results: Number of cycles of each pressure range for each defect.

Defect	Number of cycles for a given pressure range (ΔP)				
	52 bar	**58 bar**	**128 bar**	**192 bar**	**242 bar**
D1 – Groove (CD_{max}=0.19)	358,614	98,992	236,050	18,606	9,019
D2 – Groove (CD_{max}=0.39)	358,614	98,992	236,050	18,606	
D3 – Groove (CD_{max}=0.59)	358,614	98,992	5,231		
D4 – Patch (CD_{max}=0.59)	358,614	98,992	236,050		

Table 21. Vessel 2 (pipe 2) results: Number of cycles of each pressure range for each defect.

Defect	Experimental SCF	Minimum local wall, mm	Maximum local wall, mm	Location of maximum stress
Vessel 1 (pipe 1): 323.9mm x 8.4mm, seamless pipe, grade X52				
D1 – Groove	2.15	8.9	9.1	Centre
D2 – Groove	3.87	8.6	8.7	End
D3 – Groove	5.07	9.1	9.8	Centre
D4 – Patch	3.22	8.9	9.2	Centre of short (circumferential) side
Vessel 2 (pipe 2): 323.9mm x 15.9mm, HFI pipe, grade X60				
D1 – Groove	2.03	16.5	16.6	Centre
D2 – Groove	3.74	16.4	16.5	Centre
D3 – Groove	7.76	16.4	16.5	Centre
D4 – Patch	3.07	16.4	16.6	Centre

Table 22. Experimental SCF results based on nominal wall thickness.

Defect	Pressure Range (ΔP) (Bar)	Equivalent Cycles (N_{eq})
Vessel 1 (pipe 1): 323.9mm x 8.4mm, seamless pipe, grade X52		
D1 – Groove (CD_{max}=0.22)	85.8	421,423
D2 – Groove (CD_{max}=0.40)	43.7	516,402
D3 – Groove (CD_{max}=0.57)	31.4	259,071
D4 – Patch (CD_{max}=0.68)	54.4	315,614
Vessel 2 (pipe 2): 323.9mm x 15.9mm, HFI pipe, grade X60		
D1 – Groove (CD_{max}=0.19)	242	35,957
D2 – Groove (CD_{max}=0.39)	192	67,987
D3 – Groove (CD_{max}=0.59)	128	19,172
D4 – Patch (CD_{max}=0.59)	128	249,991

Table 23. Equivalent pressure cycles.

Defect	ΔP bar	N_{eq}	$N_{BS7608\ (Class\ B)}$	Comment
D1 – Groove (CD_{max}=0.22)	85.8	**421,423**	+1SD: 280,629 Mean: 184,516 -1SD: 121,320	No failure of defect
D2 – Groove (CD_{max}=0.40)	43.7	516,402	**+1SD**: 346,338 Mean: 227,720 -1SD: 149,727	N_{eq} >> Mean +1SD
D3 – Groove (CD_{max}=0.57)	31.4	259,071	+1SD: 552,957 **Mean:** 363,573 -1SD: 239,051	N_{eq} ≡ Mean – 1SD
D4 – Patch (CD_{max}=0.68)	54.4	315,614	**+1SD:** 345,157 Mean: 226,943 -1SD: 149,217	N_{eq} ≡ Mean +1SD

Notes: ΔP is the pressure range for the final stage of the fatigue test for the individual defect, and $\mathbf{N_{eq}}$ is the number of equivalent pressure cycles of the reference pressure range.

Table 24. Vessel 1 (pipe 1): Comparison of actual and predicted fatigue lives (experimentally determined SCFs).

Defect	ΔP bar	N_{eq}	$N_{BS7608\ (Class\ B)}$	Comment
D1 – Groove (CD_{max}=0.19)	242	**35,957**	+1SD: 65,912 Mean: 43,338 -1SD: 28,495	No failure of defect
D2 – Groove (CD_{max}=0.39)	192	67,987	**+1SD**: 14,092 Mean: 9,265 -1SD: 6,092	N_{eq} >> Mean +1SD
D3 – Groove (CD_{max}=0.59)	128	19,172	**+1SD:** 3,849 Mean: 2,531 -1SD: 1,664	N_{eq} >> Mean +1SD
D4 – Patch (CD_{max}=0.59)	128	249,991	**+1SD:** 157,130 Mean: 103,314 -1SD: 67,929	N_{eq} >> Mean +1SD

Notes: ΔP is the pressure range for the final stage of the fatigue test for the individual defect and $\mathbf{N_{eq}}$ is the number of equivalent pressure cycles of the reference pressure range.

Table 25. Vessel 2 (pipe 2): Comparison of actual and predicted fatigue lives (experimentally determined SCFs).

Defect	ΔP bar	N_{eq}	$N_{BS7608\ (Class\ B)}$	Comment
D1 – Groove (CD_{max}=0.22)	85.8	**421,423**	+1SD: 14,480 Mean: 9,521 -1SD: 6,260	No failure of defect
D2 – Groove (CD_{max}=0.40)	43.7	516,402	**+1SD**: 10,874 Mean: 7,150 -1SD: 4,701	N_{eq} >> Mean +1SD
D3 – Groove (CD_{max}=0.57)	31.4	259,071	**+1SD:** 7,532 Mean: 4,953 -1SD: 3,256	N_{eq} >> Mean +1SD
D4 – Patch (CD_{max}=0.68)	54.4	315,614	**+1SD:** 15,795 Mean: 10,385 -1SD: 6,828	N_{eq} >> Mean +1SD

Notes: ΔP is the pressure range for the final stage of the fatigue test for the individual defect and $\mathbf{N_{eq}}$ is the number of equivalent pressure cycles of the reference pressure range

Table 26. Vessel 1 (pipe 1): Comparison of actual and predicted fatigue lives (predicted SCFs).

Defect	ΔP bar	N_{eq}	$N_{BS7608\ (Class\ B)}$	Comment
D1 – Groove (CD_{max}=0.19)	242	**35,957**	+1SD: 16,661 Mean: 10,955 -1SD: 7,203	No failure of defect
D2 – Groove (CD_{max}=0.39)	192	67,987	**+1SD**: 2,314 Mean: 1,522 -1SD: 1,001	N_{eq} >> Mean +1SD
D3 – Groove (CD_{max}=0.59)	128	19,172	**+1SD:** 1,124 Mean: 739 -1SD: 486	N_{eq} >> Mean +1SD
D4 – Patch (CD_{max}=0.59)	128	249,991	**+1SD:** 13,883 Mean: 9,128 -1SD: 6,002	N_{eq} >> Mean +1SD

Notes: **ΔP** is the pressure range for the final stage of the fatigue test for the individual defect, and $\mathbf{N_{eq}}$ is the number of equivalent pressure cycles of the reference pressure range.

Table 27. Vessel 2 (pipe 2): Comparison of actual and predicted fatigue lives (predicted SCFs).

Diameter (mm)	CCL mm	ACL mm	CD	SCF t=9.5mm	SCF t=15.9mm	SCF t=19.1mm
914.4	50	100	0.4	-8.21	-5.70	-3.92
914.4	200	100	0.4	-6.32	-8.75	-8.71
914.4	20	50	0.6	-31.78	-19.63	-12.41
914.4	20	100	0.6	-16.49	-3.72	1.96
914.4	50	100	0.6	-16.15	-18.04	-19.00
914.4	200	100	0.6	-2.02	-8.61	-11.46

Table 28. Percentage errors in calculated SCFs for varying wall thickness (t) for the 914.4mm (36”) diameter pipe

Defect	Experimental SCF	Predicted SCFs		
		Nominal wall	Minimum local wall	Maximum local wall
D1 – Groove	2.15	4.87	4.51	4.38
D2 – Groove	3.87	9.57	9.19	9.02
D3 – Groove	5.07	17.18	14.84	12.99
D4 – Patch	3.22	7.61	6.96	6.62

Table 29. Experimental and calculated numerical SCFs for varying wall thicknesses (Vessel 1, pipe 1).

.

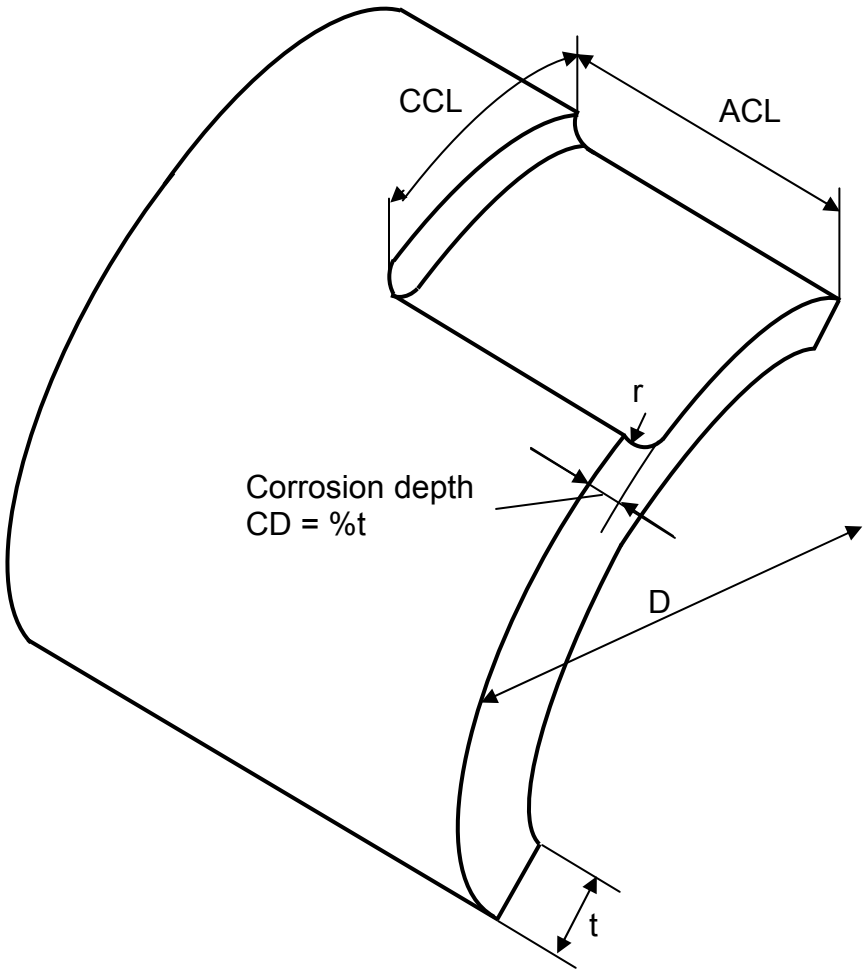

Figure 1. Geometrical Definition of Corroded Pipe

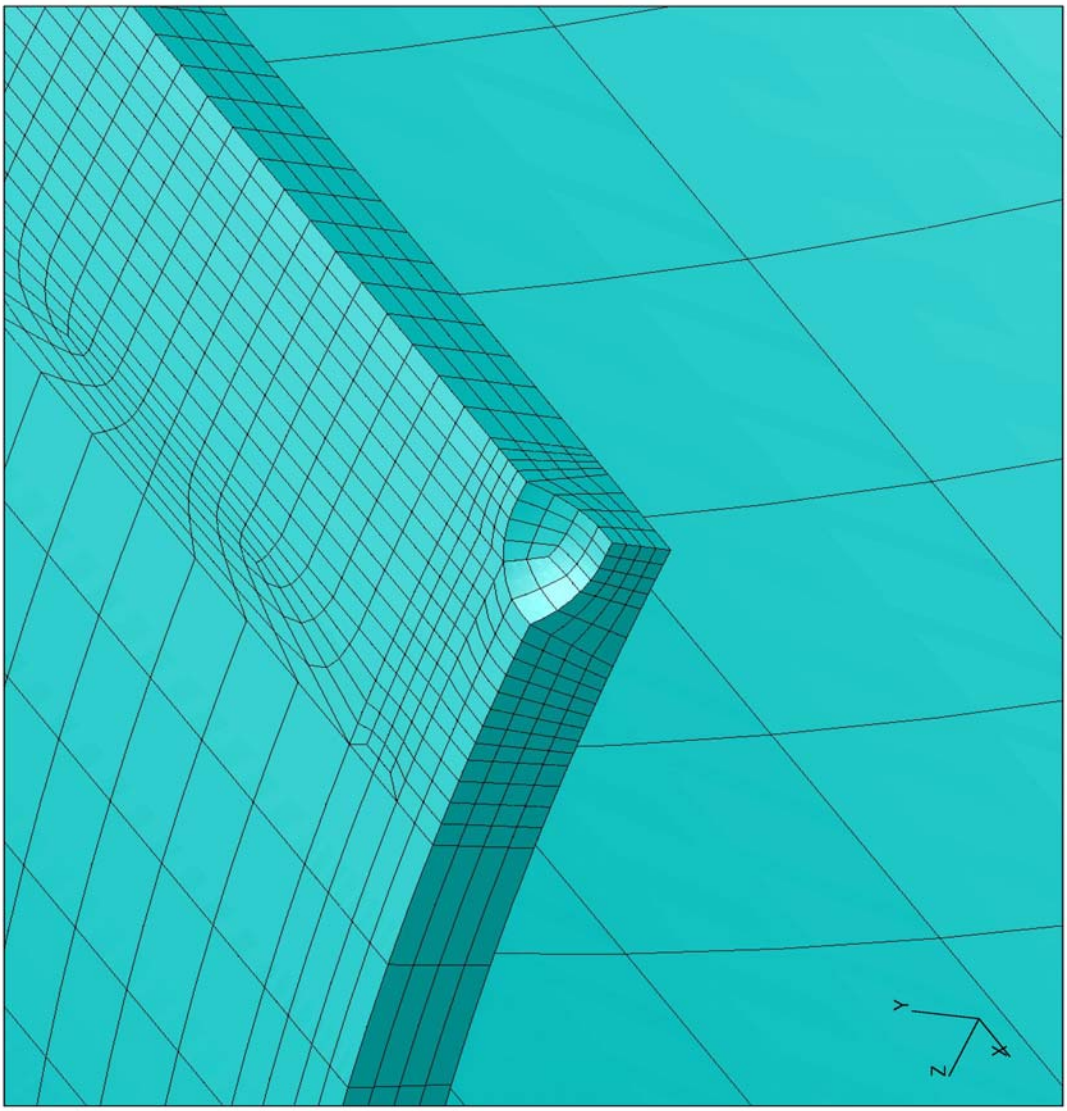

Figure 2. Finite element mesh of 914.4x12.7 mm (36x0.5”) pipe with a pit defect (size: 13x13 mm [0.5x0.5”]), CD=0.4, r/t=1.

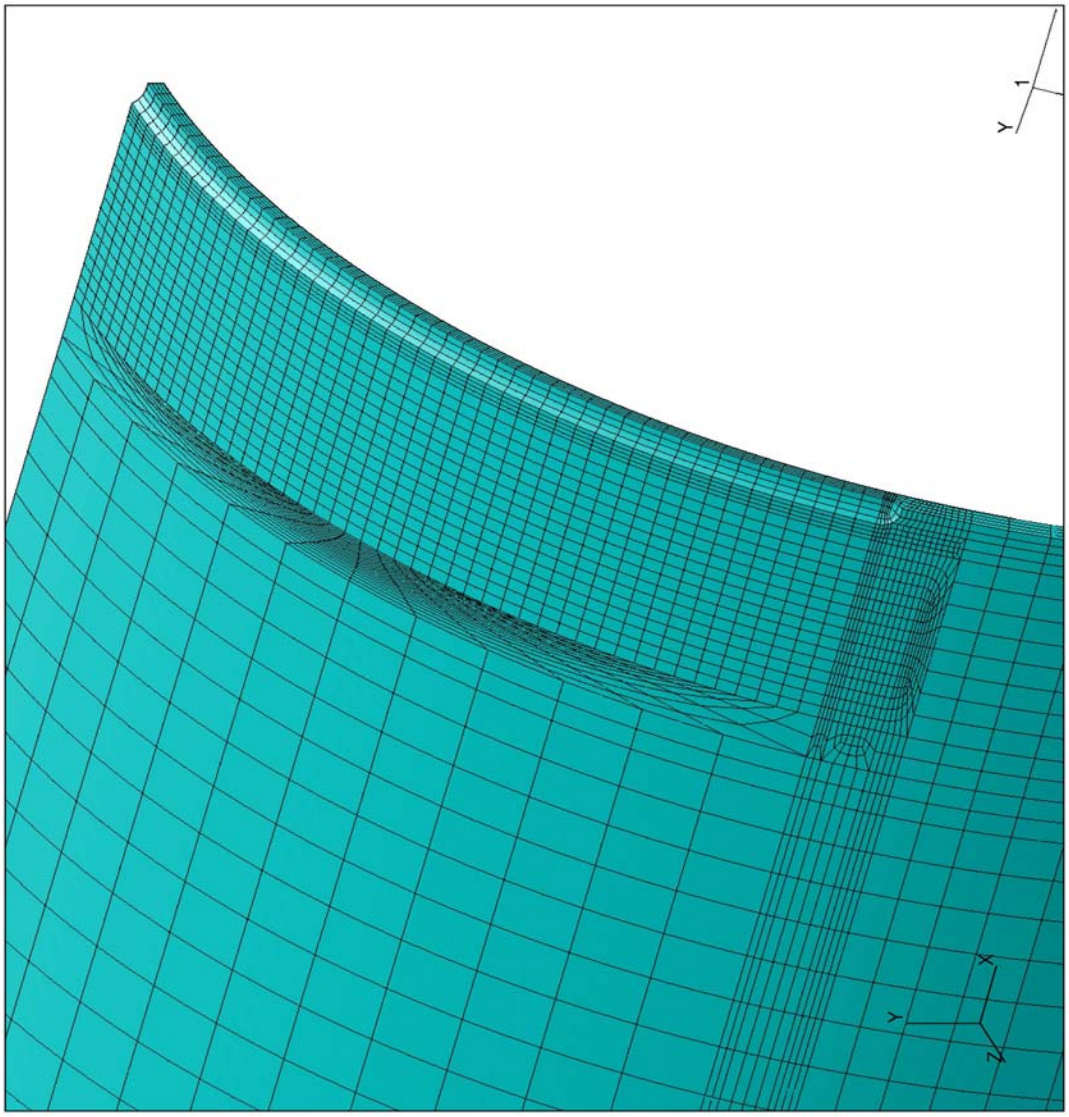

Figure 3. Finite element mesh of 914.4x12.7 mm (36x0.5”) pipe with a circumferential groove defect (size: 13x500 mm [0.5x20”]), CD=0.4, r/t=1.

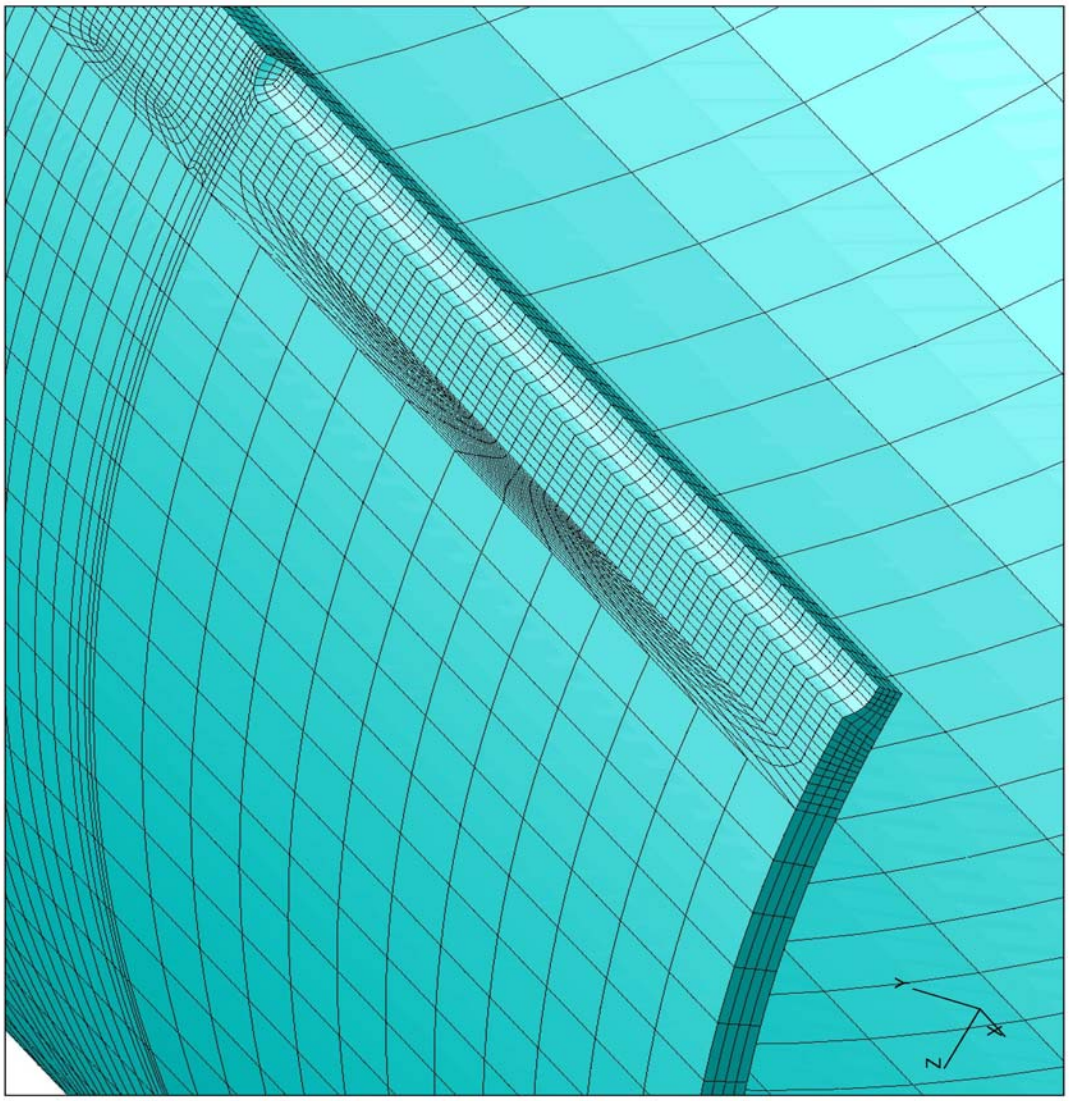

Figure 4. Finite element mesh of 914.4x12.7 mm (36x0.5”) pipe with an axial groove defect (size: 500x13 mm [20x0.5”]), CD=0.4, r/t=1.

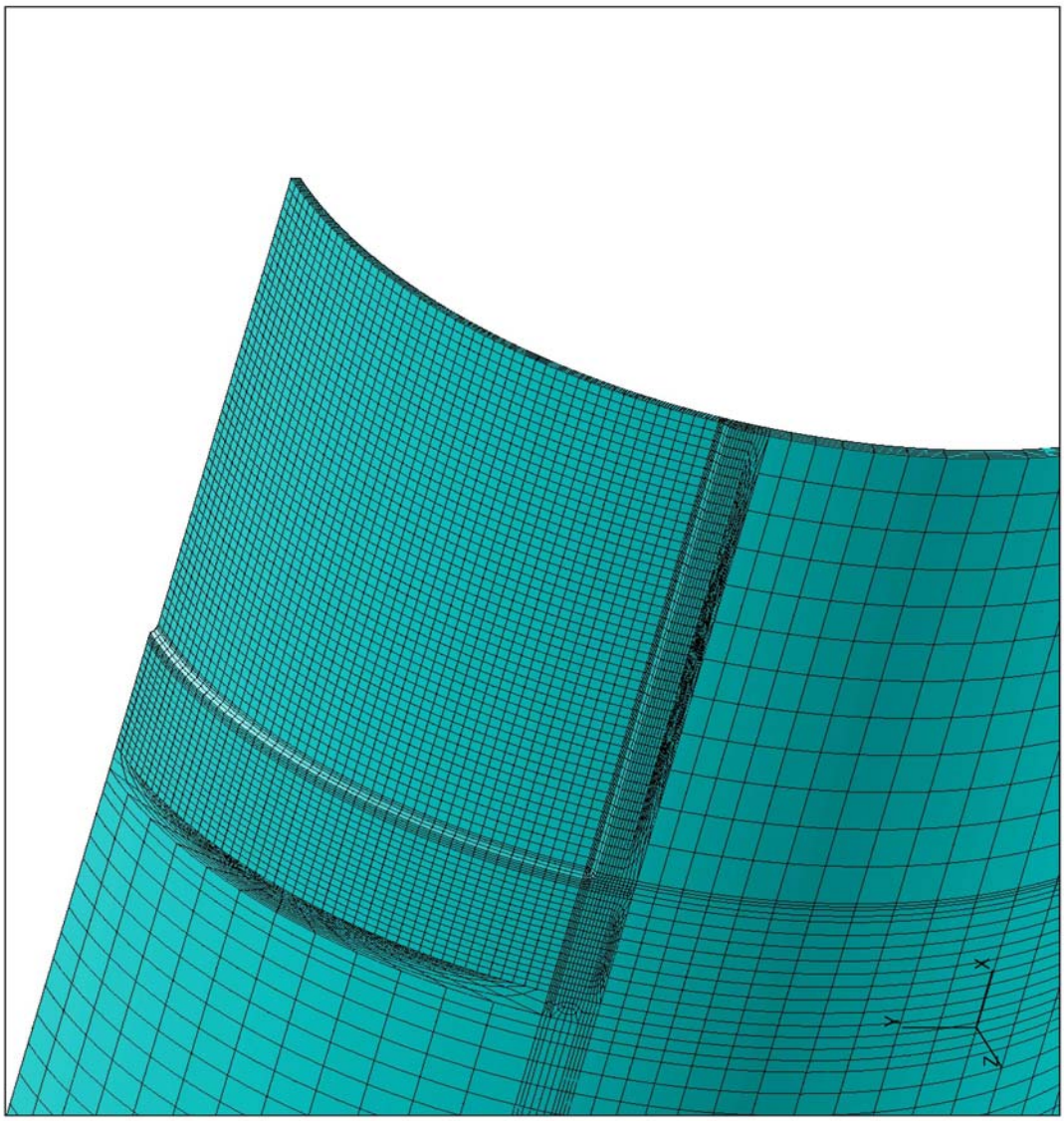

Figure 5. Finite element mesh of 914.4x12.7 mm (36x0.5”) pipe with a patch defect (size: 500x500 mm [20x20”]), CD=0.4, r/t=1.

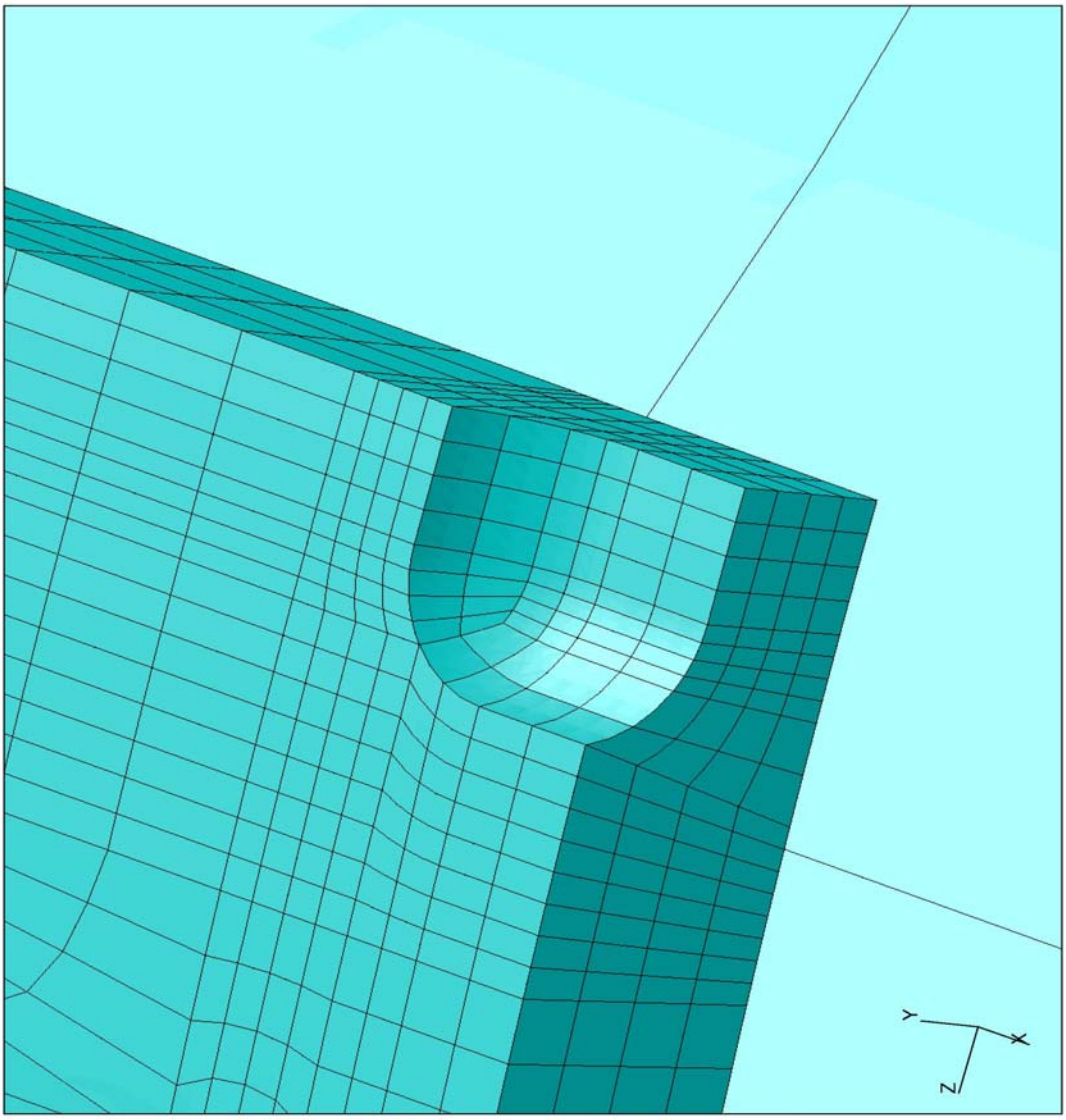

Figure 6. Finite element mesh of 914.4x12.7 mm (36x0.5”) pipe with a pit defect (size: 13x13 mm [0.5x0.5”]), CD=0.4, r/t=0.5.

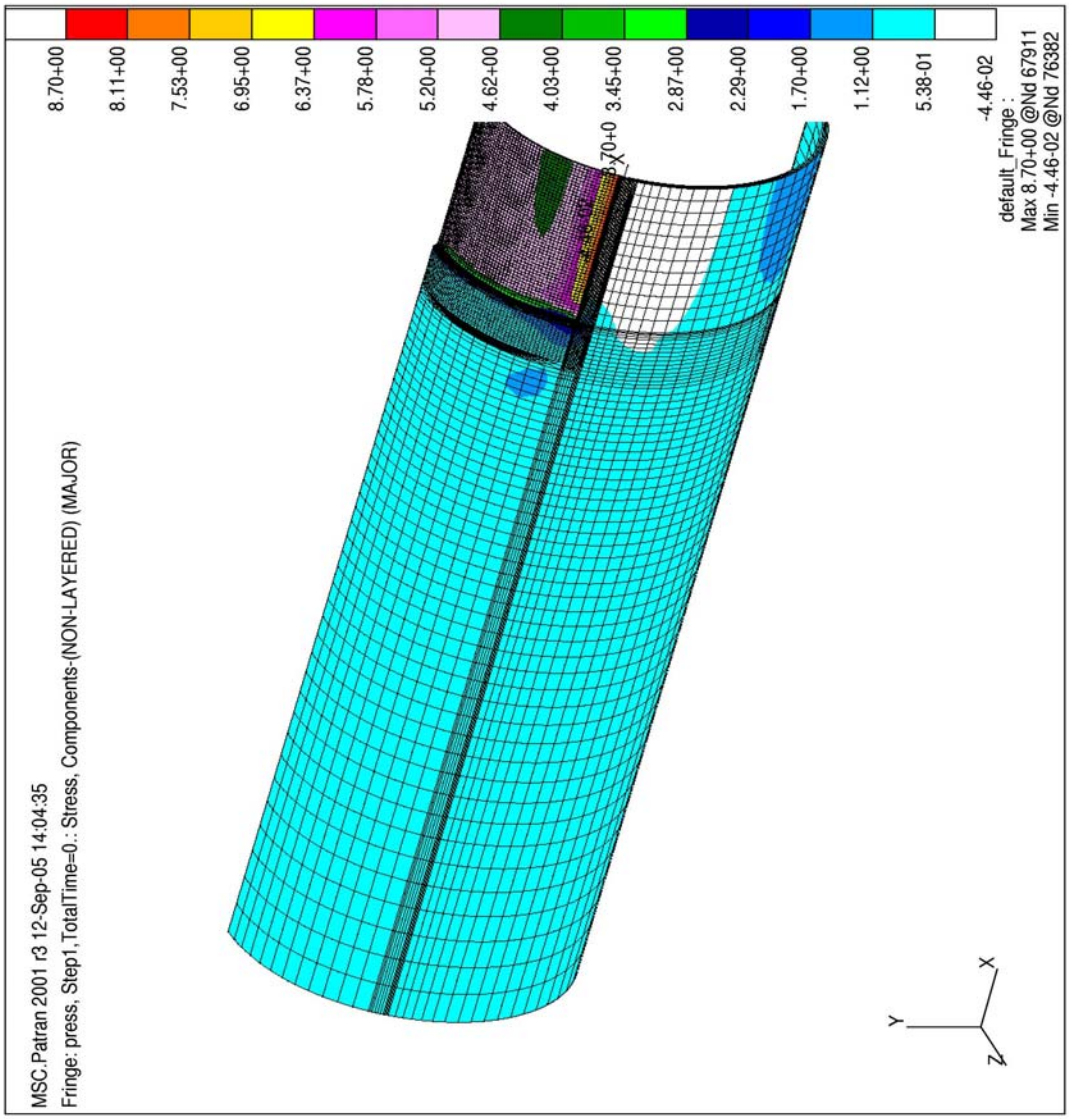

Figure 7. Maximum Principal Stress of 914.4x12.7 mm (36x0.5”) pipe with a patch defect (size: 500x500 mm [20x20”]), CD=0.8.

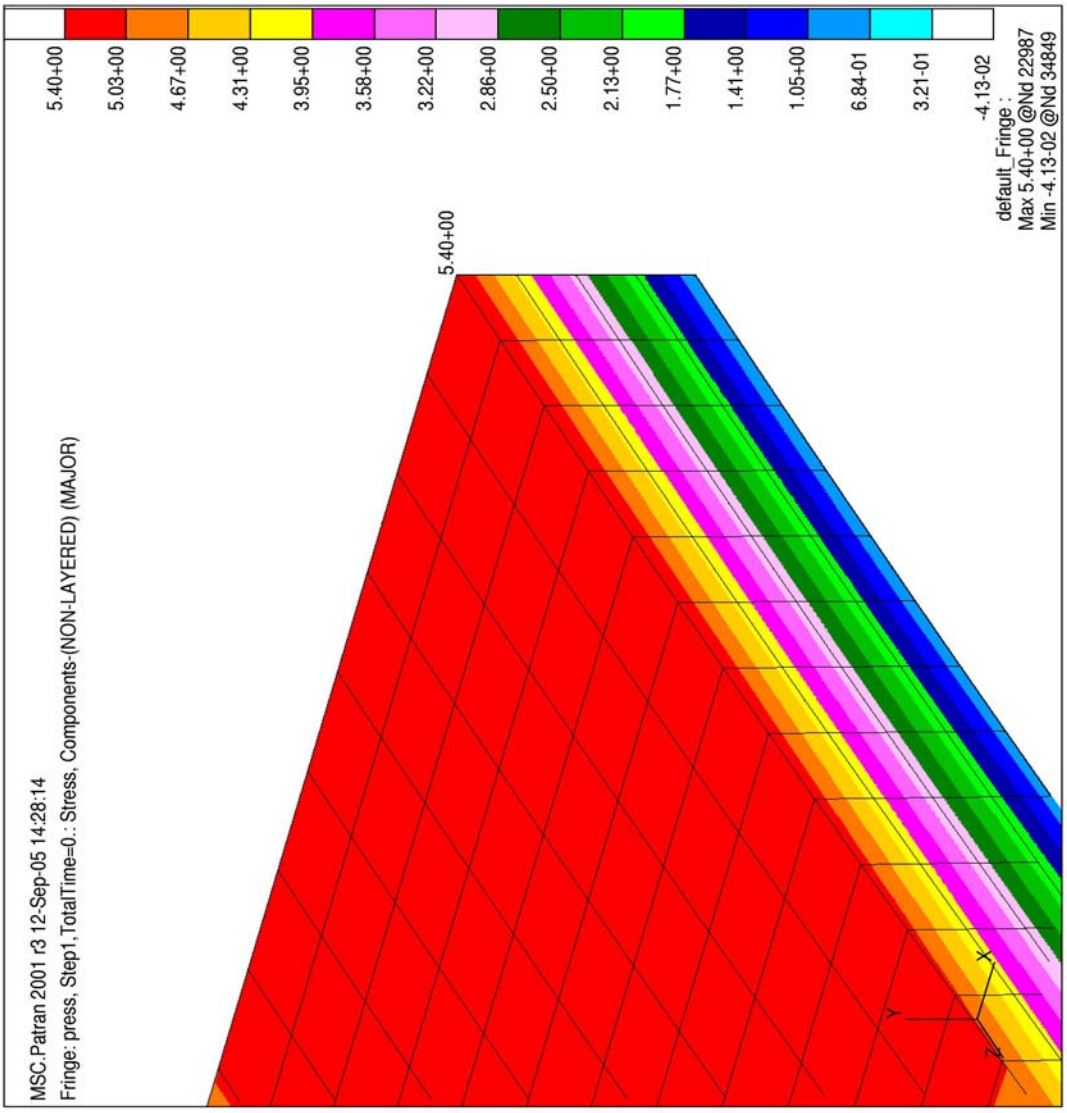

Figure 8. Local view of Maximum Principal Stress of 914.4x12.7 mm (36x0.5”) pipe with a patch defect (size: 50x50 mm [2x2”]), CD=0.8.

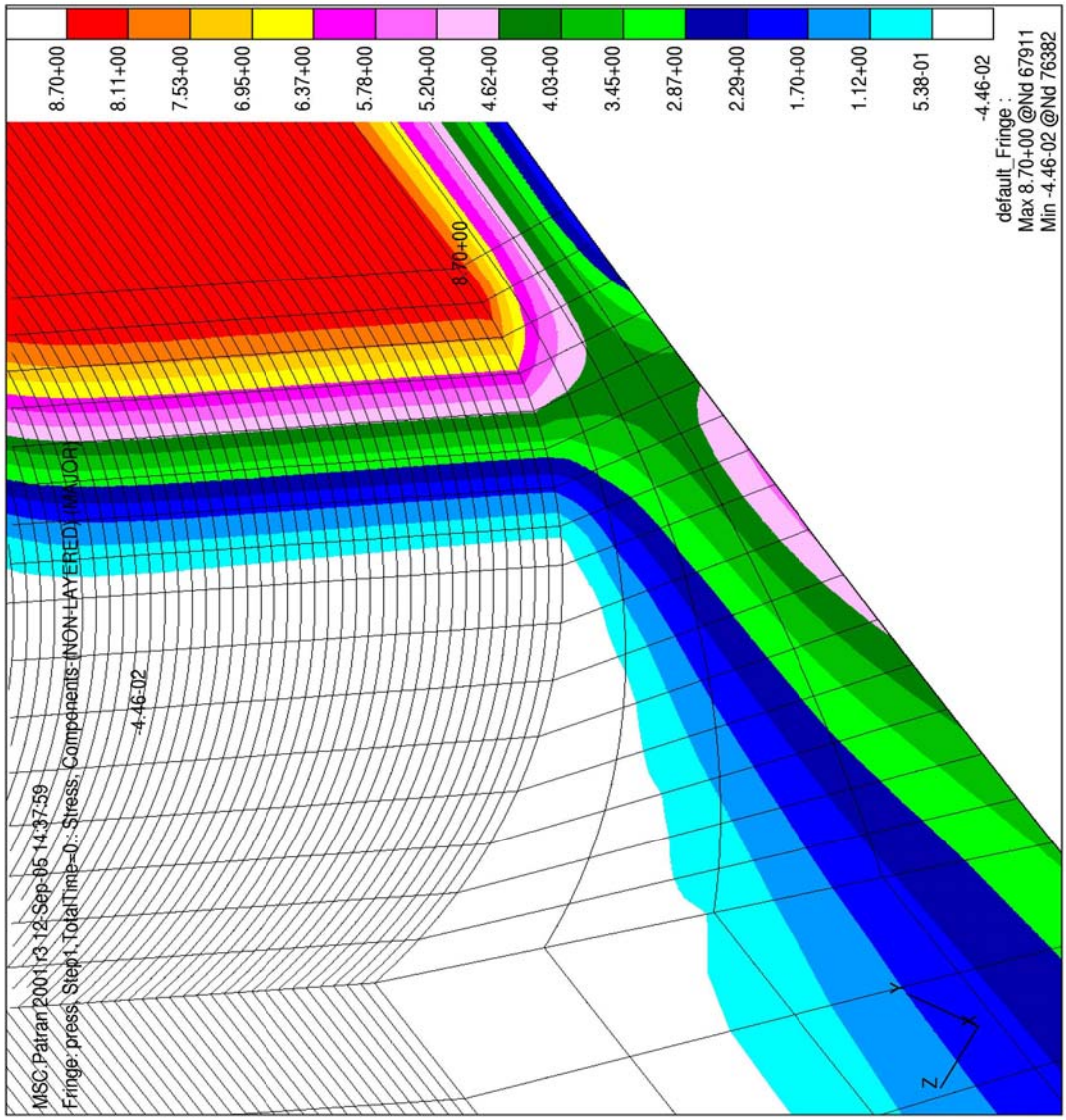

Figure 9. Local view of Maximum Principal Stress of 914.4x12.7 mm (36x0.5”) pipe with a patch defect (size: 500x500 mm [20x20”]), CD=0.8.

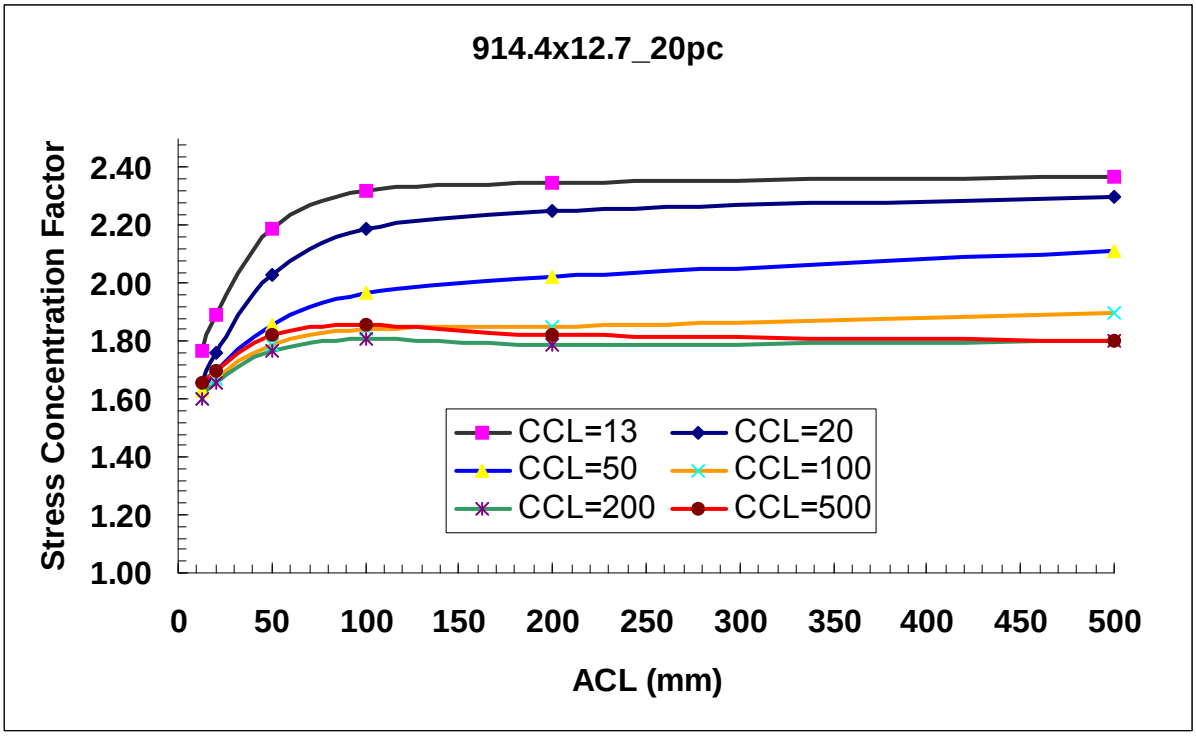

a): SCF with variation of axial corrosion length

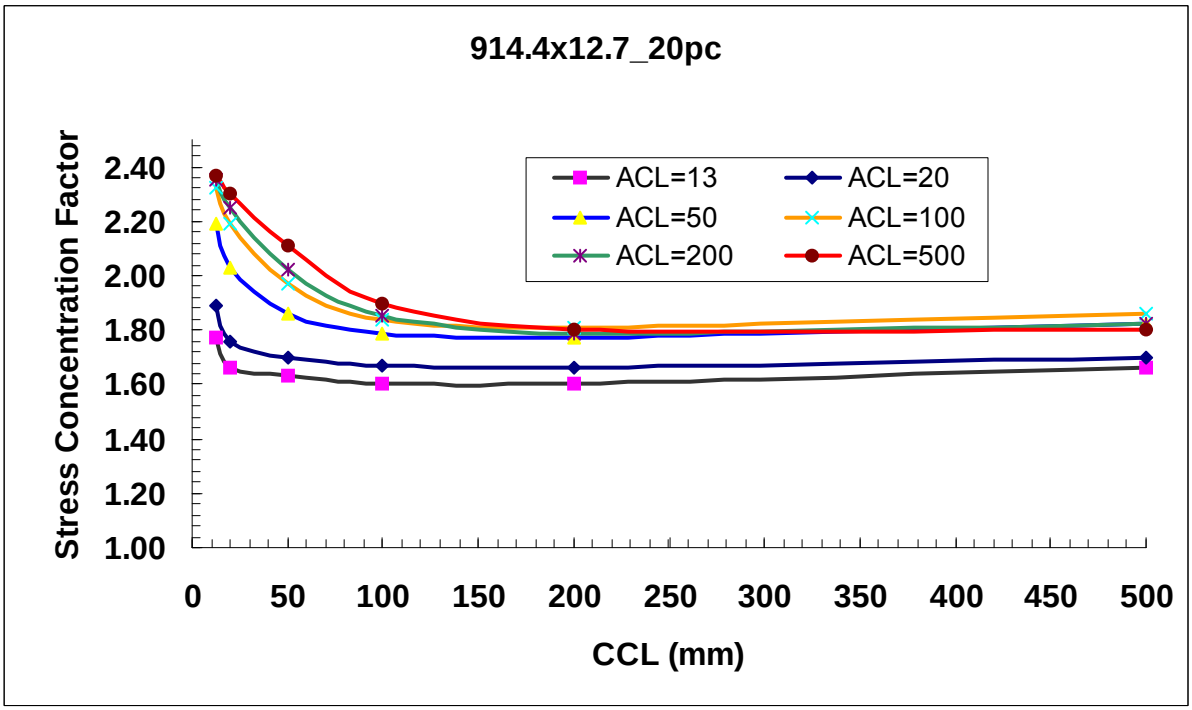

b): SCF with variation of circumferential corrosion length

Figure 10. SCFs for 914.4x12.7 mm (36x0.5”) pipe, CD=0.2, r/t=1.

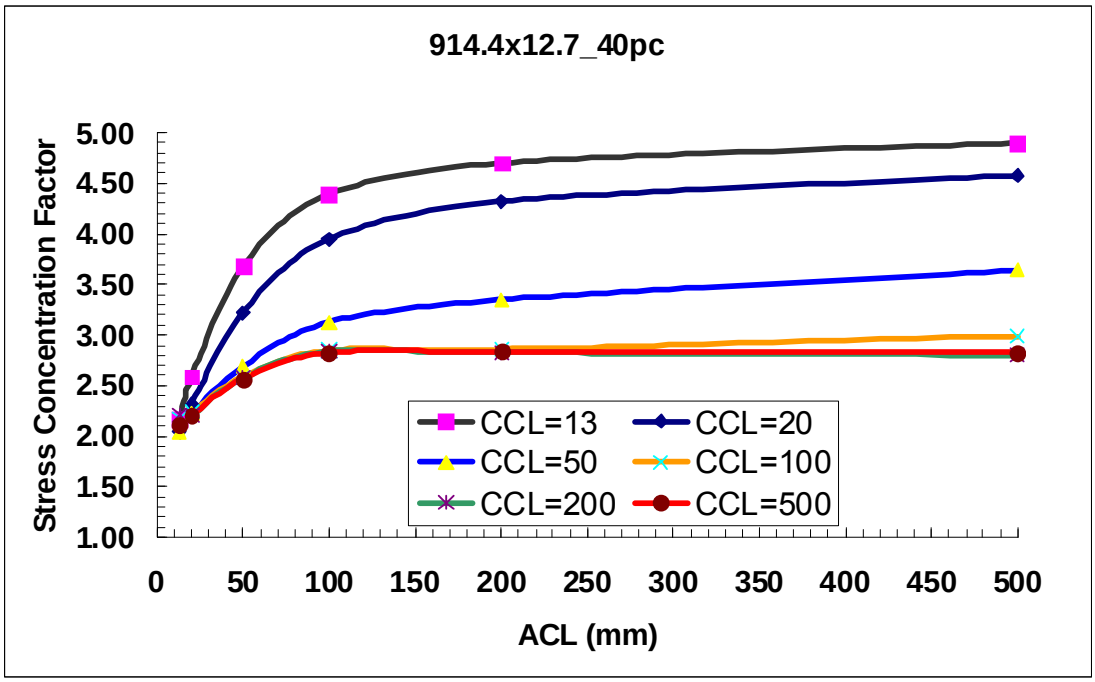

a): SCF with variation of axial corrosion length

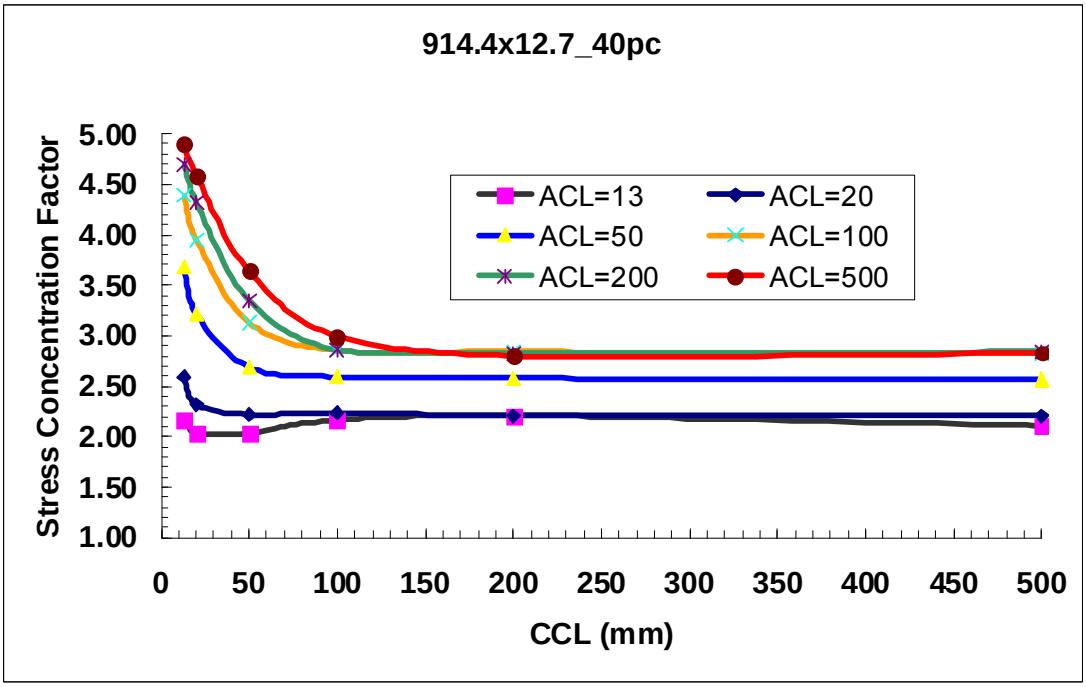

b): SCF with variation of circumferential corrosion length

Figure 11. SCFs for 914.4x12.7 mm (36x0.5”) pipe, CD=0.4, r/t=1.

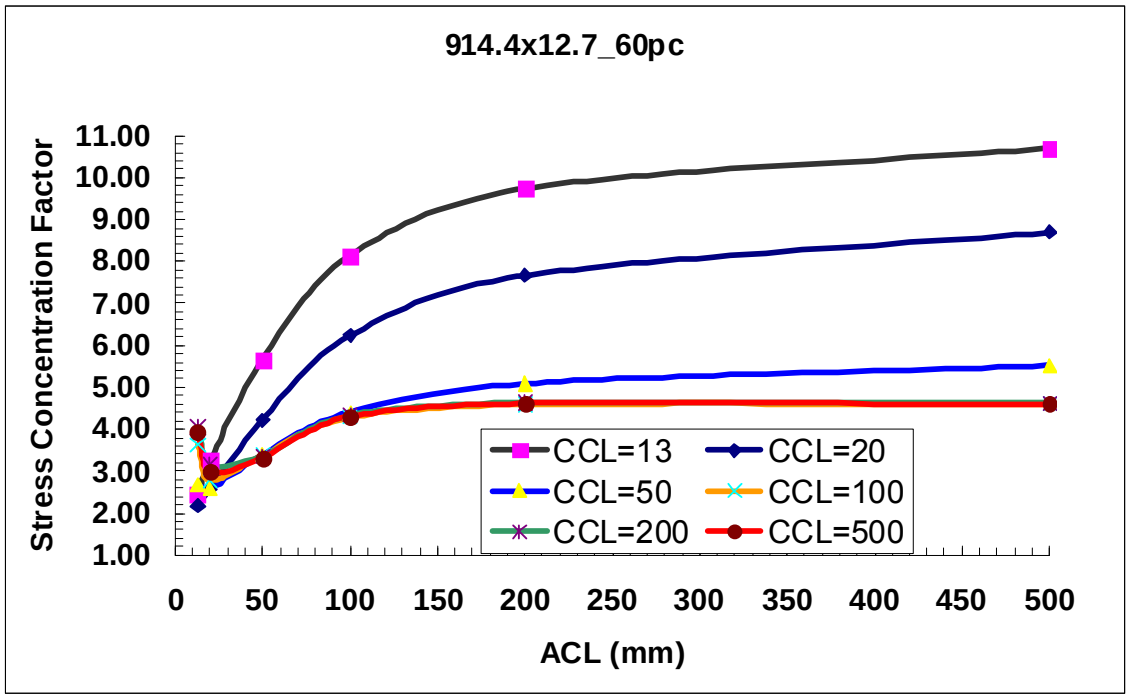

a): SCF with variation of axial corrosion length

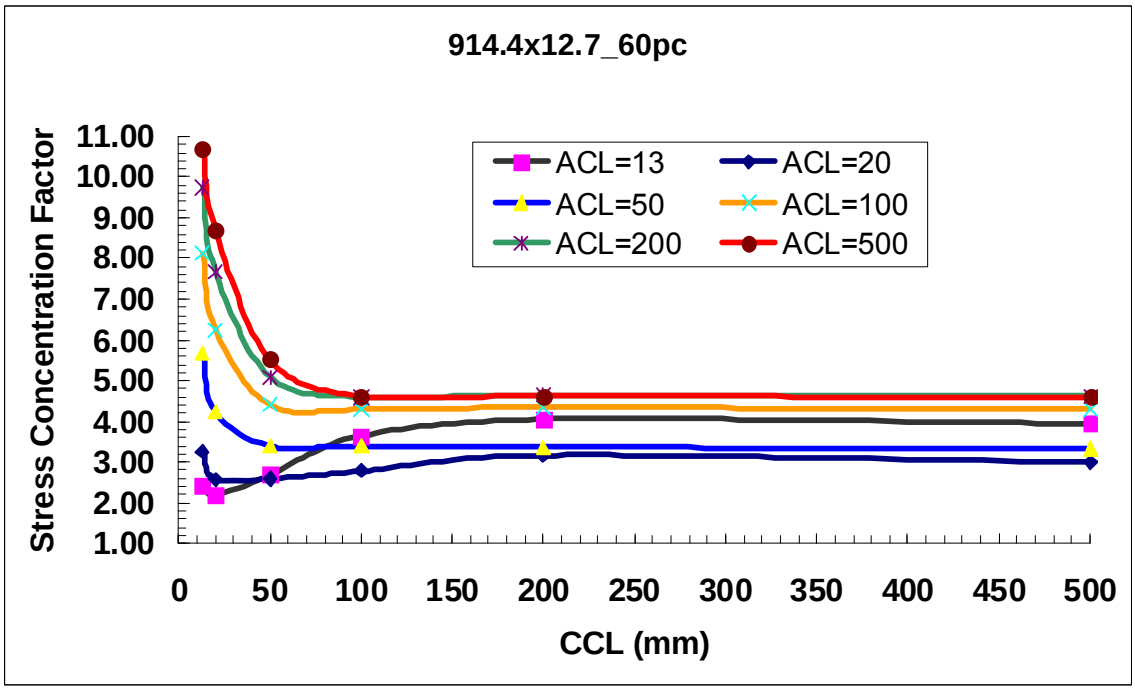

b): SCF with variation of circumferential corrosion length

Figure 12. SCFs for 914.4x12.7 mm (36x0.5”) pipe, CD=0.6, r/t=1.

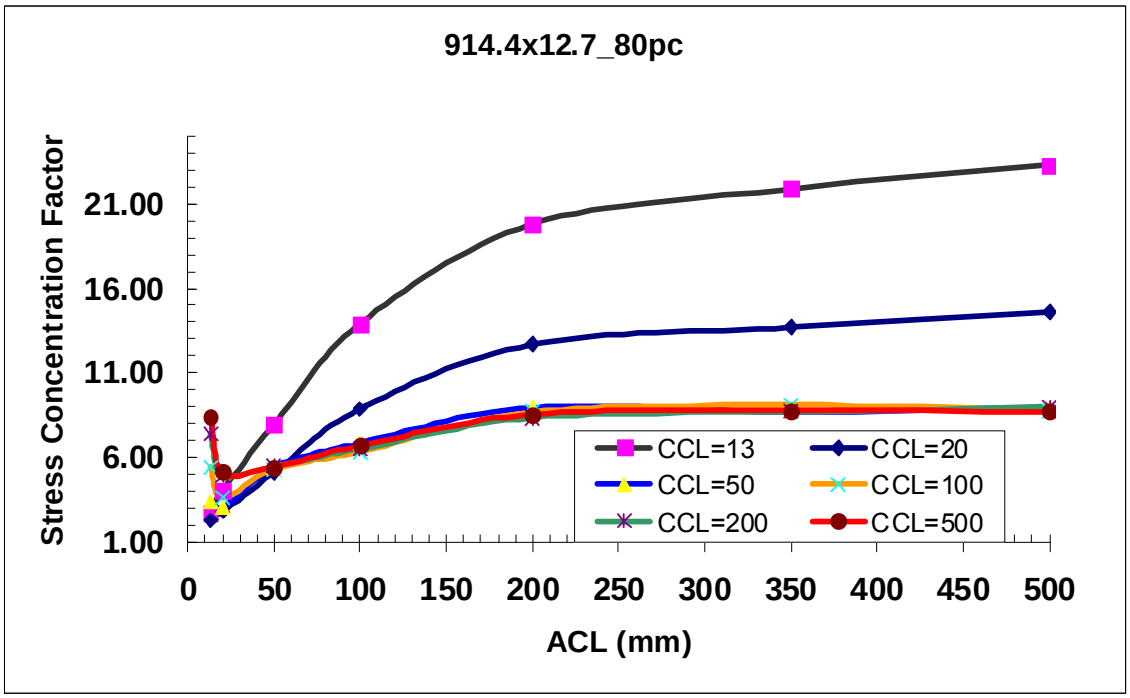

a): SCF with variation of axial corrosion length

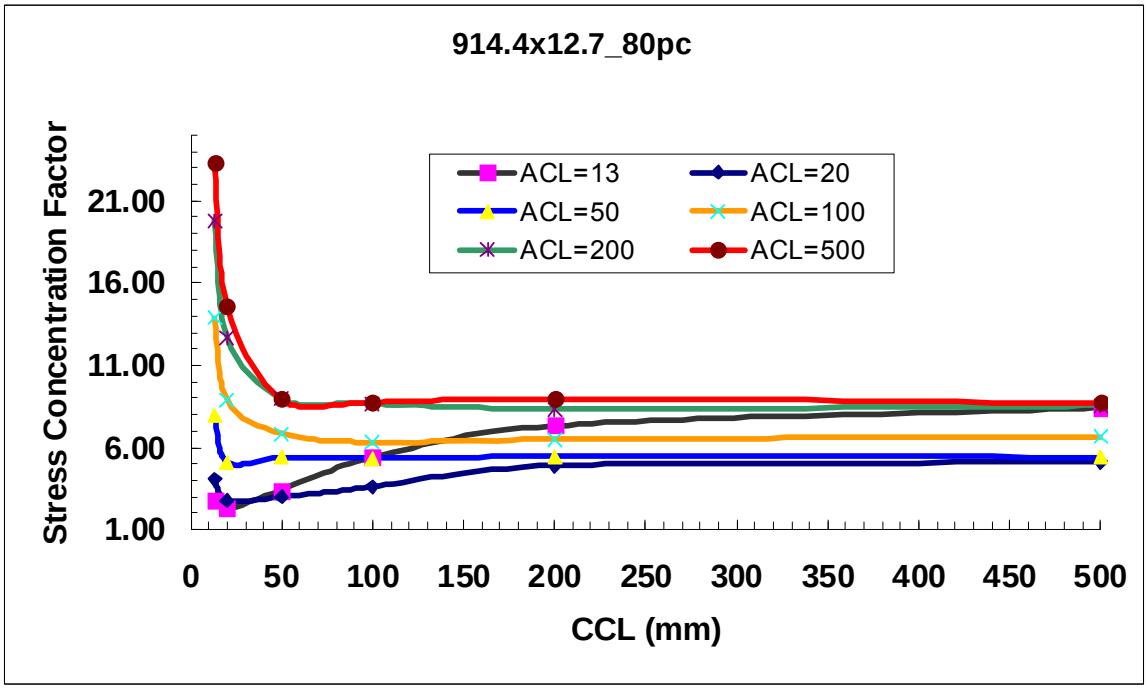

b): SCF with variation of circumferential corrosion length

Figure 13. SCFs for 914.4x12.7 mm (36x0.5”) pipe, CD=0.8, r/t=1.

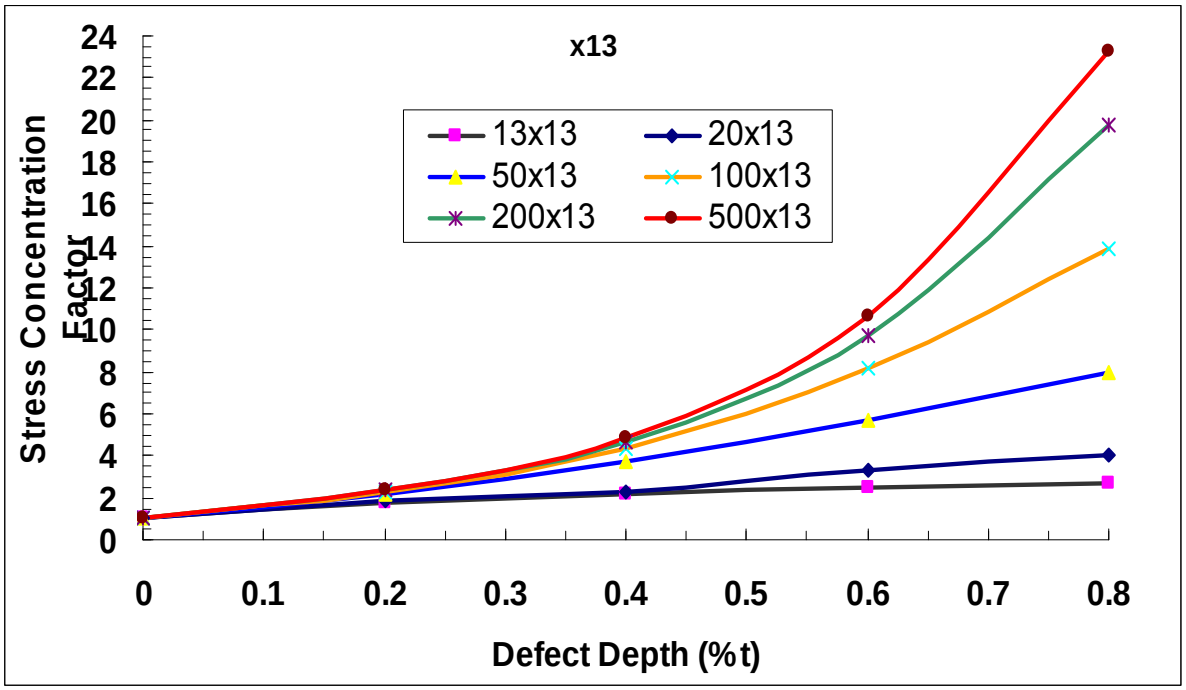

a): with CCL=13 mm and ACL=13 mm, 20 mm, 50 mm, 100 mm, 200 mm and 500 mm

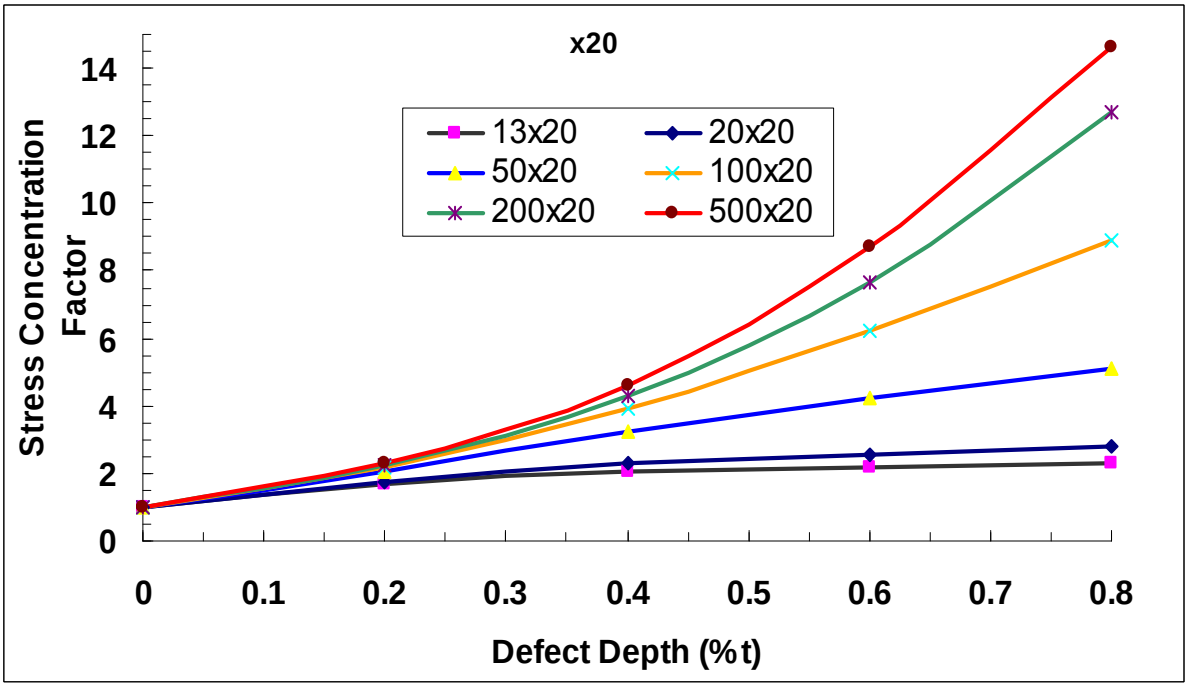

b): with CCL=20 mm and ACL=13 mm, 20 mm, 50 mm, 100 mm, 200 mm and 500 mm

Figure 14. SCFs for 914.4x12.7 mm (36x0.5”) pipe: variation in corrosion depth.

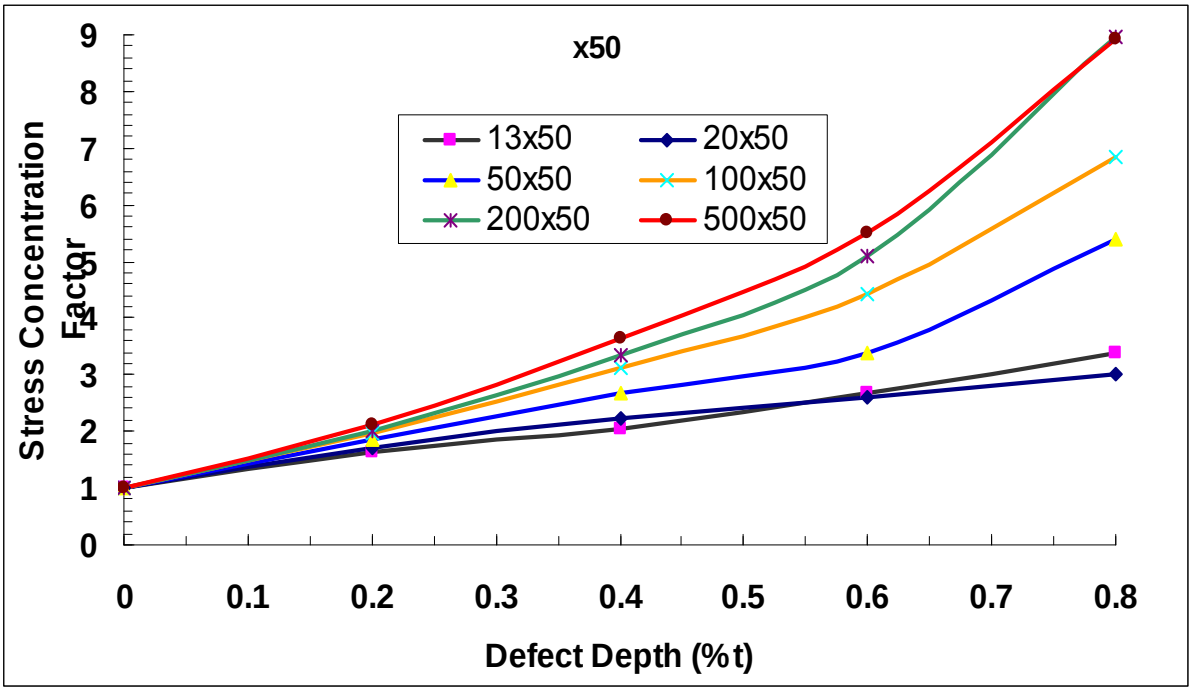

c): with CCL=50 mm and ACL=13 mm, 20 mm, 50 mm, 100 mm, 200 mm and 500 mm

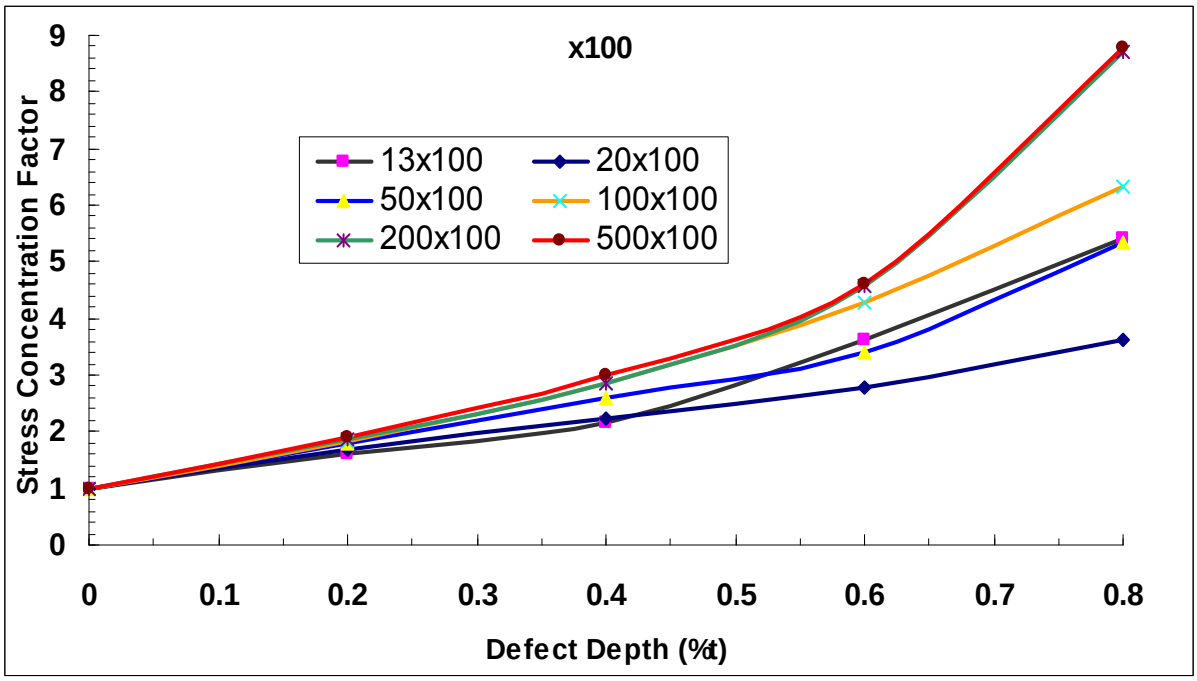

d): with CCL=100 mm and ACL=13 mm, 20 mm, 50 mm, 100 mm, 200 mm and 500 mm

Figure 14. SCFs for 914.4x12.7 mm (36x0.5”) pipe: variation in corrosion depth.

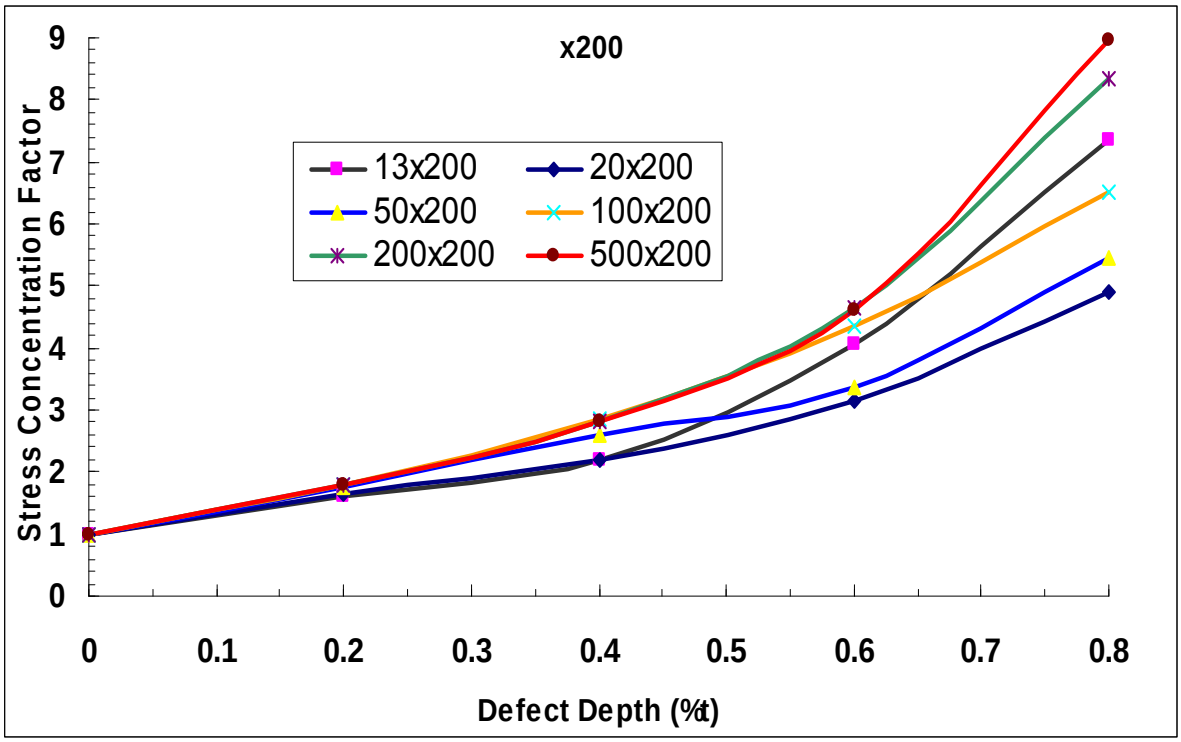

e): with CCL=200 mm and ACL=13 mm, 20 mm, 50 mm, 100 mm, 200 mm and 500 mm

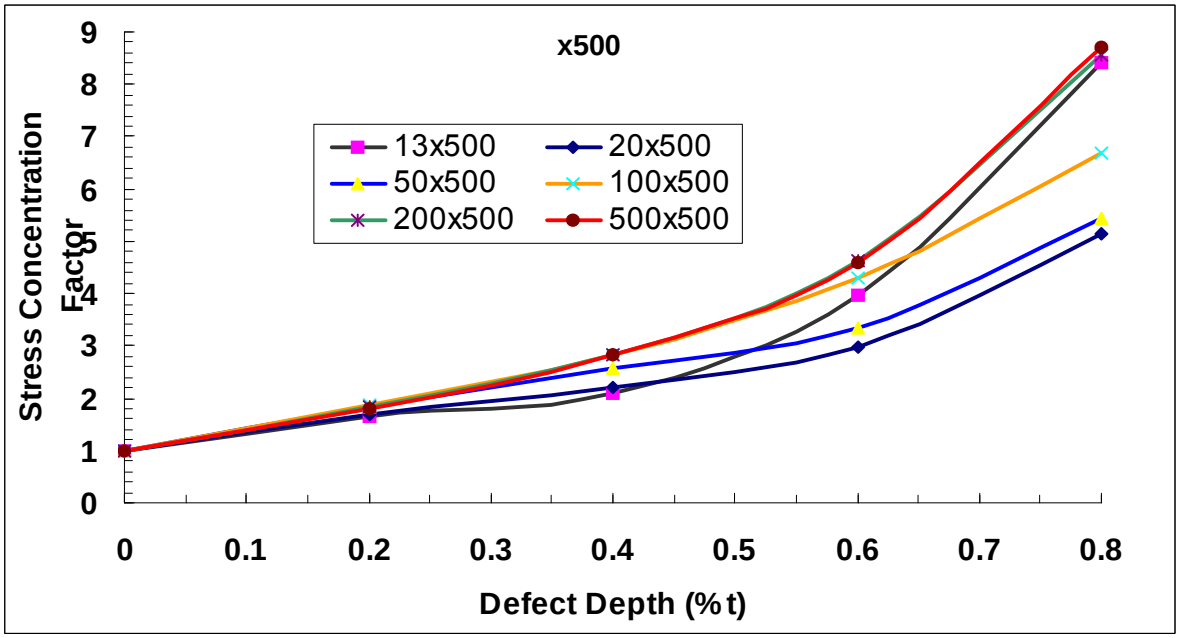

f): with CCL=500 mm and ACL=13 mm, 20 mm, 50 mm, 100 mm, 200 mm and 500 mm

Figure 14. SCFs for 914.4x12.7 mm (36x0.5”) pipe: variation in corrosion depth.

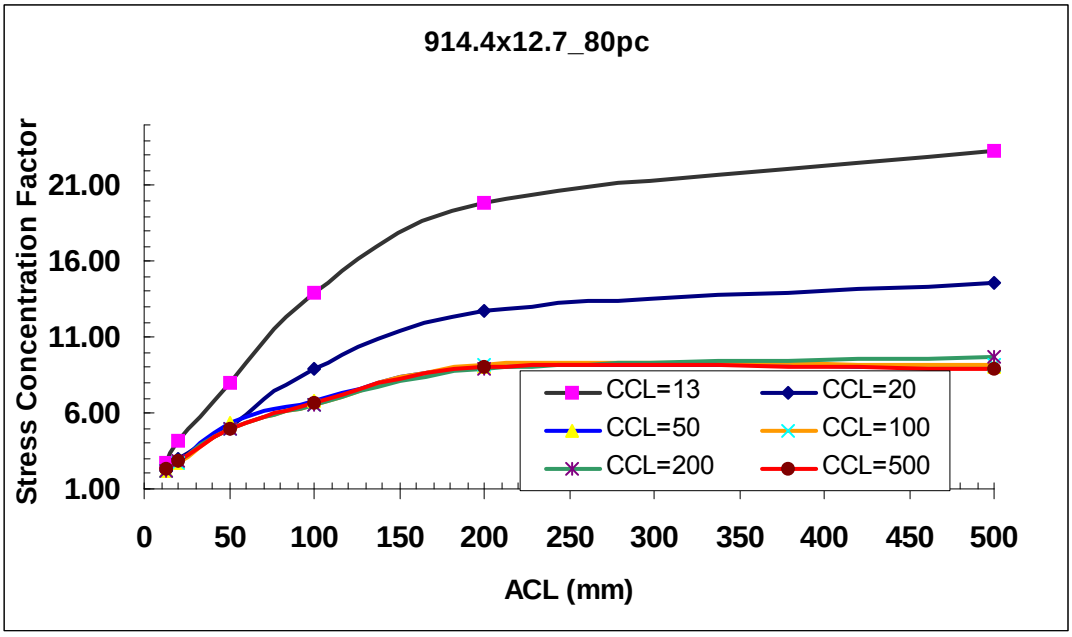

a): SCF with variation of axial corrosion length

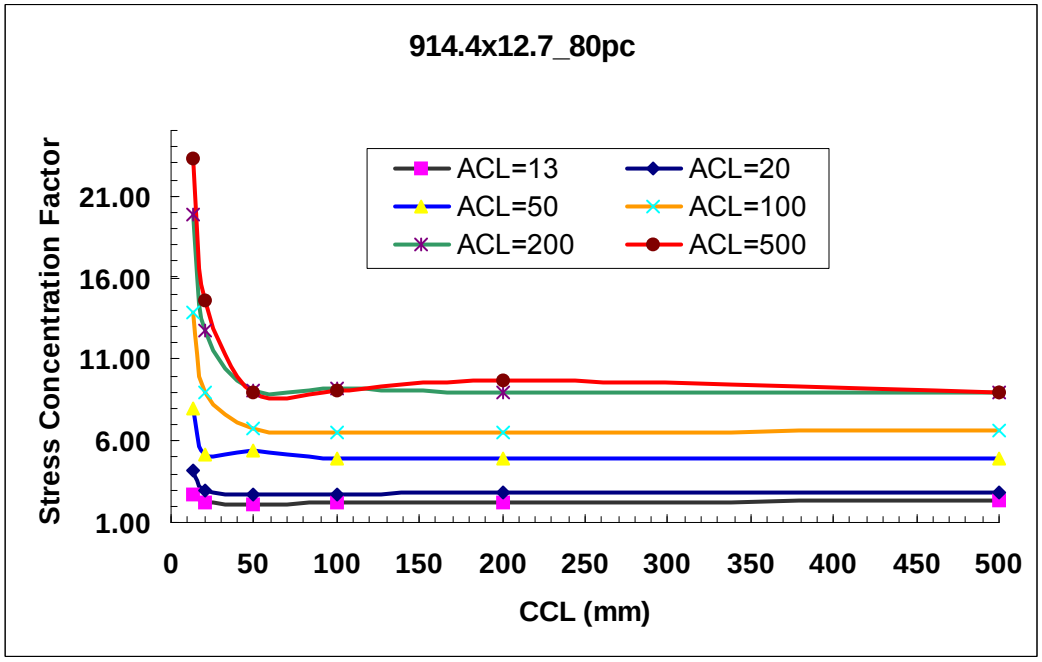

b): SCF with variation of circumferential corrosion length

Figure 15. SCFs for 914.4x12.7 mm (36x0.5”) pipe, CD=0.8, r/t=1, without ‘capped end force’.

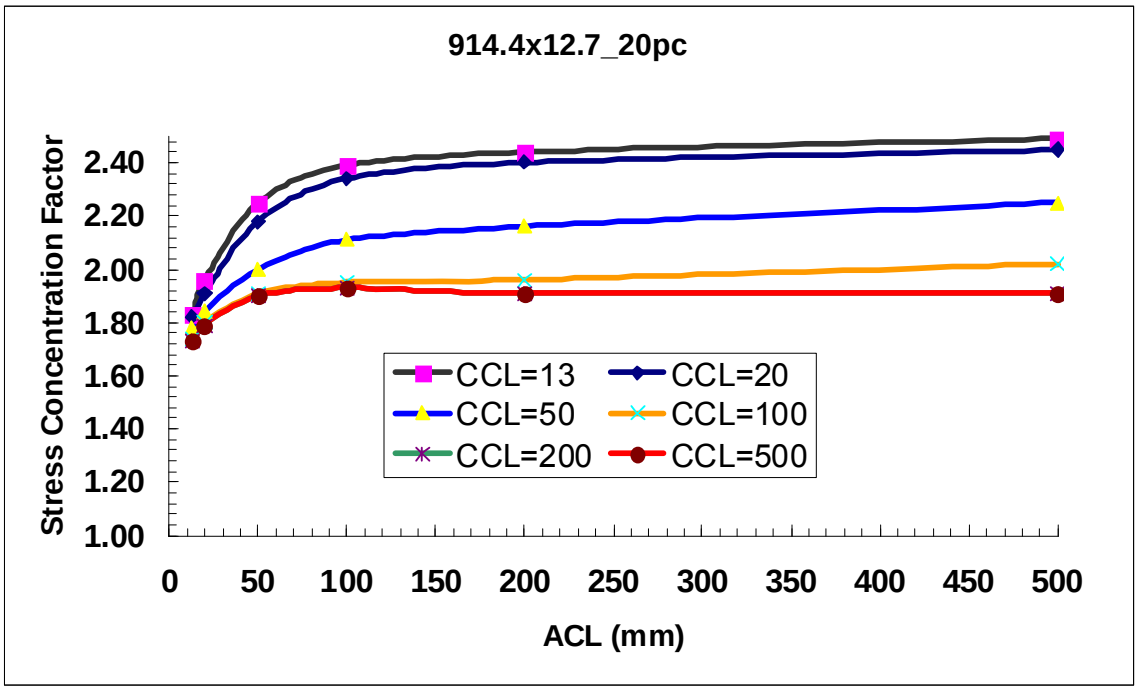

a): SCF with variation of axial corrosion length

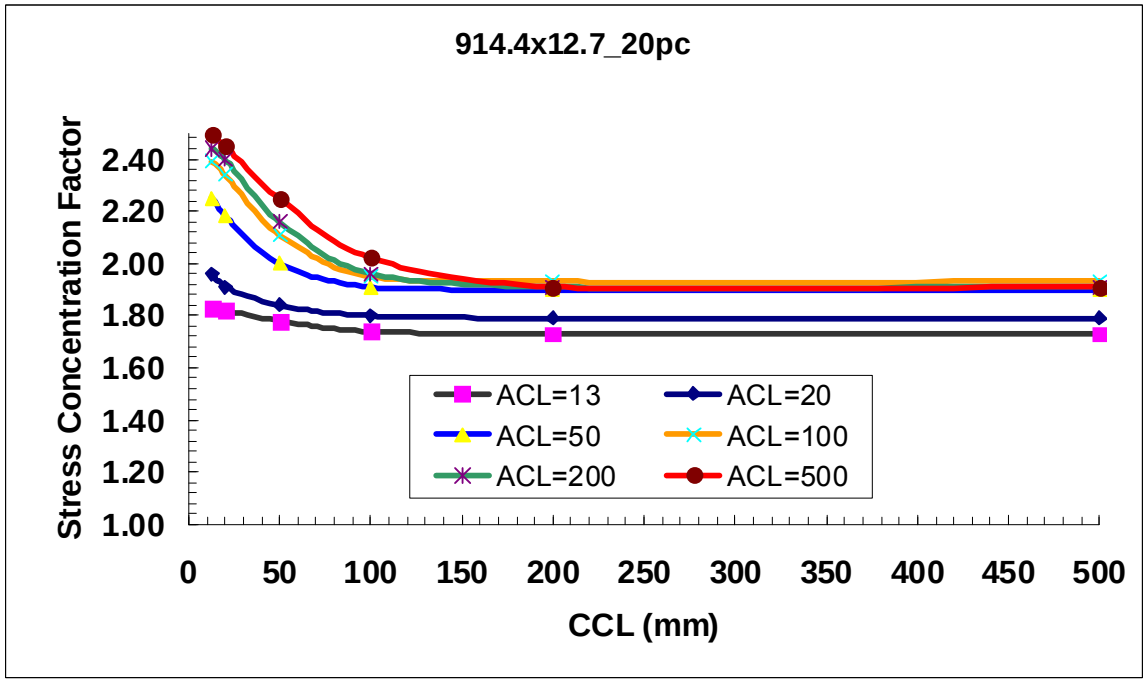

b): SCF with variation of circumferential corrosion length

Figure 16. SCFs for 914.4x12.7 mm (36x0.5”) pipe, CD=0.2, r/t=0.5.

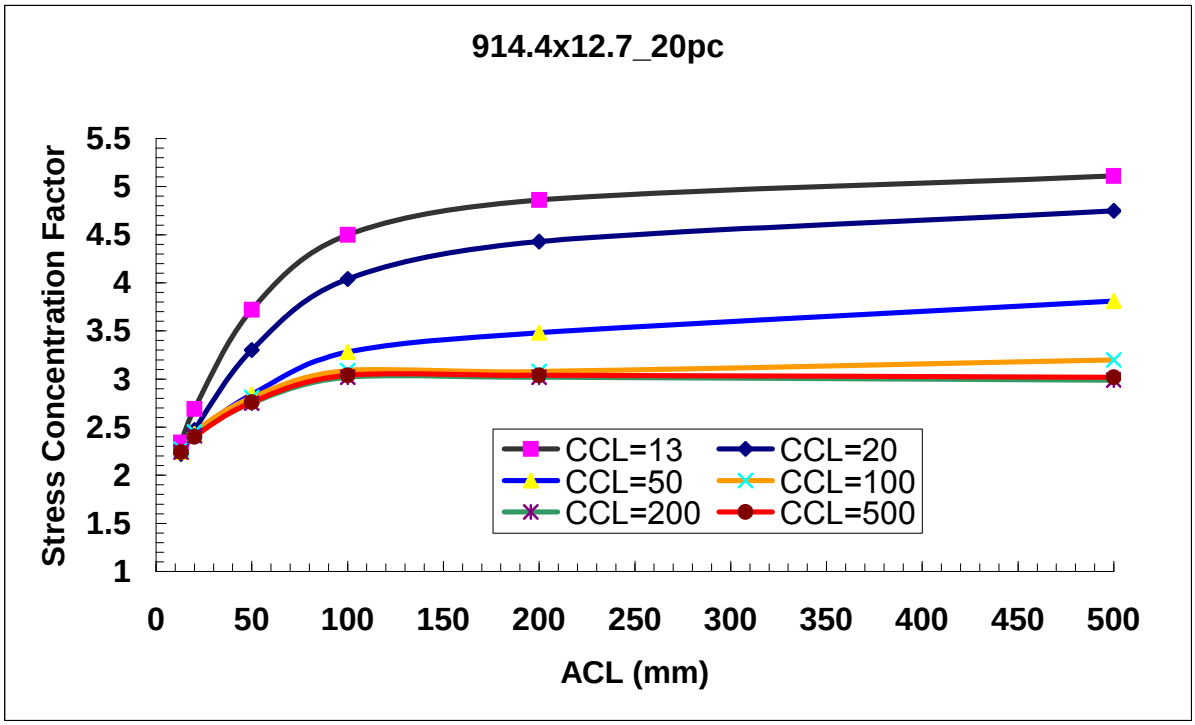

a): SCF with variation of axial corrosion length

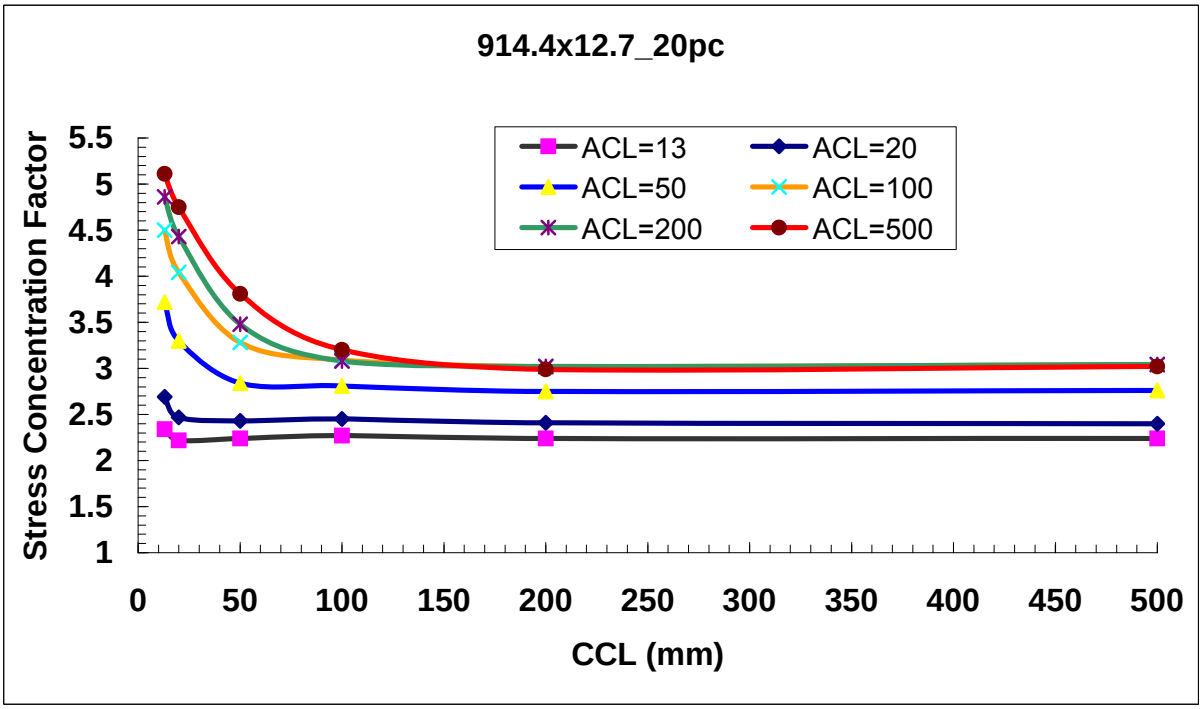

b): SCF with variation of circumferential corrosion length

Figure 17. SCFs for 914.4x12.7 mm (36x0.5”) pipe, CD=0.4, r/t=0.5.

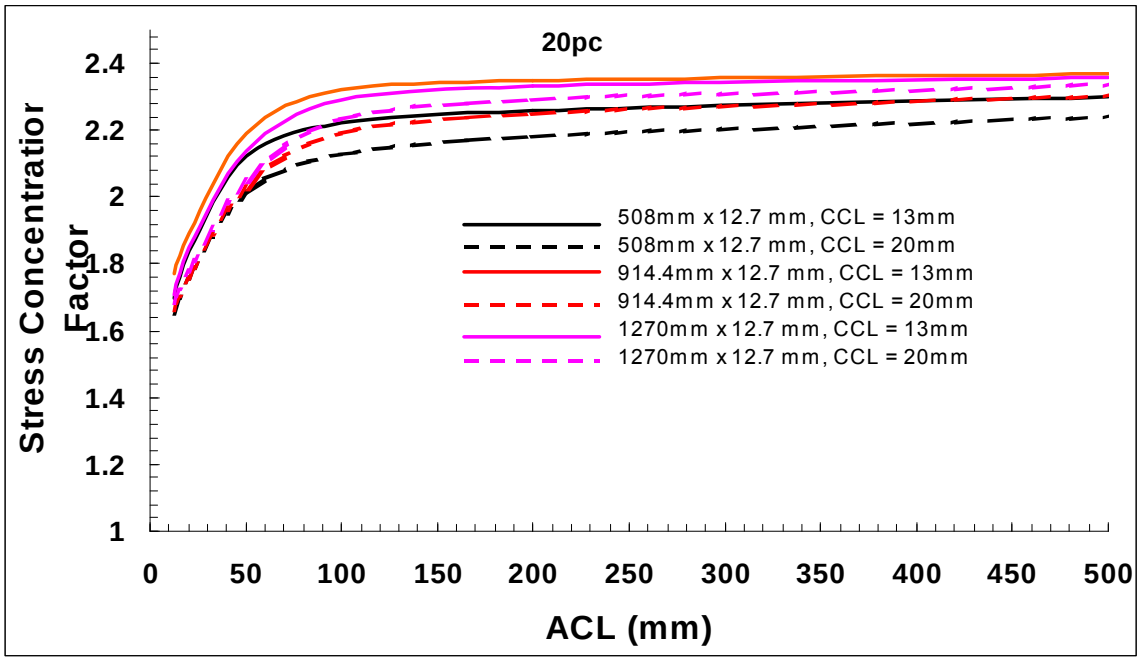

Figure 18. SCF for 508 x12.7 mm (20x0.5”), 914.4x12.7 mm (36x0.5”) and 1270x12.7 mm (50x0.5”) pipe, CD=0.2, r/t=1.

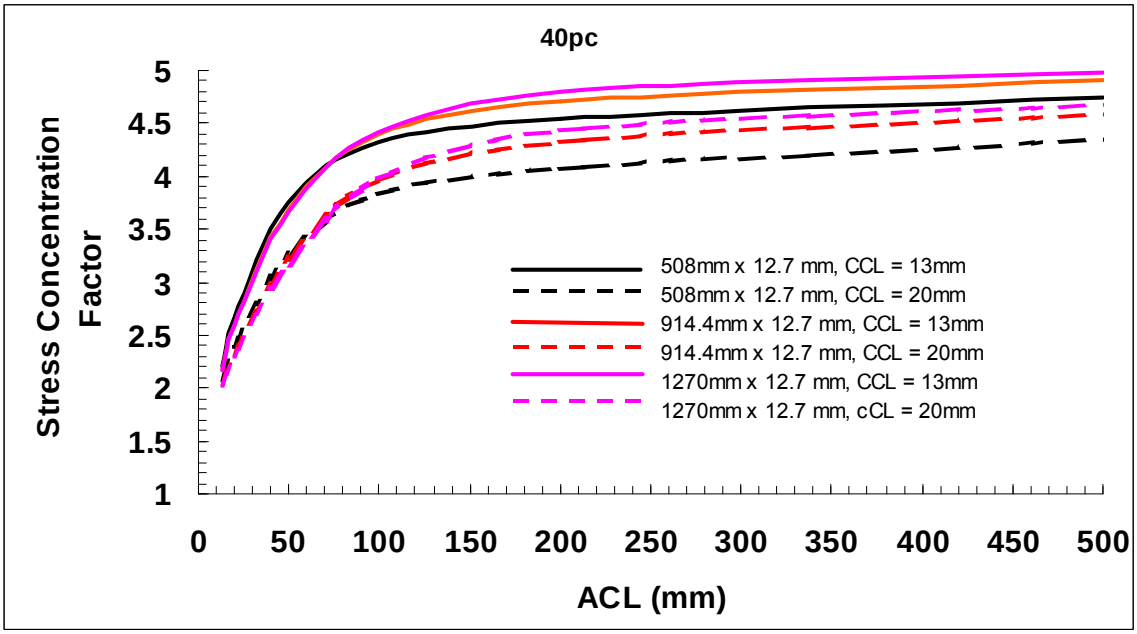

Figure 19. SCF for 508x12.7 mm (20x0.5”), 914.4x12.7 mm (36x0.5”) and 1270x12.7 mm (50x0.5”) pipe, CD=0.4, r/t=1.

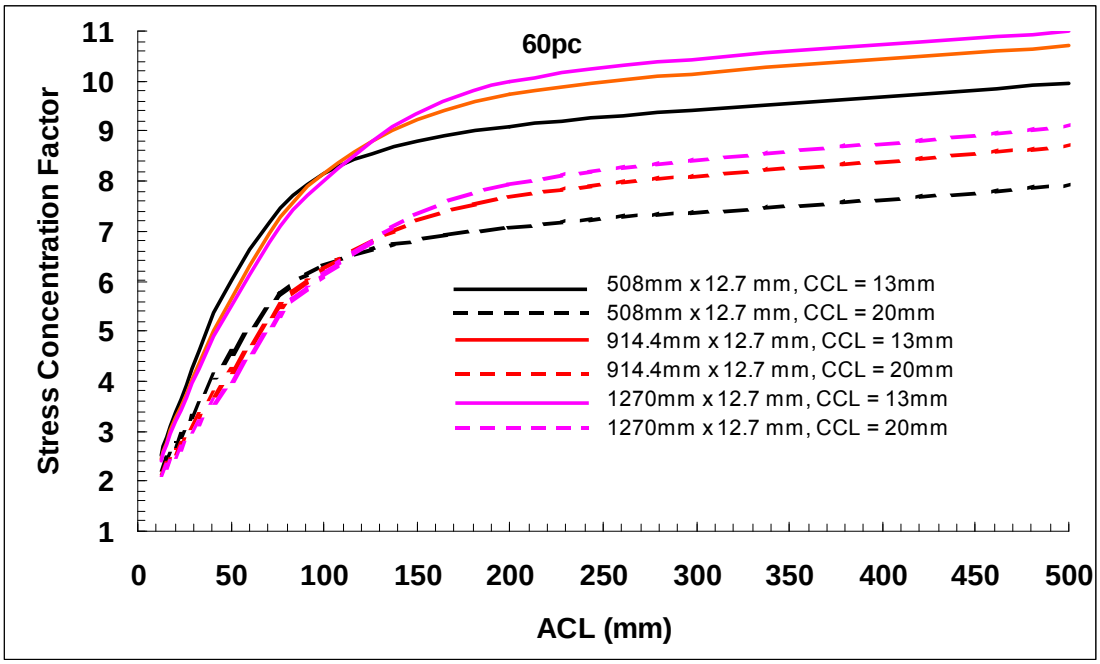

Figure 20. SCF for 508 x12.7 mm (20x0.5”), 914.4x12.7 mm (36x0.5”) and 1270x12.7 mm (50x0.5”) pipe, CD=0.6, r/t=1.

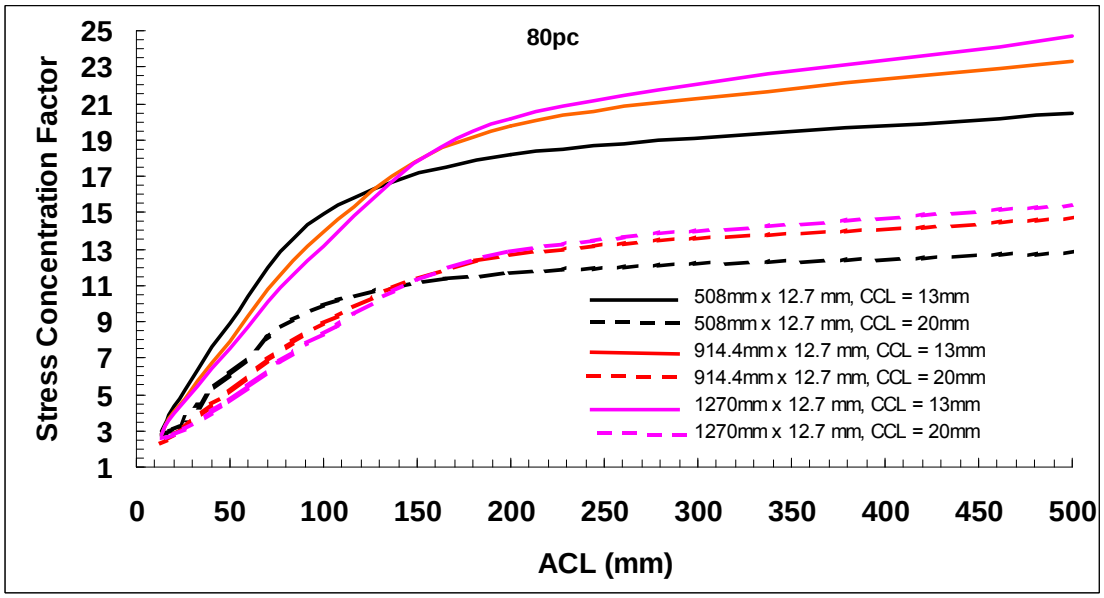

Figure 21. SCF for 508 x12.7 mm (20x0.5”), 914.4x12.7 mm (36x0.5”) and 1270x12.7 mm (50x0.5”) pipe, CD=0.8, r/t=1.

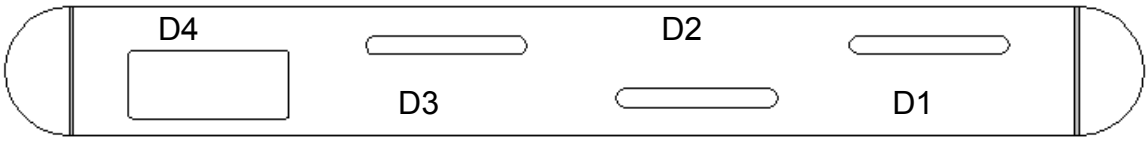

Notes: D1, D2, D3 and D4 refer to defects 1, 2, 3 and 4 respectively. For defect dimensions refer to Table 17.

Figure 22. Illustration of test vessel and defect locations (not to scale).

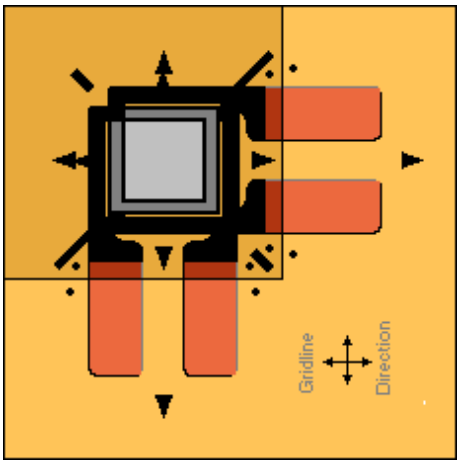

Type 1: CEA-06-062WT-350

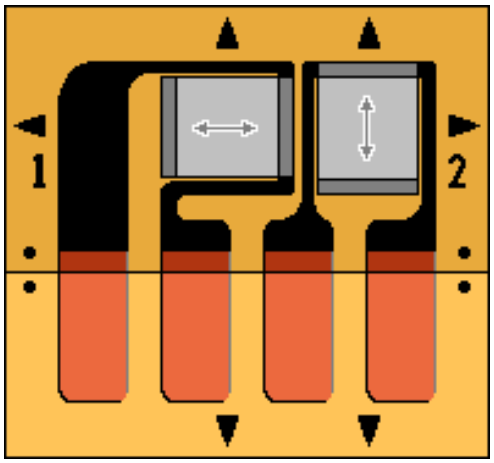

Type 2: CEA-06-062UT-350

Figure 23. Strain gauge rosettes used to measure the pipe axial and circumferential strains in the defect area.

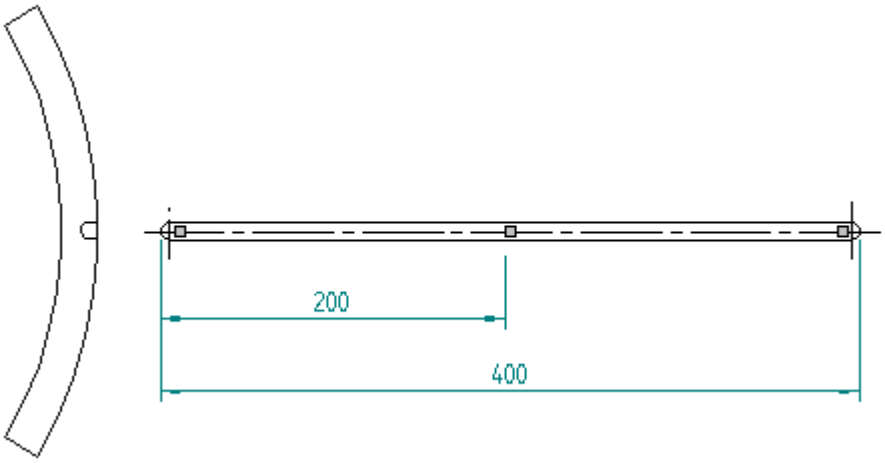

(a) Groove defect (dimensions in mm)

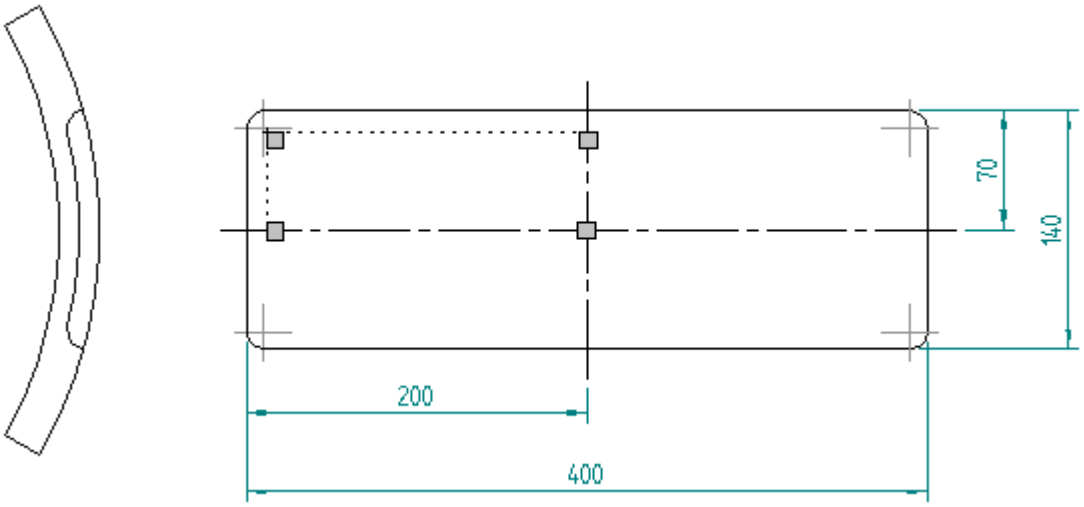

(b) Patch defect (dimensions in mm)

Figure 24. Strain gauge locations within the groove and patch defects.

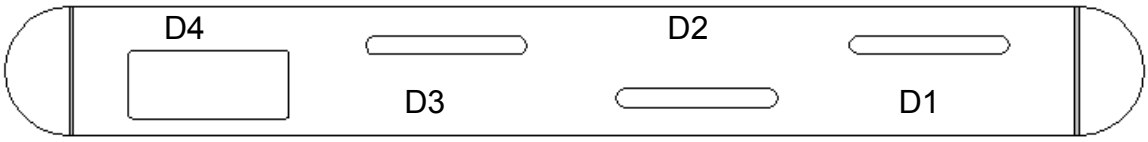

(a) through wall cracking observed in defect D2

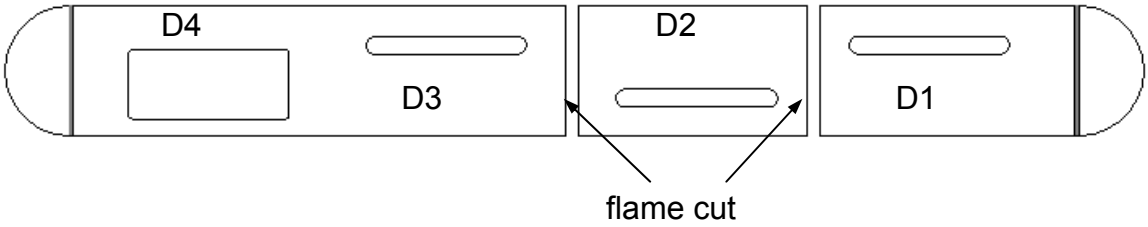

(b) removal of defect D2 via flame cutting (cutting process cuts a weld prep onto the ends of the pup pieces containing defects D1, D3 and D4)

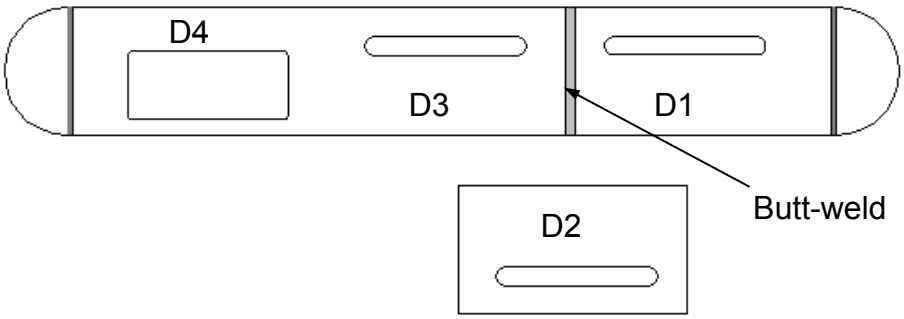

(c) defect D2 is extracted and the two vessel ends are butt welded together. Pressure cycling is then resumed.

Figure 25. Illustration of repair methodology (not to scale).

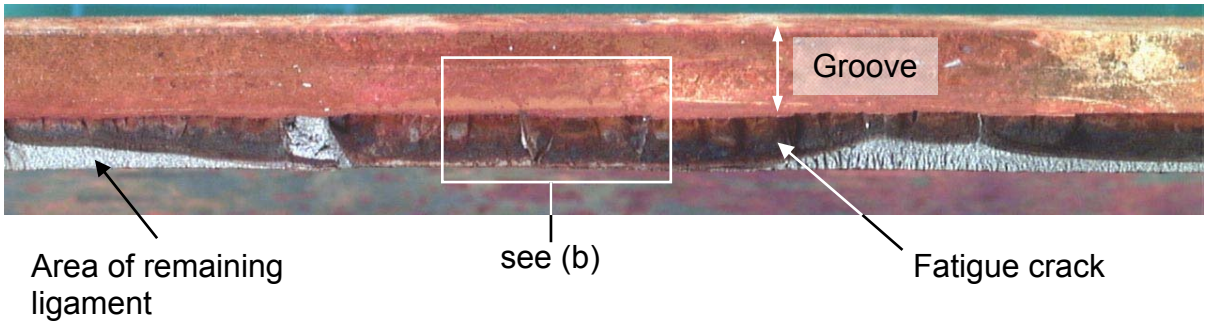

(a) Multiple crack initiation sites along outer surface of defect, which eventually coalesce to form one large fatigue crack

(b) Cleaned up image of typical crack initiation site at location of through wall breach, as enveloped in (a) above.

Note: inner surface to bottom in all images

Figure 26. Pipe 1, Defect D3: Stereo optical microscope images of crack face features.

(a) Crack initiation site along outer surface of defect

(b) Cleaned up image of crack initiation site and location of through wall breach. Beach markings clearly visible, showing crack propagation from the outer to the inner surface (top to bottom in image).

Note: inner surface to bottom in all images

Figure 27. Pipe 1, Defect D2: Stereo optical microscope images of crack face features.

(a) Crack initiation site along inner surface of defect

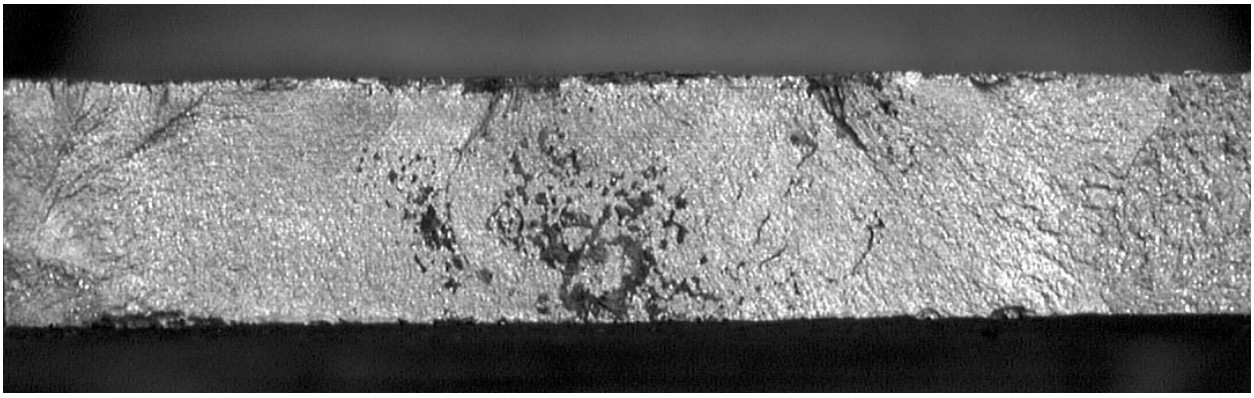

(b) Cleaned up image of multiple crack initiation sites and location of through wall breach. Crack propagation from the inner to the outer surface (top to bottom in image).

Note: outer surface to bottom in all images

Figure 28. Pipe 1, Defect D4: Stereo optical microscope images of crack face features.

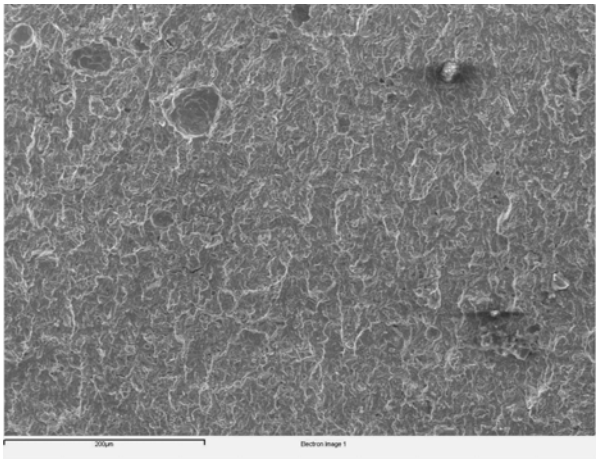

Fatigue crack surface features – **outer**, 200μm scale

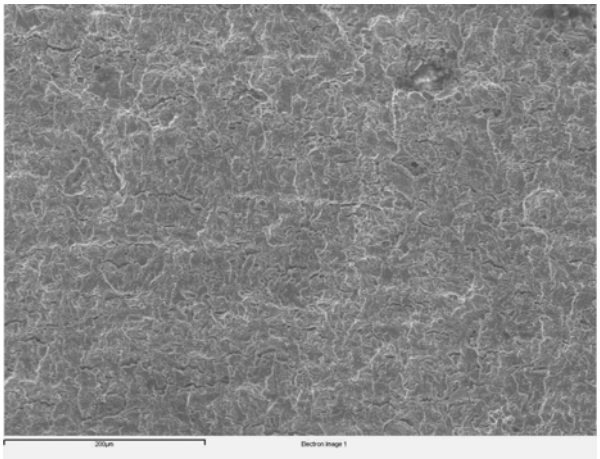

Fatigue crack surface features – **inner**, 200μm scale

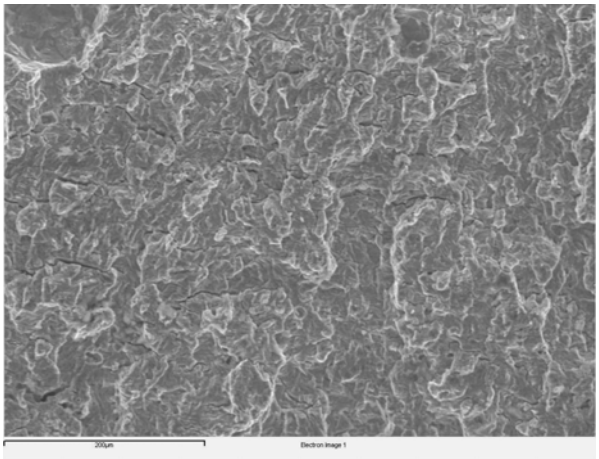

Fatigue crack surface features – **outer**, 100μm scale

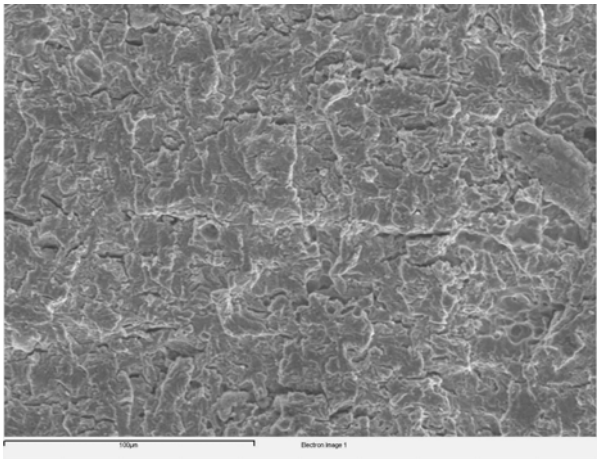

Fatigue crack surface features – **inner**, 100μm scale

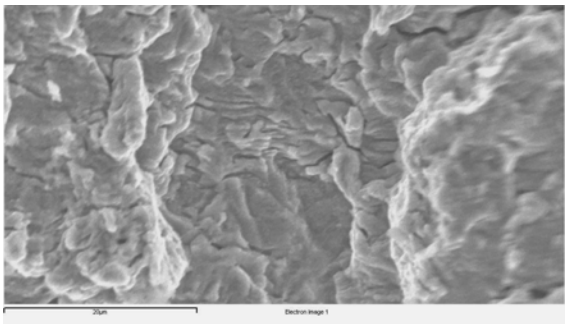

Striations – outer, 20μm scale

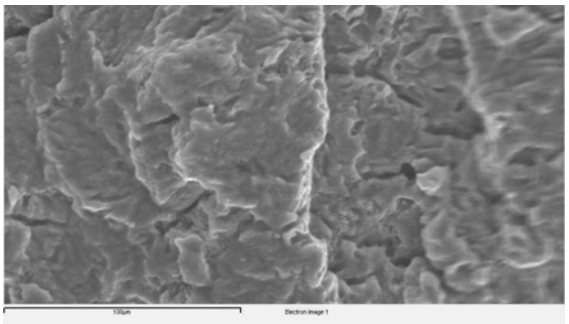

Striations – inner, 20μm scale

Notes: outer and **inner** refer to crack face areas in relation to the outer and inner pipe surfaces

Figure 29. Pipe 1, Defect D3: Scanning electron microscope images (crack growth direction is top to bottom in all images).

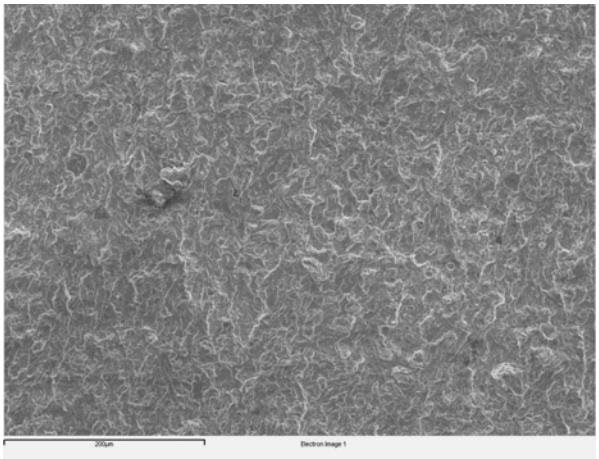

Fatigue crack surface features – outer, 200μm scale

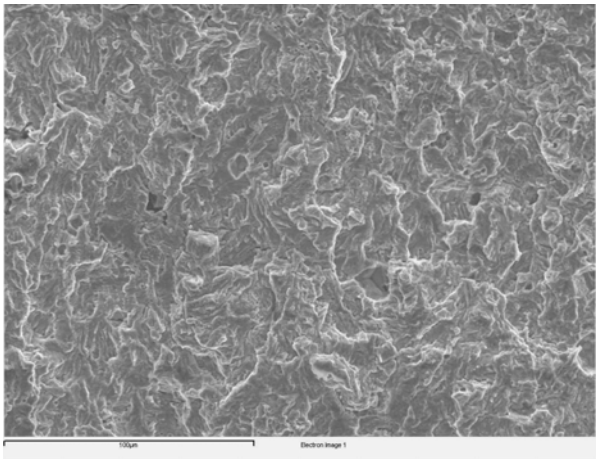

Fatigue crack surface features – outer, 100μm scale

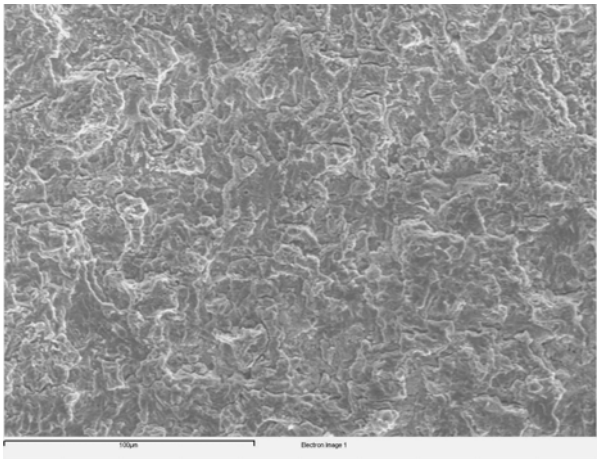

Fatigue crack surface features – inner, 100μm scale

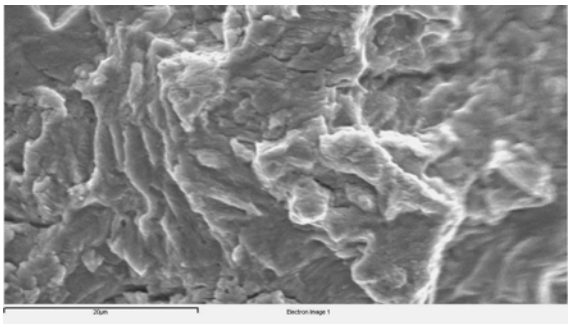

Striations – outer, 20μm scale

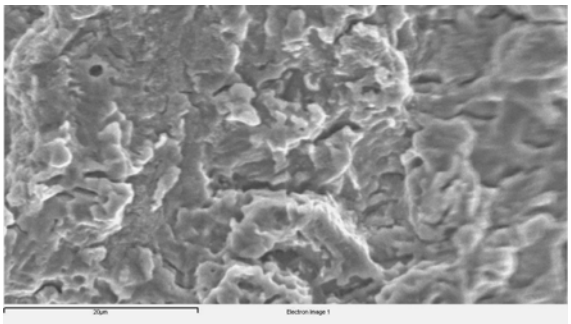

Striations – inner, 20μm scale

Notes: outer and **inner** refer to crack face areas in relation to the outer and inner pipe surfaces

Figure 30. Pipe 1, Defect D2: Scanning electron microscope images (crack growth direction is top to bottom in all images).

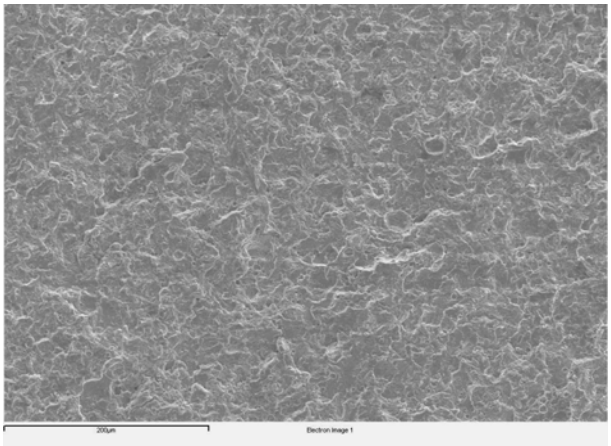

Fatigue crack surface features – outer, 200μm scale

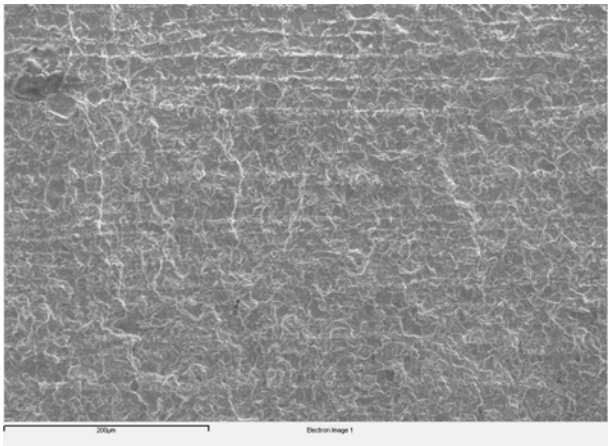

Fatigue crack surface features – inner, 200μm scale

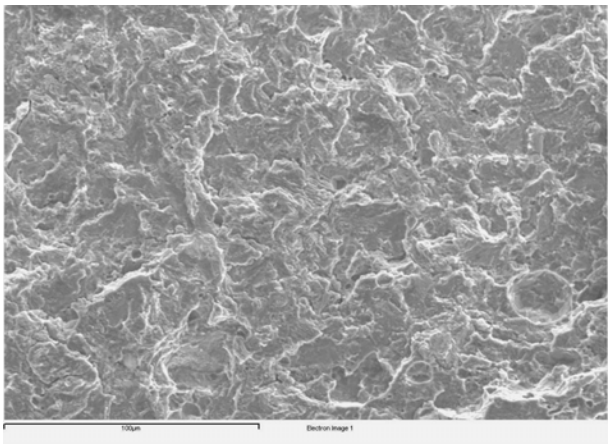

Fatigue crack surface features – outer, 100μm scale

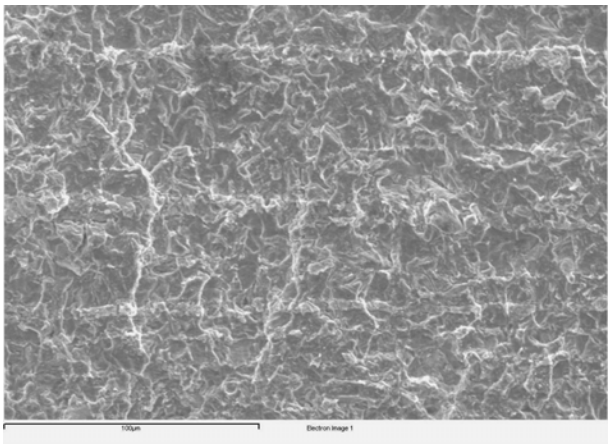

Fatigue crack surface features – inner, 100μm scale

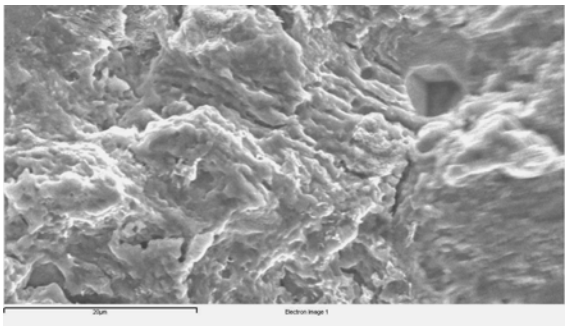

Striations – outer, 20μm scale

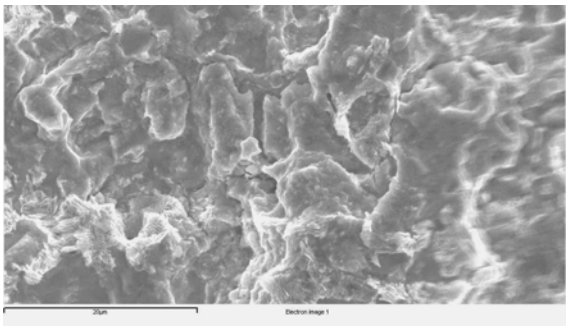

Striations – inner, 20μm scale (not as clear as on outer surface)

Notes: outer and **inner** refer to crack face areas in relation to the outer and inner pipe surfaces

Figure 31. Pipe 1, Defect D4: Scanning electron microscope images (crack growth direction is top to bottom in all images).

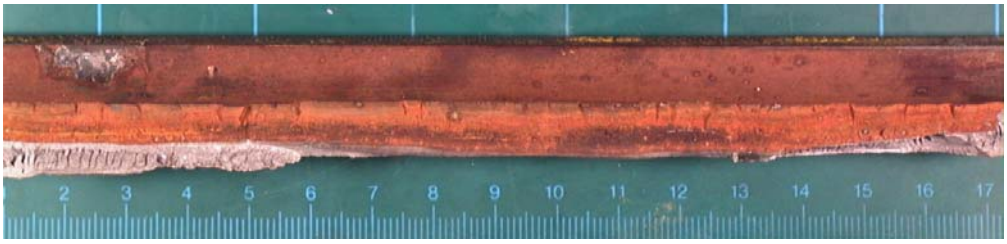

(a) As opened

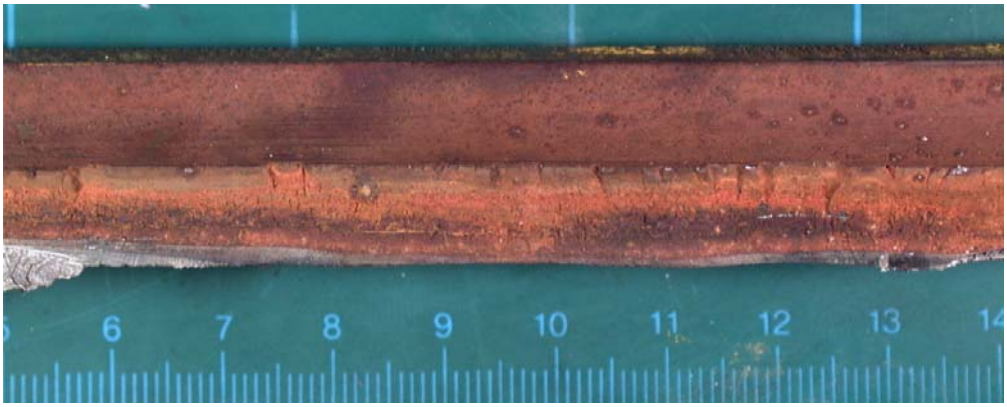

(b) Close up view of central through wall area.

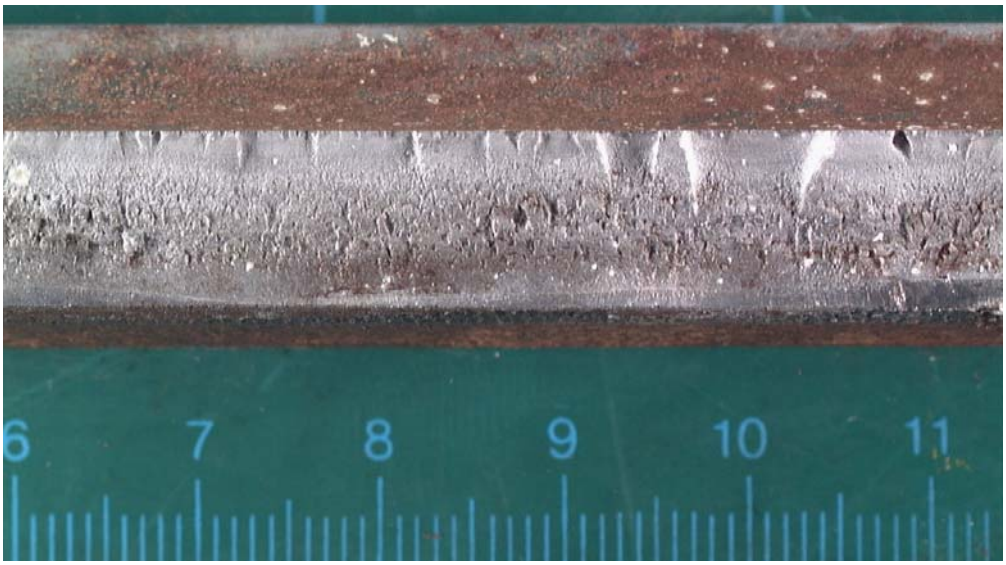

(c) Central through wall area after cleaning of deposits.

Note: inner surface to bottom in all images

Figure 32. Pipe 2, Defect D2: Stereo optical microscope images of crack face features.

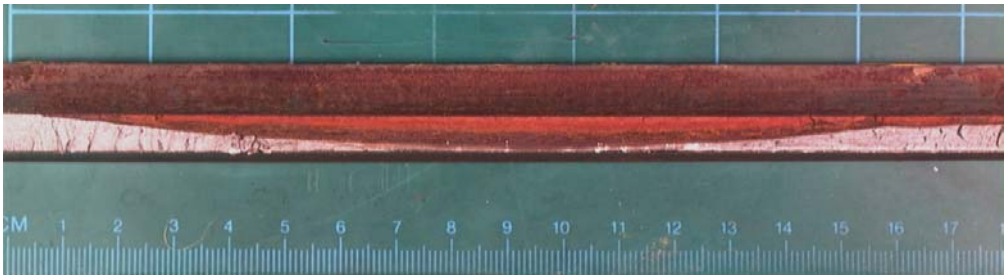

(a) As opened

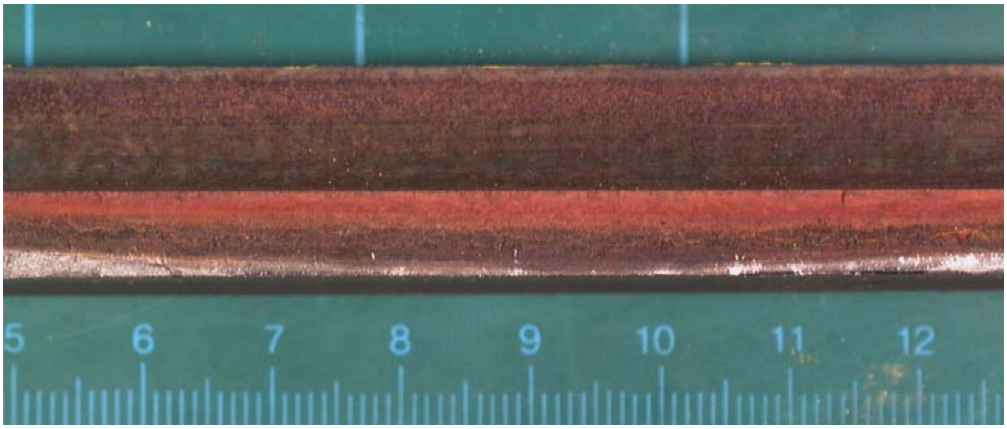

(b) Close up view of central through wall area

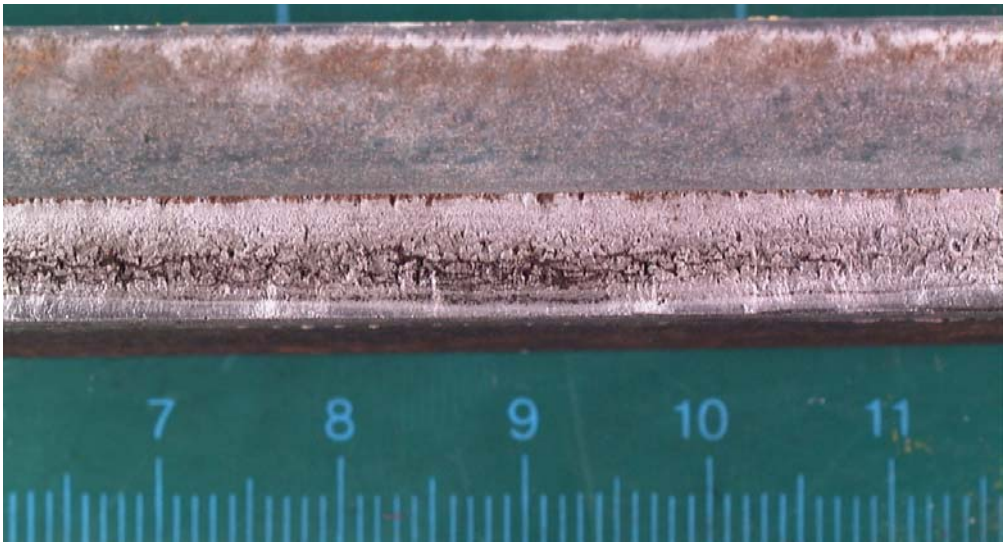

(c) Central through wall area after cleaning of deposits

Note: inner surface to bottom in images

Figure 33. Pipe 2, Defect D3: Stereo optical microscope images of crack face features.

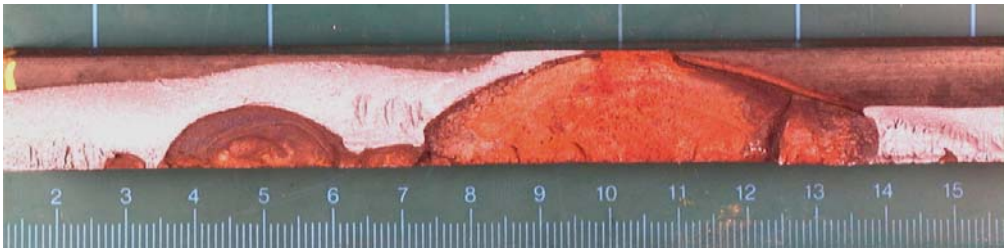

(a) As opened.

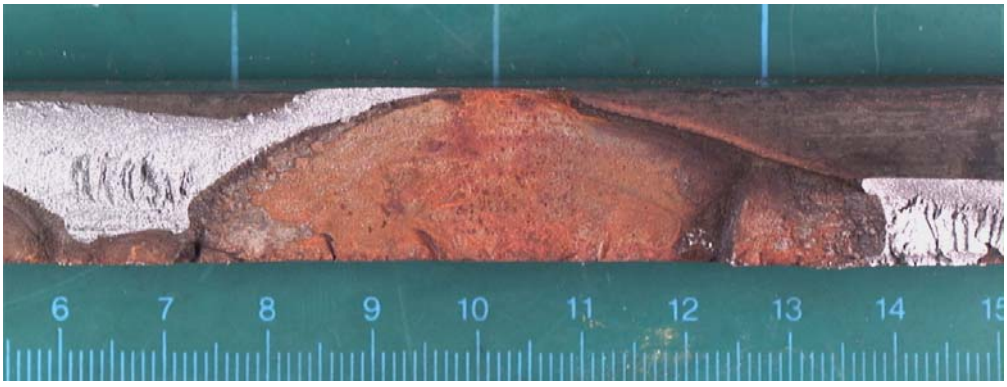

(b) Close up view of through wall area.

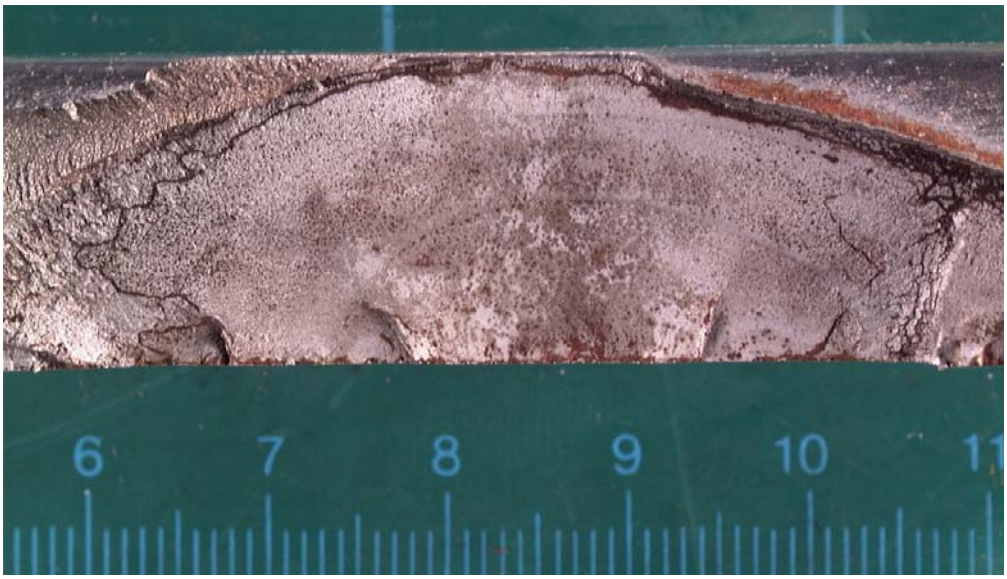

(c) Through wall area after cleaning of deposits.

Note: inner surface to bottom in images

Figure 34. Pipe 2, Defect D4: Stereo optical microscope images of crack face features.

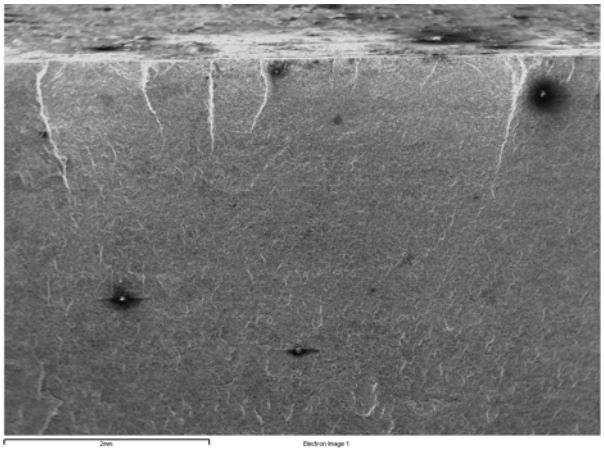

Fatigue crack surface features – **outer**, 2mm scale

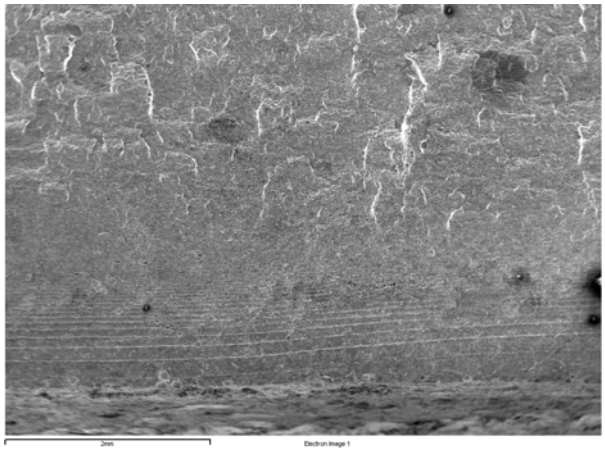

Fatigue crack surface features – **inner**, 2mm scale

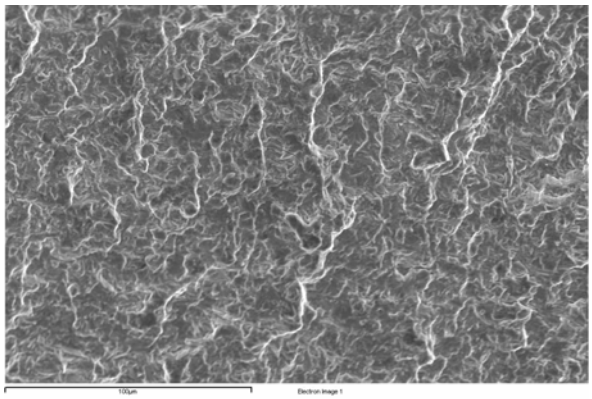

Fatigue crack surface features – **outer**, 100μm scale

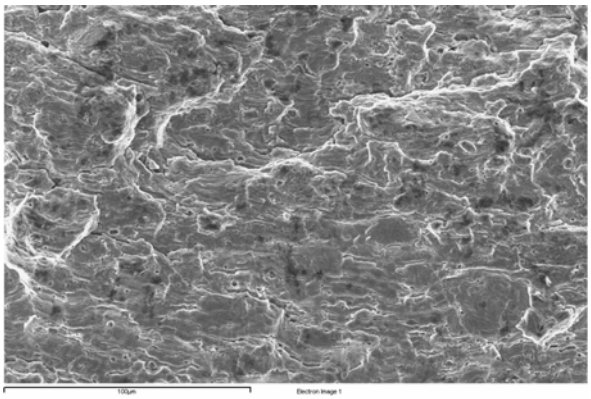

Fatigue crack surface features – **inner**, 100μm scale

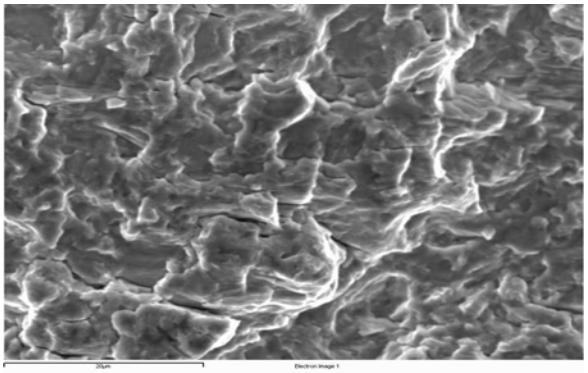

Striations – **outer**, 20μm scale

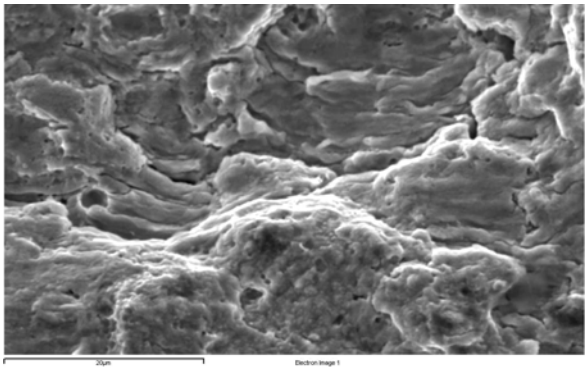

Striations – **inner**, 20μm scale

Notes: outer and **inner** refer to crack face areas in relation to the outer and inner pipe surfaces

Figure 35. Pipe 2, Defect D2: Scanning electron microscope images (crack growth direction is top to bottom in all images).

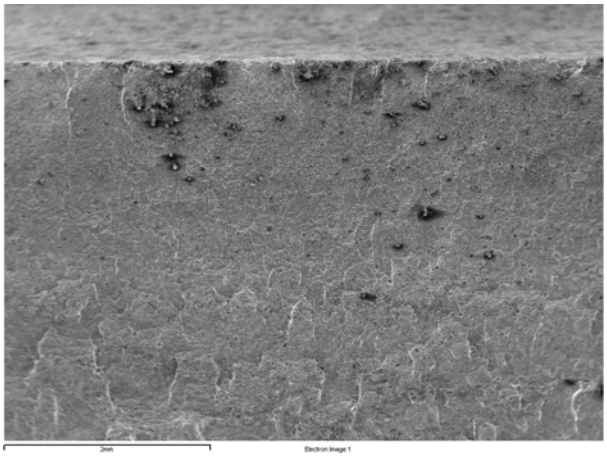

Fatigue crack surface features – **outer**, 2mm scale

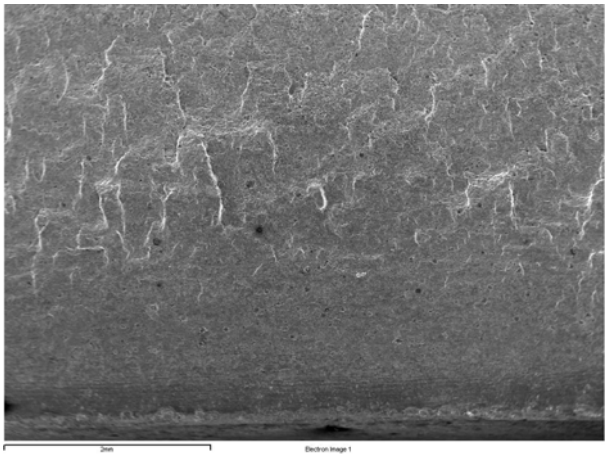

Fatigue crack surface features – **inner**, 2mm scale

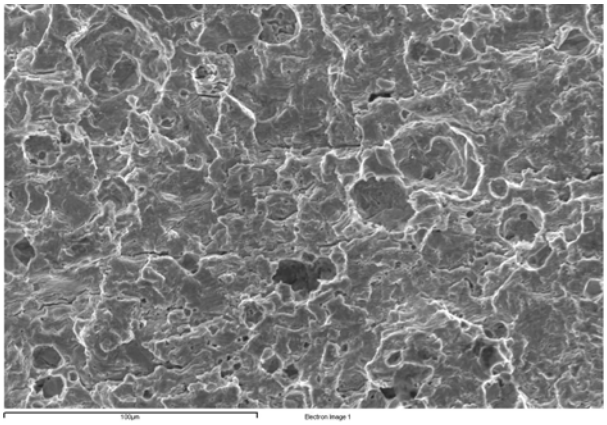

Fatigue crack surface features – **outer**, 100μm scale

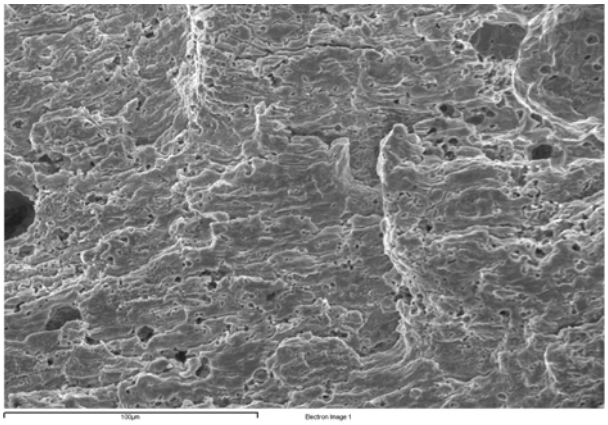

Fatigue crack surface features – **inner**, 100μm scale

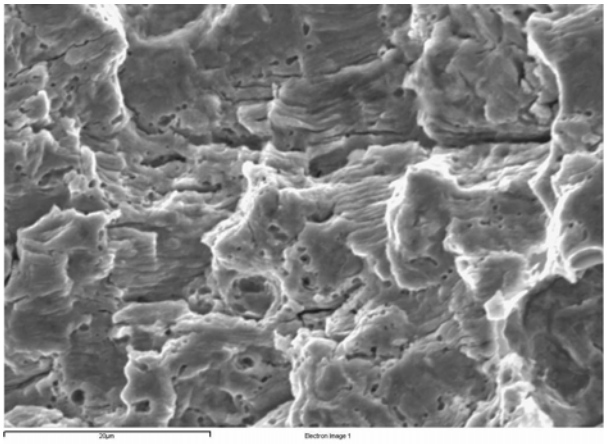

Striations – **outer**, 20μm scale

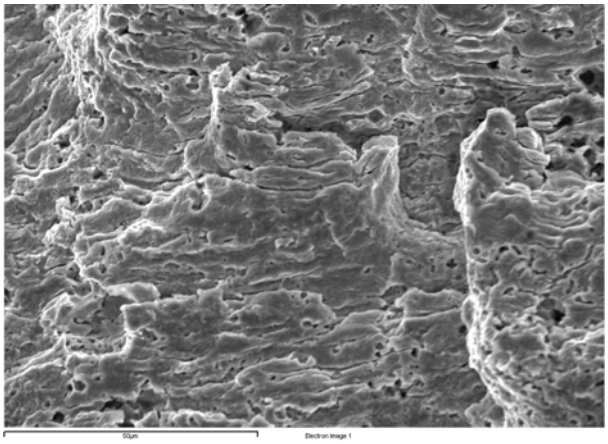

Striations – **inner**, 50μm scale

Figure 36. Pipe 2, Defect D3: Scanning electron microscope images (crack growth direction is top to bottom in all images).

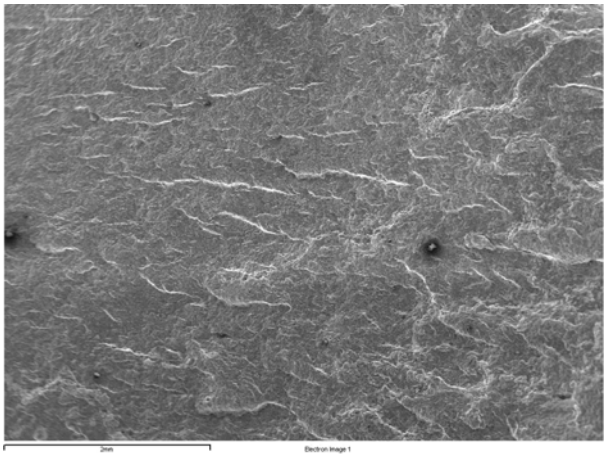

Fatigue crack surface features – **outer**, 2mm scale

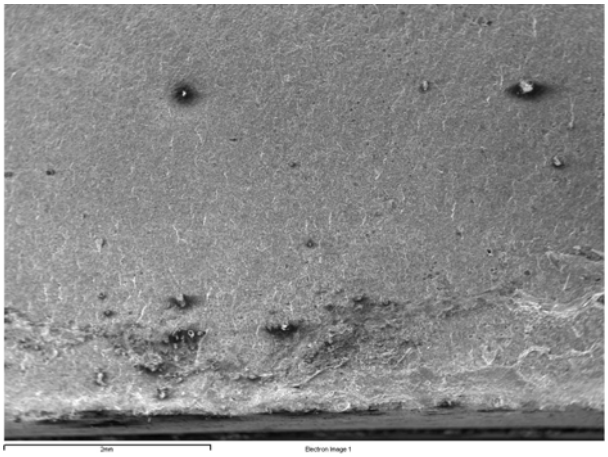

Fatigue crack surface features – **inner**, 2mm scale

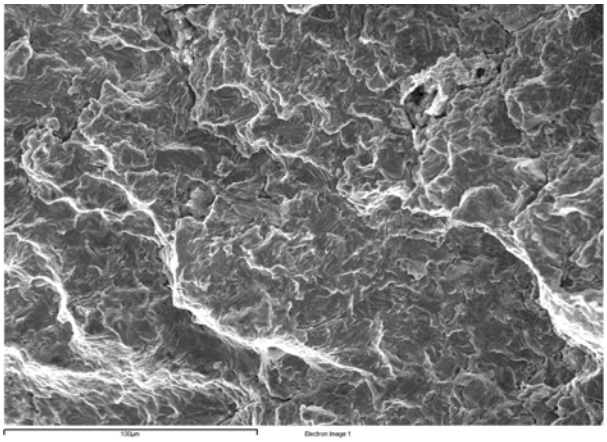

Fatigue crack surface features – **outer**, 100μm scale

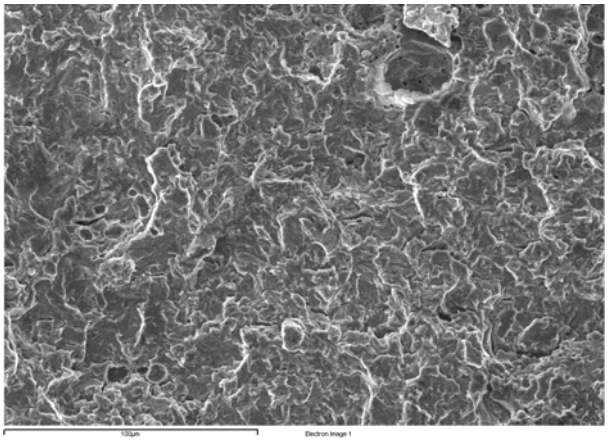

Fatigue crack surface features – **inner**, 100μm scale

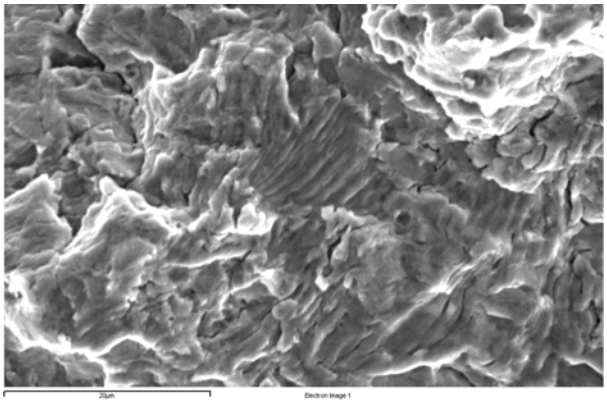

Striations – **outer**, 20μm scale

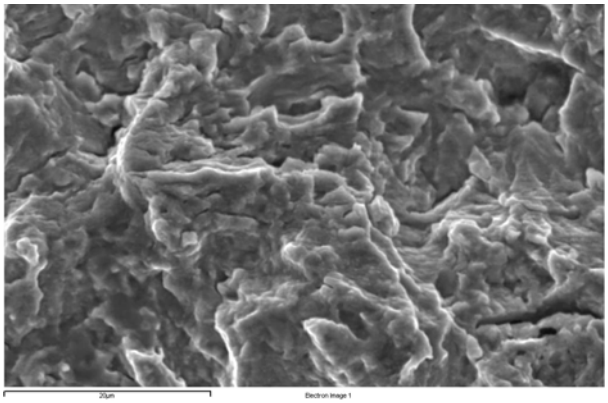

Striations – **inner**, 20μm scale

Figure 37. Pipe 2, Defect D4: Scanning electron microscope images (crack growth direction is top to bottom in all images).

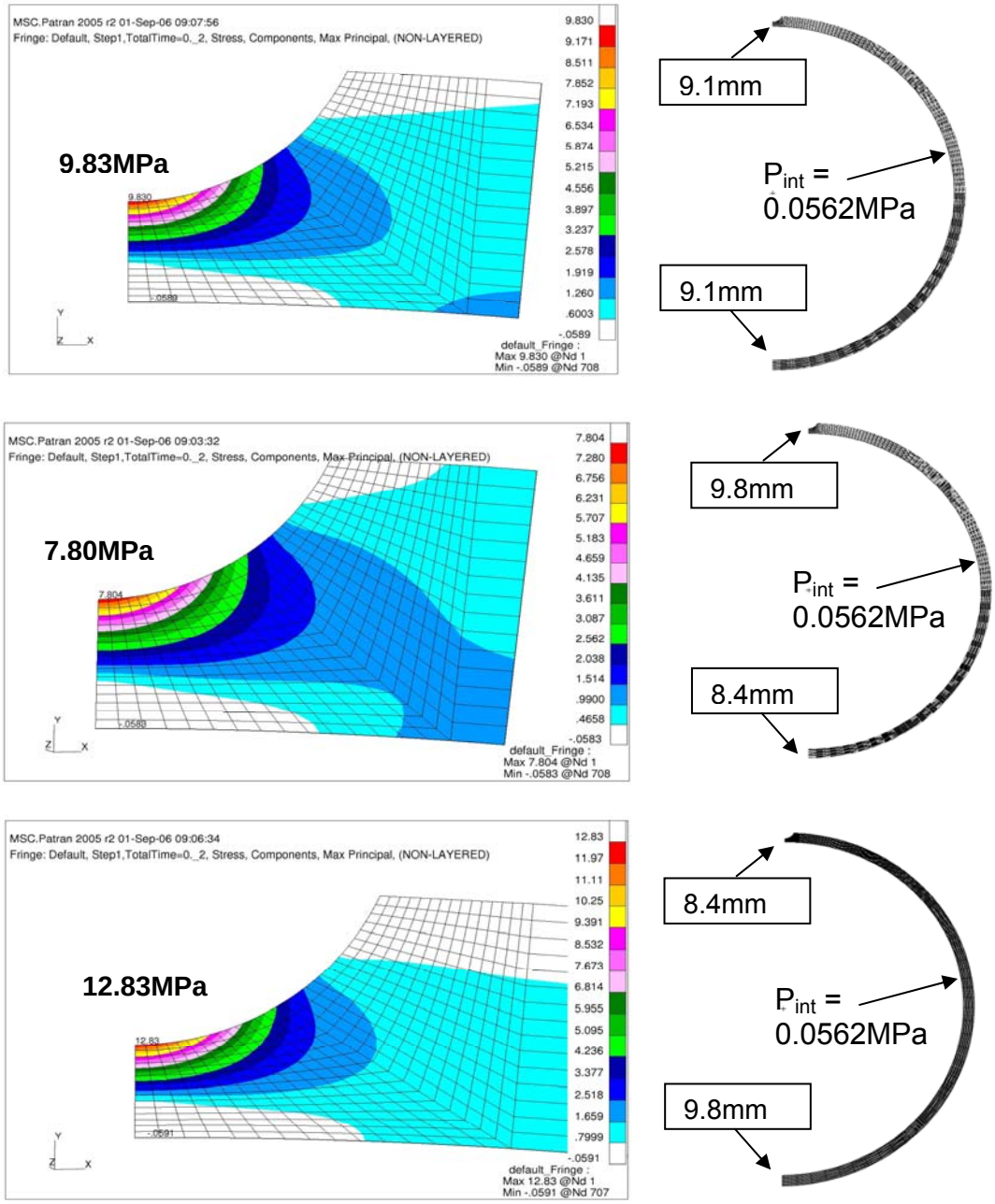

Figure 38. Plane strain finite element models showing the effect of an eccentric bore on the SCF (Hoop stress of 1.0 N/mm^2 in each case).

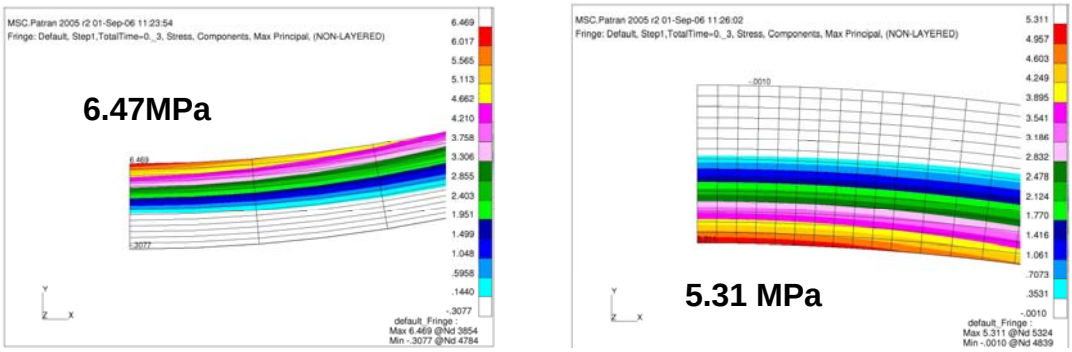

Figure 39. Local Maximum Principal Stress contours for defect free pipe with an eccentric bore (Left - thinnest area; right - thickest area).

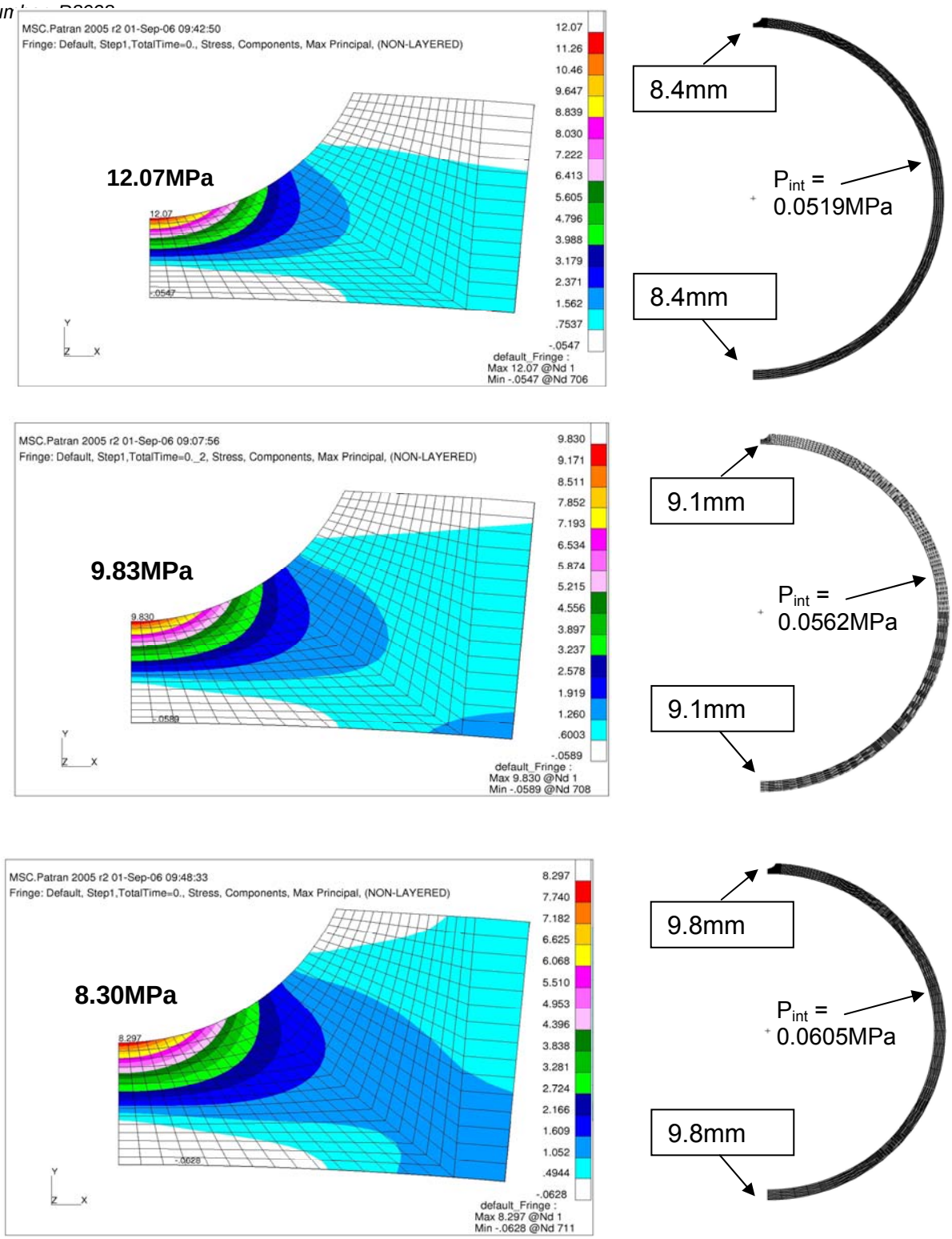

Figure 40. Effect of varying pipe wall thickness for a constant groove depth (Hoop stress of 1.0 N/mm^2 in each case).

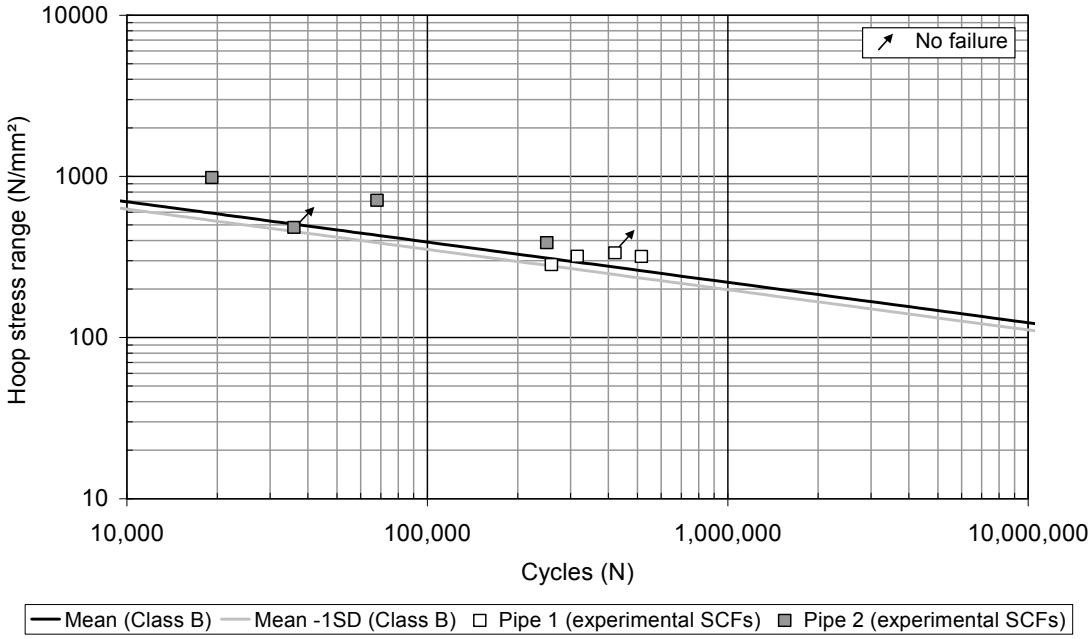

Figure 41. Comparison of the fatigue test results with the BS 7608 Class B fatigue design curve: SCFs derived from strain gauge data.

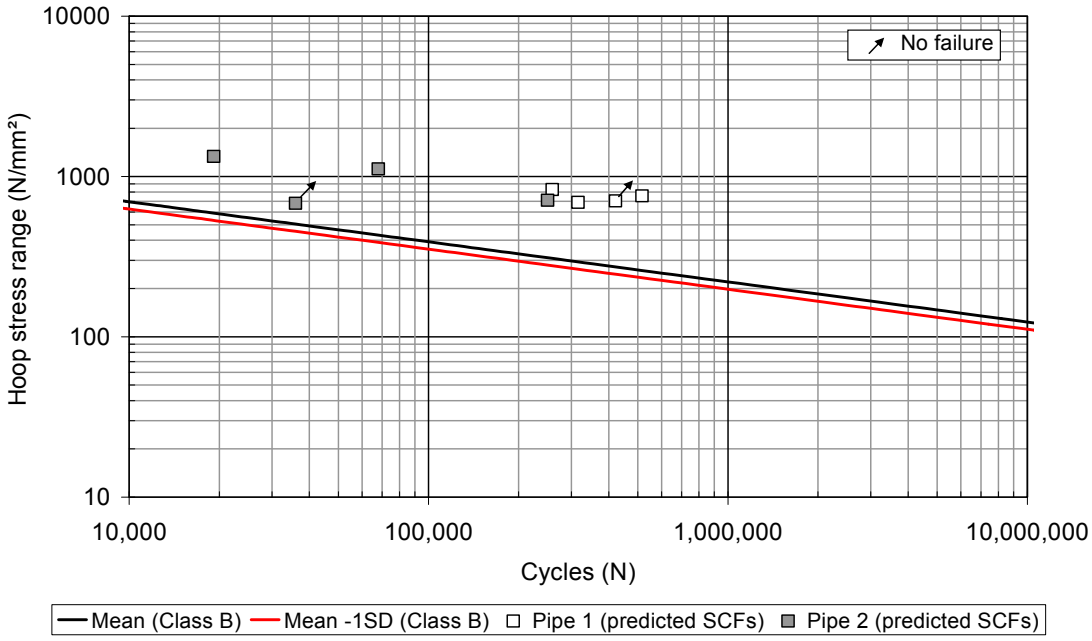

Figure 42. Comparison of the fatigue test results with the BS 7608 Class B fatigue design curve: SCFs predicted using closed form equations.

APPENDIX A MATERIAL INFORMATION.

Vessel 1 was constructed from pipe 1 (323.9x8.4mm [12.75x0.331”]). The test certificate is given in Figure A1.

Vessel 2 was constructed from pipe 2 (323.9x15.9mm [12.75x0.626”]). The test certificate is given in Figure A2 (note, the two certificates provided are for two pipes from the same cast/heat as pipe 2 – a certificate specific to pipe 2 was not available) and the measured material properties are given in Figure A3. The measurements were undertaken to confirm the material properties given that the test certificates (Figure A2) are not specific to pipe 2.

Dalmine PLANT: DALMINE	INSPECTION CERTIFICATE (UNI EN 10204 3.1.B) TO 23884	N. 99/02010 Page 1

CUSTOMER'S ORDER 14208 9900043347 TUBE DEVELOPMENTS LTD

MILL ORDER / ITEM 1902243/002
EXP REFERENCE c/16604

QUEENZIEBURN IND. ESTATE
G659BN KILSYTH GLASGOW
GB.

PRODUCT SEAMLESS STEEL LINEPIPE ACC. TO API 5L AND BS 7191 - STEEL GRADE X52 OF API 5L AND 355 EM - S 0,008% MAX,N 0,012% MAX- NORMALIZED - BLACK INSIDE OUTSIDE OILED - BEVELLED ENDS ACCORDING TO API

DIMENSIONS:	Lg. From	Lg. To	O.D. mm	W.T. mm
	8000	11800	323,900	8,400

QUANTITY : Nr 18 Mt 198,29 Kg 13612 Ft 650' 7" Lbs 30009,2

TEST N. R7132 HEAT N. 990178

TENSION TEST + 20,0^C
TEST SPEC. : TRANSVERSAL WIDTH 37,90 THICK. 8,40 SECTION 318,4 mm2
YIELD POINT 0,5% (N/MM2): requir min 358 result 395,0
TENSILE STRENGTH (N/MM2): requir min 460 max 620 result 553,0
ELONGATION : CALIBRATED ON 2" 50,8 mm
(%): requir.min 25,0 result 36,8
1^IMPACT TEST - 50,0^C REMARKS OR SPEC. : KCV LONG - 050 C JOULE
TEST SPECIMEN : LONGIT. 10 X 7,50 MM requ.JOULE min 28,0 avg 40,0
: result 219,0 205,0 195,0
2^IMPACT TEST - 50,0^C REMARKS OR SPEC. : KCV TRASV - 050 C JOULE
TEST SPECIMEN : TRANSV. 10 X 5,00 MM requ.JOULE min 17,5 avg 24,5
: result 103,0 83,0 90,0
HARDNESS HRC requ. max 22,0 result 0,0
HARDNESS HRB requ. max 100,0 result 86,0

TEST N. R7132/10 HEAT N. 990178

TENSION TEST + 20,0^C
TEST SPEC. : LONGITUDINAL WIDTH 16,00 THICK. 8,50 SECTION 136,0 mm2
YIELD POINT 0,5% (N/MM2): requir min 358 result 444,0
TENSILE STRENGTH (N/MM2): requir min 460 max 620 result 547,0
ELONGATION : CALIBRATED ON 5D 65,0 mm
(%): requir.min 20,0 result 26,1
HARDNESS HRC requ. max 22,0 result 0,0
HARDNESS HRB requ. max 100,0 result 85,4

TEST N. R7133 HEAT N. 990178

TENSION TEST + 20,0^C
TEST SPEC. : TRANSVERSAL WIDTH 38,10 THICK. 8,50 SECTION 323,9 mm2
YIELD POINT 0,5% (N/MM2): requir min 358 result 390,0
TENSILE STRENGTH (N/MM2): requir min 460 max 620 result 555,0
ELONGATION : CALIBRATED ON 2" 50,8 mm

Questo certificato è emesso da un sistema compiuterizzato ed è valido senza firma. Il certificato originale riporta il marchio D in colore verde lungo una diagonale. Il possessore dell'originale, qualora rilasci copia, deve attestarne a suo nome la conformità, assumendosi ogni responsabilità per usi illeciti o semplicemente non consentiti dalla Dalmine.

Alterazioni e/o falsificazioni saranno perseguite a termini di legge.

This certificate is issued by a computerized system and it is valid without signature. On the original certificate the trade-mark D green coloured along the diagonal is stamped. In case the owner of the original certificate would release a copy of it, he must attest its conformity to the original one taking upon himself the responsability for any unlawful or not allowed use.

Any alteration and/or falsification will be subject to the law.

Le certificat est rédigé par un système d'ordinateur et il est valable sans signature. Le certificat original mantionne la marque D de couleur verte en diagonal. Dans le cas où le possesseur de l'original délivrera une copie, il devra attester la conformité en son nom, en s'endossant toute la responsabilité pour des usages illicites ou, tout simplement, pas permis par Dalmine.

Toute alteration ou contrefaction seront susceptibles d'entraîner des poursuites légales.

VERIFIED TRUE COPY OF ORIGINAL

D A T E	QUALITY CERTIFICATION DPT	CHIEF OF QUALITY CERTIFICATION DPT
03/02/1999	Flaviana CERRI	Marco BELLOLI

Figure A1 Vessel 1 (pipe 1): materials test certificate.

Dalmine
PLANT:
DALMINE

INSPECTION CERTIFICATE
(UNI EN 10204 3.1.B) ND 23884

N. 99/02010
Page 2
99000 43347

```
                          (%): requir.min  25,0                    result   36,8
1^IMPACT TEST -  50,0^C  REMARKS OR SPEC. : KCV     LONG  - 050 C  JOULE
    TEST SPECIMEN  : LONGIT. 10 X  7,50 MM     requ.JOULE  min  28,0 avg  40,0
                   :                                result 220,0  218,0  213,0
2^IMPACT TEST -  50,0^C  REMARKS OR SPEC. : KCV   TRASV   - 050 C  JOULE
    TEST SPECIMEN  : TRANSV. 10 X  5,00 MM     requ.JOULE  min  17,5 avg  24,5
                   :                                result 106,0   92,0   86,0
  HARDNESS   HRC    requ.            max  22,0     result     0,0
  HARDNESS   HRB    requ.            max 100,0     result    86,2

TEST     N. R7133/10       HEAT N. 990178
====================
  TENSION TEST + 20,0^C
    TEST SPEC. : LONGITUDINAL    WIDTH 16,10 THICK.  8,40   SECTION  135,2 mm2
    YIELD POINT  0,5% (N/MM2 ): requir min   358                result  439,0
    TENSILE STRENGTH  (N/MM2 ): requir min   460  max   620     result  551,0
    ELONGATION                : CALIBRATED ON 5D   65,0 mm
                          (%): requir.min  20,0                    result   26,1
  HARDNESS   HRC    requ.            max  22,0     result     0,0
  HARDNESS   HRB    requ.            max 100,0     result    85,7

HEAT   N. 990178
================
  HEAT ANALYSIS %
     C   0,12    Mn  1,28    Si  0,29    P   0,011   S   0,002   Cu  0,17
     Sn  0,014   Ni  0,12    Cr  0,10    Mo  0,04    Al  0,035   Ti  0,004
     Nb  0,024   V   0,06    N   0,0078  B   0,0002  Ca  0,0018  As  0,0108
     Sb  0,0032  Pb  0,0014  Bi  0,0018
     SOLUBLE ELEMENTS       :   Al  0,033
          (Cr+Mo+Ni+Cu)    =     0,43
          (Nb+V )          =     0,079
          (Nb+Ti+V )       =     0,083
          (Al-A@)          =     0,002
          (A@/N )          =     4,231
     CARBON EQUIVALENT      : L.F. (C+Mn/6+(Cr+Mo+V)/5+(Ni+Cu)/15)   0,39
     --->  A@ = soluble  Al

  PRODUCT ANALYSIS %                        TEST     N. R7132
     C   0,12    Mn  1,28    Si  0,28    P   0,010   S   0,002   Cu  0,17
     Sn  0,013   Ni  0,12    Cr  0,10    Mo  0,04    Al  0,036   Ti  0,004
     Nb  0,023   V   0,06    N   0,0077  B   0,0002  Ca  0,0018  As  0,0098
     Sb  0,0024  Pb  0,0013  Bi  0,0017
     SOLUBLE ELEMENTS       :   Al  0,036
          (Cr+Mo+Ni+Cu)    =     0,43
          (Nb+V )          =     0,078
          (Nb+Ti+V )       =     0,082
          (Al-A@)          =     0,00
          (A@/N )          =     4,675
     CARBON EQUIVALENT      : L.F. (C+Mn/6+(Cr+Mo+V)/5+(Ni+Cu)/15)   0,39
     --->  A@ = soluble  Al
```

SUBS DEVELOPMENTS
U.A. DEPT
APPROVED
SIGN.
DATE 17/2/99

Questo certificato è emesso da un sistema compiuterizzato ed è valido senza firma. Il certificato originale riporta il marchio ☐ in colore verde lungo una diagonale. Il possessore dell'originale, qualora rilasci copia, deve attestarne a suo nome la conformità, assumendosi ogni responsabilità per usi illeciti o semplicemente non consentiti dalla Dalmine.

Alterazioni e/o falsificazioni saranno perseguite a termini di legge.

This certificate is issued by a computerized system and it is valid without signature. On the original certificate the trade-mark ☐ green coloured along the diagonal is stamped. In case the owner of the original certificate would release a copy of it, he must attest its conformity to the original one taking upon himself the responsability for any unlawful or not allowed use.

Any alteration and/or falsification will be subject to the law.

Le certificat est rédigé par un système d'ordinateur et il est valable sans signature. Le certificat original mantionne la marque ☐ de couleur verte en diagonal. Dans le cas où le possesseur de l'original délivrera une copie, il devra attester la conformité en son nom, en s'endossant toute la responsabilité pour des usages illicites ou, tout simplement, pas permis par Dalmine.
Toute altération ou contréfaction seront susceptibles d'entrainer des poursuites légales.

D A T E	QUALITY CERTIFICATION DPT	CHIEF OF QUALITY CERTIFICATION DPT
03/02/1999	Flaviana CERRI	Marco BELLOLI

Figure A1 Vessel 1 (pipe 1): materials test certificate (continued).

Dalmine PLANT: DALMINE	INSPECTION CERTIFICATE (UNI EN 10204 3.1.B)	N. 99/02010 Page 3

PRODUCT ANALYSIS % TEST N. R7133

C	0,12	Mn	1,29	Si	0,28	P	0,010	S	0,002	Cu	0,18
Sn	0,014	Ni	0,12	Cr	0,11	Mo	0,04	Al	0,035	Ti	0,004
Nb	0,023	V	0,05	N	0,0075	B	0,0002	Ca	0,0017	As	0,0101
Sb	0,0027	Pb	0,0010	Bi	0,0016						

SOLUBLE ELEMENTS : Al 0,034
(Cr+Mo+Ni+Cu) = 0,45
(Nb+V) = 0,077
(Nb+Ti+V) = 0,081
(Al-A@) = 0,001
(A@/N) = 4,533

CARBON EQUIVALENT : L.F. (C+Mn/6+(Cr+Mo+V)/5+(Ni+Cu)/15) 0,40

---> A@ = soluble Al

LEAK-TIGHTNESS TEST PERFORMED WITH SATISFACTORY RESULTS BY:
HYDRAULIC TEST PRESSURE 15,9 MPA FOR 5 Sec

VISUAL AND DIMENSIONAL CONTROL OF THE TUBES HAS BEEN CARRIED OUT WITH SATISFACTORY RESULT

STEEL IS FULLY KILLED AND PRODUCED BY ELECTRIC FURNACE

REMARKS:

ALL TUBES HAVE BEEN NORMALIZED AT 920^C FOR 20 MINS.

HEAT TREATMENT BY CONTINUOS METHOD - FINE GRAIN PRACTICE.

HARDNESS HRC 22 MAX., ACC. TO NACE MR-01-75 L.E.

ALL TUBES HAVE BEEN TESTED BY ULTRASONIC INSPECTION FOR LONGITUDINAL INSIDE/OUTSIDE DEFECTS (NOTCH 5%), ACCORDING TO API 5L-SR4 AND PT COQU 10.05 R.0, WITH SATISFACTORY RESULT.

THE WALL THICKNESS CONTROLLED ON FULL LENGTH BY U.T. OF EACH PIPE IS WITHIN THE TOLERANCE REQUESTED (GQ 13.022/Da L.R.).

ALL PIPES HAVE BEEN TESTED BY U.T. ON FULL LENGTH FOR LAMINATION DETECTION, ACCORDING TO GQ 13.020/Da L.R. - BS 5996 L4, WITH SA-SATISFACTORY RESULT.

THE BEVELLED ENDS (for 300 mm.) HAVE BEEN TESTED WITH WET FLUORESCENT MAGNETIC PARTICLES (P.T. COQU 10.76 R.0), WITH SATISFACTORY RESULT.

----
* CERTIFIED FACTORY UNI EN ISO 9001: I.G.Q. Nr. 8603 *

Questo certificato è emesso da un sistema compiuterizzato ed è valido senza firma. Il certificato originale riporta il marchio ◐ in colore verde lungo una diagonale. Il possessore dell'originale, qualora rilasci copia, deve attestarne a suo nome la conformità, assumendosi ogni responsabilità per usi illeciti o semplicemente non consentiti dalla Dalmine.

Alterazioni e/o falsificazioni saranno perseguite a termini di legge.

This certificate is issued by a computerized system and it is valid without signature. On the original certificate the trade-mark ◐ green coloured along the diagonal is stamped. In case the owner of the original certificate would release a copy of it, he must attest its conformity to the original one taking upon himself the responsability for any unlawful or not allowed use.

Any alteration and/or falsification will be subject to the law.

Le certificat est rédigé par un système d'ordinateur et il est valable sans signature. Le certificat original mentionne la marque ◐ de couleur verte en diagonal. Dans le cas où le possesseur de l'original délivrera une copie, il devra attester la conformité en son nom, en s'endossant toute la responsabilité pour des usages illicites ou, tout simplement, pas permis par Dalmine.

Toute altération ou contrefaction seront susceptibles d'entrainer des poursuites légales.

DATE	QUALITY CERTIFICATION DPT	CHIEF OF QUALITY CERTIFICATION DPT
03/02/1999	Flaviana CERRI	Marco BELLOLI

Figure A1 Vessel 1 (pipe 1): materials test certificate (continued).

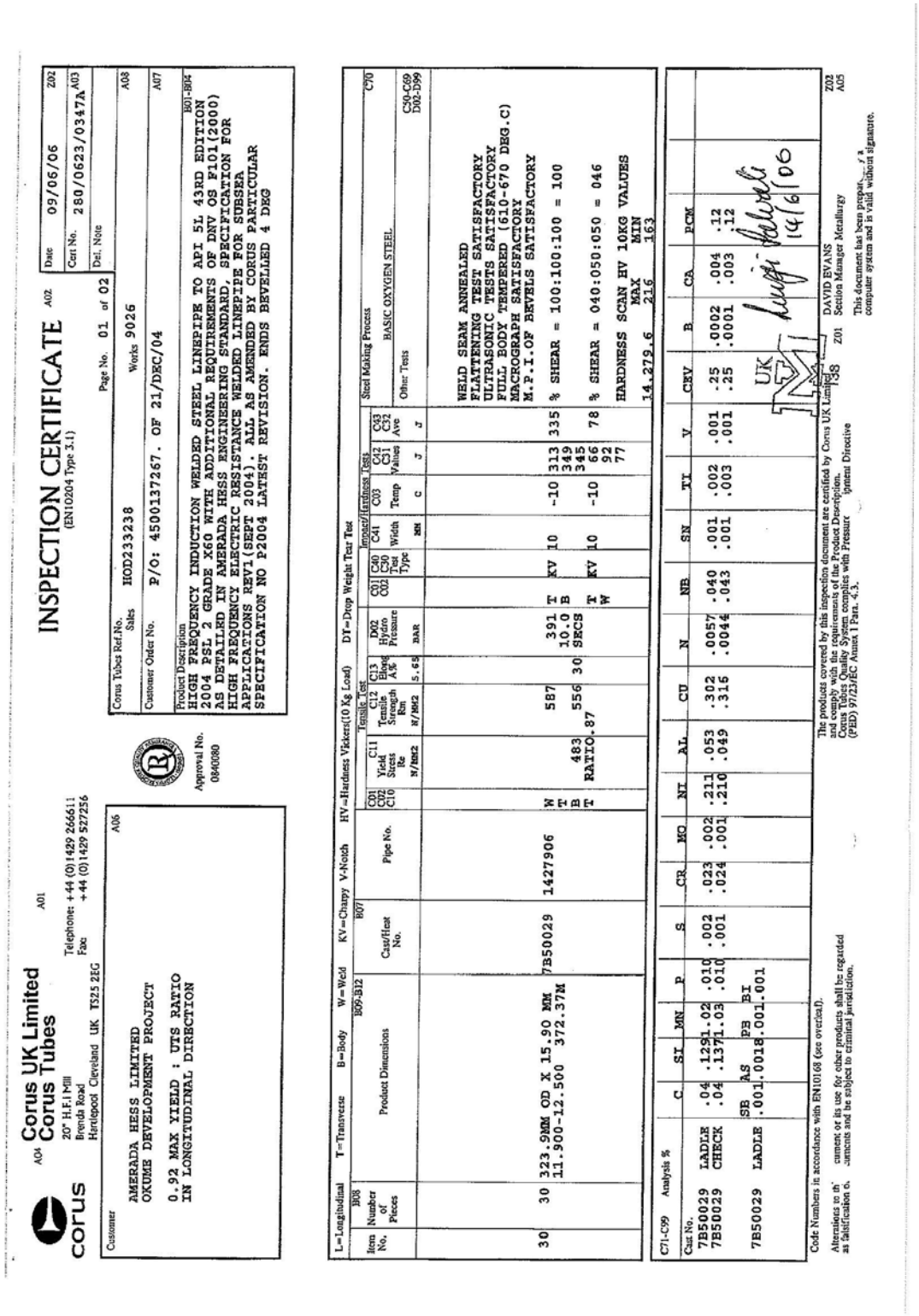

Corus
A04 Corus UK Limited
Corus Tubes
A01
20" H.F.I Mill
Brenda Road
Hartlepool Cleveland UK TS25 2EG
Telephone: +44 (0)1429 266611
Fax +44 (0)1429 527256

Approval No. 0840080

INSPECTION CERTIFICATE
(EN10204 Type 3.1)

A02

Page No. 01 of 02

Date 09/06/06 Z02
Cert No. 280/0623/0347A A03
Del. Note

Customer A06
AMERADA HESS LIMITED
OKUME DEVELOPMENT PROJECT

0.92 MAX YIELD : UTS RATIO
IN LONGITUDINAL DIRECTION

Corus Tubes Ref.No. HOD233238 Works 9026
Sales
A08

Customer Order No. P/O: 4500137267. OF 21/DEC/04
A07

Product Description B01-B04
HIGH FREQUENCY INDUCTION WELDED STEEL LINEPIPE TO API 5L 43RD EDITION
2004 PSL 2 GRADE X60 WITH ADDITIONAL REQUIREMENTS OF DNV OS F101(2000)
AS DETAILED IN AMERADA HESS ENGINEERING STANDARD. SPECIFICATION FOR
HIGH FREQUENCY ELECTRIC RESISTANCE WELDED LINEPIPE FOR SUBSEA
APPLICATIONS REV1(SEPT 2004). ALL AS AMENDED BY CORUS PARTICULAR
SPECIFICATION NO P2004 LATEST REVISION. ENDS BEVELLED 4 DEG

L=Longitudinal T=Transverse B=Body W=Weld KV=Charpy V-Notch HV=Hardness Vickers(10 Kg Load) DT=Drop Weight Tear Test

Item No.	B08 Number of Pieces	Product Dimensions B09-B12	Cast/Heat No. B07	Pipe No.	C01 C02 C10	Yield Stress Re N/MM2	C11	Tensile Test C12 Tensile Strength Rm N/MM2	C13 Elong. A%	D02 Hydro Pressure BAR	C01 C02	C40 C30 Test Type	C41 Width MM	Impact/Hardness Test C03 Temp C	C42 C31 Values J	C43 C32 Ave J	Steel Making Process BASIC OXYGEN STEEL	C70
	30	323.9MM OD X 15.90 MM 11.900-12.500 372.37M	7B50029	1427906	W T B T	483 RATIO.87	587	556	30	391 10.0 SECS	T B W	KV	10	-10	313 349 345 66 92 77	335 78	Other Tests	C50-C59 D02-D99
																	WELD SEAM ANNEALED FLATTENING TEST SATISFACTORY ULTRASONIC TESTS SATISFACTORY FULL BODY TEMPERED (610-670 DEG.C) MACROGRAPH SATISFACTORY M.P.I.OF BEVELS SATISFACTORY	
																	% SHEAR = 100:100:100 = 100	
																	% SHEAR = 040:050:050 = 046	
																	HARDNESS SCAN HV 10KG VALUES MAX MIN 14.279.6 216 163	

C71-C99 Analysis %

Cast No.		C	SI	MN	P	S	CR	MO	NI	AL	CU	N	NB	SN	TI	V	CEV	B	CA	PCM
7B50029	LADLE	.04	.129	1.02	.010	.002	.023	.002	.211	.053	.302	.0057	.040	.001	.002	.001	.25	.0002	.004	.12
7B50029	CHECK	.04	.137	1.03	.010	.001	.024	.001	.210	.049	.316	.0044	.043	.001	.003	.001	.25	.0001	.003	.12
		SB	AS	PB	BI															
7B50029	LADLE	.001	.001	8.001	.001															

Code Numbers in accordance with EN10168 (see overleaf).

Alterations to this document or its use for other products shall be regarded as falsification of documents and be subject to criminal jurisdiction.

The products covered by this inspection document are certified by Corus UK Limited and comply with the requirements of the Product Description. Corus Tubes Quality System complies with Pressure Equipment Directive (PED) 97/23/EC Annex 1 Para. 4.3.

UK
138 Z01

DAVID EVANS
Section Manager Metallurgy

Z02
A05

This document has been produced by a computer system and is valid without signature.

Figure A2 Vessel 2 (pipe 2): materials test certificate.

A04 **Corus UK Limited**
Corus Tubes A01

corus

20" H.F.I Mill
Brenda Road
Hartlepool Cleveland UK TS25 2EG

Telephone: +44 (0)1429 266611
Fax: +44 (0)1429 527256

INSPECTION CERTIFICATE A02

(EN10204 Type 3.1)

Page No. 02 of 02

Date	09/06/06 Z02
Cert No.	280/0623/0347A A03
Del. Note	

Customer A06

AMERADA HESS LIMITED
OKUME DEVELOPMENT PROJECT

0.92 MAX YIELD : UTS RATIO
IN LONGITUDINAL DIRECTION

Approval No.
0840080

Corus Tubes Ref.No. Sales HOD233238 Works 9026 A08

Customer Order No. P/O: 4500137267. OF 21/DEC/04 A07

Product Description B01-B04
HIGH FREQUENCY INDUCTION WELDED STEEL LINEPIPE TO API 5L 43RD EDITION 2004 PSL 2 GRADE X60 WITH ADDITIONAL REQUIREMENTS OF DNV OS F101(2000) AS DETAILED IN AMERADA HESS ENGINEERING STANDARD, SPECIFICATION FOR HIGH FREQUENCY ELECTRIC RESISTANCE WELDED LINEPIPE FOR SUBSEA APPLICATIONS REV1(SEPT 2004). ALL AS AMENDED BY CORUS PARTICULAR SPECIFICATION NO P2004 LATEST REVISION. ENDS BEVELLED 4 DEG

L=Longitudinal T=Transverse B=Body W=Weld KV=Charpy V-Notch HV=Hardness Vickers(10 Kg Load) DT=Drop Weight Tear Test

Item No.	B08 Number of Pieces	B09-B12 Product Dimensions	B07 Cast/Heat No.	Pipe No.	C01 C02 C10	C11 Yield Stress Re N/MM2	C12 Tensile Strength Rm N/MM2	C13 Elong A% 5.65	D02 Hydro Pressure BAR	C01 C02	C40 C30 Test Type	C41 Width MM	C03 Temp C	C42 C31 Values J	C43 C32 Ave J	C70 Steel Making Process BASIC OXYGEN STEEL / C50-C69 D02-D99 Other Tests
30	30	323.9MM OD X 15.90 MM 11.900-12.500 372.37M	7B50029	1428406	W		605		391	T	KV	10	-10	326	338	% SHEAR = 100:100:100 = 100
					T				10.0	B				354		
					B	490	560	31	SECS					334		
					T	RATIO.88				T	KV	10	-10	129	237	% SHEAR = 060:100:100 = 086
										W				311		
														271		HARDNESS SCAN HV 10KG VALUES
																MAX MIN
																14.284.6 213 162
**********					***	END OF TEST CERTIFICATE										**********

C71-C99 Analysis % Cast No.	C	SI	MN	P	S	CR	MO	NI	AL	CU	N	NB	SN	TI	V	CEV

UK

Luigi Salvati 14/6/06

Code Numbers in accordance with EN10168 (see overleaf).

Alterations to th' current or its use for other products shall be regarded as falsification o... documents and be subject to criminal jurisdiction.

The products covered by this inspection document are certified by Corus UK Limited and comply with the requirements of the Product Description.
Corus Tubes Quality System complies with Pressure Equipment Directive (PED) 97/23/EC Annex I Para. 4.3.

DAVID EVANS
Z05 Section Manager Metallurgy
Z02 A05

This document has been prepar... by a computer system and is valid without signature.

Figure A2 Vessel 2 (pipe 2): materials test certificate (continued).

UKAS TESTING 1046

The TEST HOUSE

Certificate of Test

Page 1 of 1

Client: Advantica Ltd, Holywell Business Park, Ashby Road, Loughborough, Leicestershire LE11 3GR

Date of receipt: 25 July 2007 *Date of test:* 2 August 2007
Reference No.: T71431 *MI No.:* 2502
Order No.: 9900050246 *Specification:* Clients own

Description: 15.9mm WT x 12" Diameter Section of Grade X60 Steel Pipe
Identity: **'HLW'**
Test methods: *Procedure:* TP01a-1, BSEN 10002-1:2001, TP06, BSEN 10045-1:1990
Inspection Authority: N/A

TENSILE TEST(S) Test machine calibrated to class 1.0 requirements of BS EN ISO 7500-1:1999

Identity/Position	Mark	Dimensions Size Mm	CSA mm²	GL mm	Proof Stress Rp 0.2% Load kN	Stress N/mm²	Max Stress Load kN	Stress N/mm²	El %	RA %
Longitudinal Tensile	1	10.04 Dia	79.17	5d	38.70	489	42.74	540	32.5	79
Longitudinal Tensile	2	10.04 Dia	79.17	5d	39.01	493	42.74	540	31.5	80
Transverse Tensile	3	8.01 Dia	50.39	5d	25.77	512	28.07	557	25.0	78
Transverse Tensile	4	7.98 Dia	50.01	5d	25.21	504	27.98	559	25.5	78
Fracture Description:					-	-	-	-	-	-

Note: The mk1 to mk4 inclusive specimens exhibited upper yield stress values of 505N/mm², 524N/mm², 531N/mm², and 536N/mm² respectively.
Comments: Extensometer number V1006, calibrated to BS EN ISO 9513:2002 class 1, was used for these tests.
Note: Specimens mk3 and mk4 fractured outside the central third of one marked gauge length.

IMPACT TESTS 300 Joules nominal striking energy machine calibrated to BS EN 10045-2:1993

Identity/Position	Mark	Size (mm)	Charpy notch	Test Temp (degrees C)	Results (Joules KV)	Crystallinity (%)
Longitudinal specimens machined within 2mm of the surface and notched through thickness	5,6,7	10 x 10	2mm V	-10	290, 289, 290 Av = 290	0, 0, 0
Transverse specimens machined within 2mm of the surface and notched through thickness	8,9,10	10 x 10	2mm V	-10	290, 289, 289 Av = 289	0, 0, 0

Note: The % crystallinity was determined in accordance with BS 131-5.
Note: Specimens mk5 to mk10 inclusive did not completely fracture. The values for specimens mk5 to mk10 inclusive exceeded 80% of the machine capacity and should be regarded as appropriate.

- End of Test Results -

Note - The test results detailed above apply only to the sample(s) of material submitted to the laboratory.

Tests Performed by: *N Green* *Witnessed by:*

Certificate Approved by: *D Ellin, Managing Director*

Signed ..... *Date* 2-8-07

The Test House (Cambridge) Ltd, Granta Park, Great Abington, Cambridge CB1 6AL Tel: 01223 899012 Fax: 01223 894255 E-mail: admin@testhouse.twi.co.uk www.thetesthouse.co.uk
Registered in England No. 2513984 Registered Office: Granta Park, Great Abington, Cambridge
The Test House is a trading name of The Test House (Cambridge) Ltd, a wholly owned subsidiary of TWI

Figure A3 Vessel 2 (pipe 2): measured material properties.

APPENDIX B INSPECTION CERTIFICATE (DEFECTS)

The defect metrology report for pipe 1 is given in Figure B1 and the report for pipe 2 is given in Figure B2.

PMC NO. 4011733

PMC
AMBERGATE

GENERAL INSPECTION
REPORT PAGE 1 OF 2

PROJECT CLIENT ADVANTICA	DATE 28-2-03
LOCATION: PMC AMBERGATE	INSPECTOR (CAPITALS): R. ELLIOTT
INSPECTION TECHNIQUE	

ADVANTICA 1/07620CM05

ALL MEASUREMENTS IN MILLIMETRES

	8.9		8.9		8.9	
8.9	1.94 *		1.73		1.65	8.9
	9.1	LENGTH 398.95 WIDTH 11.21	9.1	DEFECT 1	9.1	
	8.7		8.7		8.7	
8.7	3.23		3.43		3.44 *	8.7
	8.7	LENGTH 404.49 WIDTH 13.86	8.6	DEFECT 2	8.6	
	9.6	9.6		9.7	9.5	
9.8	5.17		4.90		5.21 *	9.7
	9.2	LENGTH 405.75 WIDTH 16.20	9.3	DEFECT 3	9.2	9.1
	9.2		9.2		9.2	
9.1	3.7		3.6		4.5	9.2
9.1	3.2		3.1		4.2	9.3
8.9	2.9 *		2.9		3.6	9.0
	9.0	LENGTH 398.27 WIDTH 137.76	9.1	DEFECT 4	9.0	

SIGNATURE R Elliott
APPROVAL & No. BGAS S.I. 2513
DATE 1-3-06

CIRCULATION

Document No: NDT-004 | Issue 3 Dated 3.4.00

Figure B1. Pipe 1: Metrology report.

PMC NO. 4011733

PMC AMBERGATE

GENERAL INSPECTION REPORT PAGE 2 of 2

PROJECT CLIENT ADVANTICA	DATE 28.2-03
LOCATION: PMC AMBERGATE	INSPECTOR (CAPITALS): R. ELLIOTT

INSPECTION TECHNIQUE

ADVANTICA 1/07620PMOT

DEFECT 1

MAXIMUM DEPTH OF DEFECT 1.94 mm / MINIMUM WALL THICKNESS 8.9 mm = 21.79% WALL LOSS

DEFECT 2

MAXIMUM DEPTH OF DEFECT 3.44 mm / MINIMUM WALL THICKNESS 8.6 mm = 40% WALL LOSS

DEFECT 3

MAXIMUM DEPTH OF DEFECT 5.21 mm / MINIMUM WALL THICKNESS 9.1 mm = 57.25% WALL LOSS

DEFECT 4

MAXIMUM DEPTH OF DEFECT 6.0 mm / MINIMUM WALL THICKNESS 8.9 mm = 67.41% WALL LOSS

SIGNATURE R Elliott
APPROVAL & No. BGAS SJI 2513
DATE 1-3-06

CIRCULATION

Document No: NDT-004	Issue 3 Dated 3.4.00

Figure B1. Pipe 1: Metrology report (continued).

PRC - 12" VESSEL DEFECTS 23 - 07 - 07

DEFECT DEPTH MEASURING POINTS

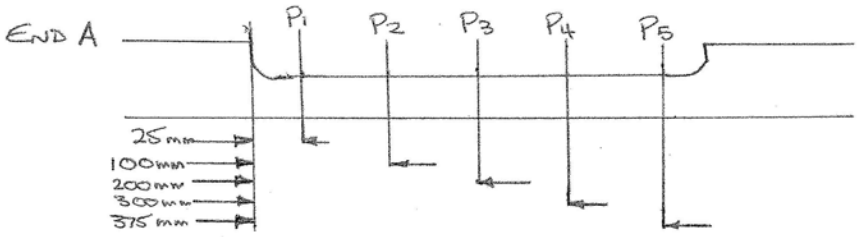

DEFECT 1	P1	P2	P3	P4	P5
DEPTH	2.92	2.94	2.95	2.93	2.93
WIDTH	16.72	16.72	16.7	16.72	16.72
DEFECT 2	P1	P2	P3	P4	P5
DEPTH	6.13	6.11	6.15	6.12	6.07
WIDTH	21.80	21.80	21.80	21.75	21.65
DEFECT 3	P1	P2	P3	P4	P5
DEPTH	9.10	9.20	9.28	9.24	9.21
WIDTH	24.0	24.0	24.0	24.0	24.0

	DEFECT 1	DEFECT 2	DEFECT 3
DEFECT LENGTH	399	399	400

PIPE W/T ADJACENT TO DEFECT.

DEFECT 1	16.5	16.6	16.6	16.6	16.5	END A
	P1	P2	P3	P4	P5	
	16.6	16.6	16.6	16.5	16.5	
DEFECT 2	16.5	16.5	16.5	16.5	16.5	END A
	P1	P2	P3	P4	P5	
	16.5	16.4	16.5	16.5	16.5	
DEFECT 3	16.5	16.5	16.5	16.5	16.5	END A.
	P1	P2	P3	P4	P5	
	16.5	16.4	16.4	16.5	16.5	

Figure B2. Pipe 2: Metrology report.

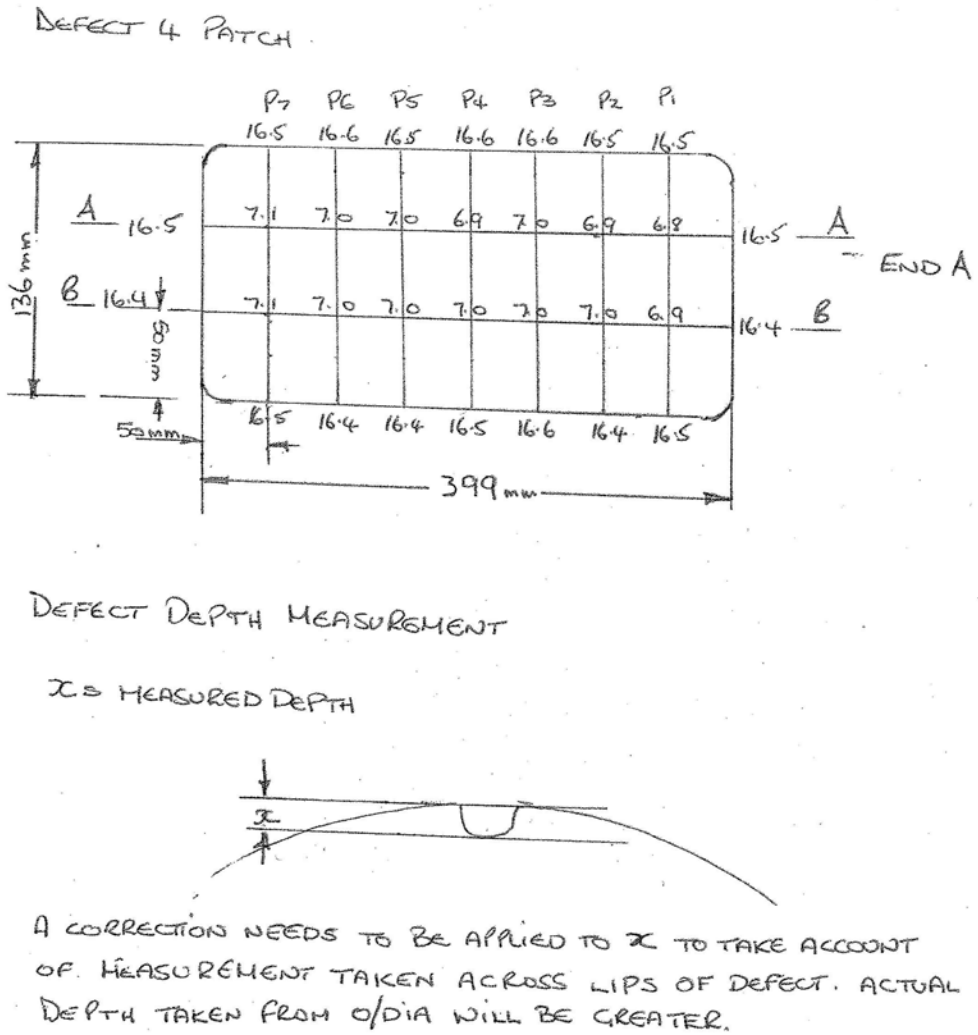

Figure B2. Pipe 2: Metrology report (continued).